THE EFFECTS OF POSTNATAL GROWTH RESTRICTION ON CARDIAC FUNCTION IN MICE

By

Joseph Visker

A DISSERTATION

Submitted to
Michigan State University
in partial fulfillment of the requirements
for the degree of

Kinesiology−Doctor of Philosophy

2020

PUBLIC ABSTRACT

THE EFFECTS OF POSTNATAL GROWTH RESTRICTION
ON CARDIAC FUNCTION IN MICE

By

Joseph Visker

The Developmental Origins of Health and Disease [DOHaD] hypothesis proposes that growth restriction in early life can lead to the development of chronic disease such as cardiovascular disease [CVD]. The objective of this dissertation is to profile cardiac function following postnatal growth restriction. To accomplish this objective three hypothesis driven investigations were conducted to elucidate differences in electrical activity, the cardiac proteome, and metabolic profile of the heart as a result of postnatal growth restriction.

To model postnatal growth restriction, FVB mice [Charles River, Wilmington, MA] were used since they are genetically similar and do not reject their newborns when handled. Two weeks before breeding, dams were fed an isocaloric diet of either a control [20% protein], or low protein [LP; 8% protein] diet. Pups nursed from LP dams undergo growth restriction from an 18% reduction of milk. Following birth [postnatal day 1; PN1], pups from LP dams were euthanized while pups from CON dams were cross fostered to a LP dam or a different CON dam. At PN21, all pups were weaned and fed CON diet *ad libitum* until adulthood at PN80. Therefore, our postnatal nutritive model isolated growth-restriction to postnatal development in early life.

In the first study, growth restriction was isolated to an early period [EUN; PN1-10], late period [LUN; PN11-21], and combined period [PUN; PN1-21] of postnatal life. ECG was used to assess the electrical conductance of the heart. At PN80, CON, EUN, LUN and PUN mice were placed under anesthesia and a 5-minute ECG was recorded at baseline. Next, the heart was stressed with an injection of dobutamine, and another 5 minutes of ECG was recorded. ECG

analysis showed that PUN mice who experienced the longest growth restriction bout had the most severe cardiac arrhythmias in adulthood. Therefore, for the remaining two studies only PUN groups were studied, since the most severe cardiac impairment was seen in this group.

In the second study, we determined proteomic differences between CON and PUN mouse hearts. At PN21, hearts were analyzed by two-dimensional in-gel electrophoresis [2D DIGE] and mass spectroscopy to identify proteomic differences. Results were confirmed with western blot and pathway analysis conducted using REACTOME and STRING. At PN80, echocardiography was performed to elucidate functional differences caused by PUN. Western blots of identified proteins were conducted at PN80 to determine if differences were persistent or recuperated. Results showed that a differential cardiac proteome [↓ Ttn, ↓ $p57^{kip2}$, and ↓ Collagen proteins] is present in the PUN hearts and led to functional impairments in adulthood.

In the third study, we determined if growth restriction impaired cardiac mitochondrial energetics in PUN mice. Mitochondria were isolated and fueled with substrates targeting Complex I [CI], Complex II [CII], and fatty acid oxidation [FAO]. Oxygen flux [JO_2], and reactive oxygen species [ROS] were recorded using high-resolution respirometry [HRR]. Results showed that PUN mitochondria have reduced mitochondrial efficiency via reductions in respiratory control with elevations in LEAK respirometry. PUN mitochondria also produce more ROS indicative of oxidative stress. Taken together, these findings suggest PUN mouse hearts have mitochondrial impairments which increase the risk for CVD in adulthood.

Conjointly, findings from this dissertation show that postnatal growth restriction causes deleterious effects to the cardiovascular system. These deficits increase the risk for CVD in adulthood, and future research should focus on the development of evidence-based practices to reduce mortality rates from growth restriction.

ABSTRACT

THE EFFECTS OF POSTNATAL GROWTH RESTRICTION
ON CARDIAC FUNCTION IN MICE

By

Joseph Visker

Annually, 15 million babies globally will undergo growth deficits from an inadequate postnatal nutritive environment. Growth restriction during key developmental windows can lead to the occurrence of chronic disease in adulthood such cardiovascular disease [CVD]. The purpose of this dissertation was to characterize heart function following postnatal growth restriction. Investigations were performed to reveal alterations in electrical conductance, cardiac protein abundance, and cardiac energetics from postnatal growth restriction.

To experimentally represent postnatal growth restriction, FVB mice were used since they do not discard their neonates when managed, thus allowing for cross fostering. Two weeks prior to mating, dams were nourished with either a control [CON; 20% protein diet], or a low protein diet [LP; 8% protein diet]. Mouse pups that are nourished from LP dams experience growth restriction from an 18% reduction of milk volume. After birth [postnatal day 1; PN1], pups from LP dams were euthanized while half of the pups from CON dams were cross fostered to a either a LP dam or a different CON dam. At PN21, all pups were weaned and fed CON diet *ad libitum* until adulthood at PN80. Therefore, our nutritive model isolated growth restriction to the postnatal developmental window in early life.

At PN80, CON, EUN, LUN and PUN mice were placed under anesthesia and a 5-minute ECG was recorded at baseline. Next, the heart was pharmacologically stressed with an intraperitoneal [IP] injection of dobutamine, and another 5 minutes of ECG was recorded for all groups. ECG showed the CON mice did not experience any abnormal arrhythmias. However, in

the restricted groups, the LUN had a higher prevalence of atrial flutter, EUN had 1st degree AV block, and PUN had an increased risk for ventricular depolarization arrhythmias. These results led to the conclusion that postnatal growth restriction increased the risk of abnormal electrical activity of the heart during adulthood, with the most severe impairments present in the PUN.

The goal for the second study was to determine proteomic alterations between the hearts of CON and PUN mice. Thus, at PN21, hearts of CON and PUN were subjected to two-dimensional in-gel electrophoresis [2D DIGE] and mass spectroscopy to identify differences in cardiac protein abundance. Cardiac function was measured in adulthood via echocardiography. Results showed a reduced protein abundance of $p57^{kip2}$, Ttn, and collagen proteins. Additionally, PUN mice had diastolic dysfunction in adulthood. Next, we constructed a potential mechanism for cardiac impairment to allow for future therapeutic countermeasures.

The last project determined if growth restriction impaired mitochondrial energetics in the hearts of the PUN mice. Oxygen flux [JO_2], and reactive oxygen species [ROS] were recorded using O2k-High resolution respirometry [HRR] at PN22 and PN80. Results from this investigation showed that postnatal growth restriction caused elevations in LEAK respirometry, which reduced the efficiency of PUN mitochondria. ROS emission was also significantly elevated in the PUN mouse hearts, indicating oxidative stress. In conclusion, postnatal growth restriction in early life impairs cardiac mitochondrial function and may increase the risk for CVD.

Results from this dissertation show postnatal growth restriction causes permanent damage to cardiac structure and function in adulthood. Future research should focus on determining evidence-based practices with therapeutic countermeasures to mitigate the damage and counteract CVD in those that have experienced postnatal growth restriction.

This dissertation is dedicated to my wife, children, and family.
Caitlin, Henderson, and Virginia thank you for always believing in me.
To my family, thanks for your love and support.

ACKNOWLEDGEMENTS

I would like to first and foremost thank my advisor, Dr. David P. Ferguson for his mentoring throughout my career at Michigan State University. Next, thanks to my committee members, Drs. James Pivarnik, Janet Hauck, and Jason Bazil. Additionally, thanks to the Neonatal Nutrition and Exercise Research laboratory of the Kinesiology Department at Michigan State University for all their help and support.

TABLE OF CONTENTS

LIST OF TABLES

LIST OF FIGURES

KEY TO ABBREVIATIONS

ADP: adenosine diphosphate

ATP: adenosine triphosphate

BCA: bicinchoninic acid assay

BSA: bovine serum albumin

CI-III: complex I-III of electron transport chain

CON: control

CV: cardiovascular

CVD: cardiovascular disease

DOHaD: developmental origins of health and disease

ECG: electrocardiography

ECHO: echocardiography

ETC: electron transport chain

EUN: early undernutrition

FAO: fatty acid oxidation

HBCS: Helsinki birth cohort study

HR: heart rate

HRR: high resolution respirometry

IUGR: intrauterine growth restriction

JO_2: oxygen flux

Kcal: kilocalories

LC: liquid chromatography

LP: low protein

LUN: late undernutrition

LV: left ventricle

MAP: mean arterial pressure

MS: mass spectrometry

PAGE: polyacrylamide gel electrophoresis

PCM: palmitoylcarnitine+malate

PM: pyruvate+malate

PN: postnatal

PPI: protein-protein interaction

PSE: pharmacological stress echocardiography

PUN: postnatal undernutrition

PVDF: polyvinylidene fluoride

Q: cardiac output

RCR: respiratory control ratio

ROS: reactive oxygen species

RP: restricted protein

SDS: sodium dodecyl sulfate

SMR: standardized mortality rate

S+R: succinate+rotenone

SV: stroke volume

TCA: tricarboxylic acid cycle

TPR: total peripheral resistance

2D DIGE: two-dimensional differential in gel electrophoresis

CHAPTER 1: INTRODUCTION

Each year, globally 15 million babies will experience growth delays due to poor postnatal nutrition[1-5]. In fact, over 7 million deaths per year, and $42.5 billion in associated healthcare costs can be attributed to CVD as a result of a suboptimal nutritive environment in early life[6]. Most of the evidence in the growth restricted literature is focused on those who experience *in utero* growth-restriction [IUGR] caused in part by placental insufficiency, while less emphasis is placed upon those who are postnatally growth restricted. The literature shows a robust volume of manuscripts associated with IUGR [~22,100] compared to the postnatal window [~1,700].

About 25% of children less than 5 years old will have growth impediments from postnatal undernutrition[7] which is related to a 47% increased mortality risk from CVD[8]. This CV morbidity rate endures even if growth is recuperated through re-feeding an appropriate diet, indicating the physiological programming into adulthood independent of body weight[9]. However, there is minimal evidence for disease mechanisms caused by postnatal growth restriction. Thus, the purpose of this dissertation is to characterize the influence of postnatal growth restriction on three key components [electrical activity, cardiac structure via global proteome screening, and metabolism] to cardiac function to lay the foundation for evidence-based practices and counteract CVD. To accomplish the objective of this dissertation the following specific aims were developed.

Research Aims

Specific Aim 1: Electrical Activity of the Heart: to determine if growth restriction during early [EUN, days 1-10], late [LUN, days 11-21], and combined [PUN, days 1-21] postnatal life induces cardiac arrhythmogenesis at rest and/or when pharmacologically stressed with dobutamine in adulthood.

Hypothesis 1.1: The postnatally growth restricted group that experience the longest [PUN, days 1-21] bout of undernutrition will exhibit the most severe ECG arrhythmias [ventricular impairments] at rest and when stimulated with dobutamine.

Hypothesis 1.2: EUN during the proliferative phase of cardiac development [days 1-10] will ascertain cardiac arrhythmias [at rest and + dobutamine] isolated to the atrial myocardium.

Hypothesis 1.3: LUN during the hypertrophy phase of cardiac development [days 11-21] will experience cardiac arrhythmias [at rest and + dobutamine] isolated to the ventricular myocardium.

Hypothesis 1.4: The CON mice will not experience any arrhythmias at rest or when stimulated with dobutamine.

Specific Aim 2.1: Cardiac Structure and Proteome: to determine the proteomic differences in the heart caused by postnatal growth restriction.

Specific Aim 2.2: To develop potential mechanisms by which postnatal growth restriction impairs cardiac function.

Hypothesis 2.1: The postnatally growth restricted mice will exhibit smaller hearts with impaired diastolic function compared to controls.

Hypothesis 2.2: The postnatally growth restricted mice will exhibit key proteomic differences from controls.

Specific Aim 3.1: Cardiac Metabolism: to determine if oxidative phosphorylation is impaired in isolated cardiac mitochondria of the postnatally growth restricted mice during juvenile [22 days old] and adult [80 days old] life.

Hypothesis 3.1: The postnatally growth restricted hearts will have reduced oxygen flux in the presence of substrates used in fatty acid oxidation [palmitoylcarnitine+malate; ETC target =

CI and quinone pool], but will be maintained in the presence of carbohydrates [pyruvate+malate; ETC target = Complex I] and TCA cycle intermediates [succinate+rotenone; ETC target = Complex II]. The control mice will not experience any deficits in oxygen flux when substrates are fueling their mitochondria.

Specific Aim 3.2: To determine if the postnatally growth restricted mouse cardiac mitochondria experience elevated oxidative stress and emit more reactive oxygen species compared to controls.

Hypothesis 3.2: Postnatally growth restricted cardiac mitochondria will experience greater amounts of oxidative stress and emit more reactive oxygen species as compared to control hearts.

In conclusion, the DOHaD literature suggests negative alterations to cardiac physiology from early life growth restriction due to suboptimal nutrition; however, minimal research has focused on the postnatal window of development. By accomplishing the objective of this dissertation, evidence-based practices could be developed to reduce CVD mortality rates.

CHAPTER 2: REVIEW OF THE LITERATURE

The purpose of this review is to examine the DOHaD literature surrounding the development of CVD from early life growth restriction with emphasis placed upon the postnatal window of development. This review will analyze early epidemiological evidence, and then a discussion about experimental research designs using animal models will follow. Importance will be placed upon the DOHaD literature surrounding the projects that have been outlined in this dissertation, mainly cardiac electrical function, cardiac proteomics, and cardiac metabolism. A review of these topics will provide the rationale for the aims and hypotheses in this dissertation.

Growth Restriction Influences Chronic Disease

Growth restriction in early life [IUGR and Postnatal] increases the risk for stroke[10] [hazard ratio = 1.62; 95% CI = 1.30 to 2.02; p=0.0001], type II diabetes[11, 12] [odds ratio = birth weight <5.5lbs = 6.6; 95% CI = 1.5 to 28], hypertension[13, 14] [odds ratio = 1.19; 95% CI = 1.01 to 1.41] and heart disease [odds ratio = 1.83; 95% CI = 1.28 to 2.60]. Researchers hypothesized that growth restriction caused impairment to physiological systems during early life such as the immune system, anti-oxidant defenses, inflammation, and neuro-endocrine systems which are linked to the increased risk for chronic disease[13]. The standardized mortality ratio [SMR] for developing heart disease in adulthood from early life growth restriction is a graded response with the lowest birth weights [<5.5 lbs. = 83 SMR, >10 lbs. = 49 SMR] associated with the highest risk of mortality.

These early associations showing chronic disease, including heart disease from growth restriction in early life have been replicated and confirmed in different parts of the world, such as Europe, China, India[15], and the United States of America[16]. As the focus of this literature review is on heart disease, readers are directed to the following reviews specific to growth restriction

and chronic disease[17, 18]. In the following paragraphs, well-known cohort studies focusing on growth restriction and CVD will be discussed in further detail.

Growth Restriction Influences Cardiovascular Disease

Hertfordshire Cohort Study

The most cited DOHaD researcher is Dr. David Barker. He was a physician and epidemiologist that proposed an adverse perinatal environment [gestational and/or postnatal] alters the body's growth, and metabolism, increasing the incidence of pathologies[19].

The original epidemiological work from Barker *et. al.* was in the county of Hertfordshire, England[1, 20]. The Hertfordshire cohort included 5,654 men born during 1911-1930. They were born across six districts of Hertfordshire and their weights in infancy recorded. Briefly, those born small for gestational age, and/or were small at one year of age were linked to having hypertension, and death from ischemic heart disease in adulthood. Growth restricted individuals who had the lowest birthweights, and lowest weight at one year of age had the highest mortality rates from CVD in adulthood[1]. Specifically, the mortality rate for CVD was increased by 62% in those who weighed 8.2 kg [18.0 lbs.] or less at one year of age[1].

The Hertfordshire cohort showed an increased mortality risk from ischemic heart disease in adulthood from low birthweight, and reduced growth rates in early life[20]. Critics of the DOHaD hypothesis contemplated that Barker and his team may have statistically over-controlled their data. Additionally, a limitation to the results presented by Barker was that too many participants were "lost to follow up" data collection[21, 22], however future studies conducted by Barker *et. al.* and others testing the DOHaD hypothesis, showed growth restriction did increase CVD[4, 8, 12, 18, 23-25].

The Dutch Hunger Winter of 1944-45

Near the end of World War II, a famine in German-occupied Netherlands caused 22,000 deaths due to starvation[26-28]. During the famine, food provisions became progressively inadequate, consisting of mostly bread and potatoes, about 1,000 kcals/day[29]. The babies that were exposed to the Dutch famine were thinner, shorter, lighter, and had a reduced head circumference, when compared to those that were not exposed to the famine[27]. The famished cohort also had a three-fold increase in coronary heart disease, which was accompanied by hypertension, impaired glucose tolerance, and an elevated atherogenic lipid profile when they became adults[1, 2, 11, 13, 26, 27, 30-33].

The studies conducted using the Dutch famine cohort are significant to the DOHaD literature since it used different subjects and locations than the Hertfordshire cohort, and came to a similar conclusion, that an adverse perinatal nutritive environment increases the risk for chronic diseases into adulthood. Therefore, the reproducibility of findings helped strengthen the causal pathway and bolstered credibility of the growing DOHaD hypothesis.

Helsinki Birth Cohort Study [1924-1944]

During World War II [1939-1945], Finland fought against the Soviet Union, and nearly 70,000 Finnish children were evacuated unaccompanied by their parents to Sweden and Denmark to escape the war zone[34]. The participants involved in the Helsinki Birth Cohort Study [HBCS] included 20,346 individuals who were born at Helsinki University Central Hospital between 1924-44[7]. These historical circumstances made it possible to study longitudinally the health consequences from an adverse early life environment. The HBCS included data on birth weight, placental weight, length, and head circumference[3]. Information about mothers who gave birth, included age, height, weight, and parity. Follow-up studies have been conducted on this

cohort during early childhood[35] [every year from 2-11 years of age], adolescents[36] [16 years of age], and later in adulthood[37] [males; 61.2±2.6 years, females; 61.3±2.9 years]. A smaller sub-cohort of individuals [n=2000] were randomly selected for a clinical study including information on metabolism, dietary information, and other lifestyle factors. In those individuals, fasting plasma glucose levels via standard oral glucose testing showed insulin resistance and impaired glucose regulation[38].

Those who experienced a restrictive nutritive environment were more likely to develop CVD in adulthood. Additionally, children [n=1,726; 4.6±2.4 years old] that experienced the longest separation [1.8±1.1 years] were more likely to use medications for heart disease as adults compared to the non-separated group [hazard ratio=1.29; 95% CI=1.04-1.59; p=0.02][39]. Several studies have continued to use this cohort as a reliable dataset to study the effects of developmental programming[3, 34, 39-41]. Limitations to the HBCS include the inability to untangle undernutrition from other variables, such as mental health status and childhood trauma, which may influence development.

The literature shows developmental programming occurs in humans and increases the risk for chronic disease in adulthood, including CVD. However, there are currently limited evidence-based practices specific to CVD from growth restriction. By focusing on how postnatal growth restriction influences cardiac function, it will allow for accurate understanding of how developmental programming of the heart occurs. In order to address chronic disease from postnatal growth restriction, biological mechanisms need elucidation. Thus, animal models are used as an experimental model for growth restriction.

Animal Models for Growth Restriction

Experimental animals are regularly used as proxy for humans and allow for research designs that are not feasible or ethical for human subjects. Much of the knowledge relating to the short and long term effects in the DOHaD literature comes from experimental animals including non-human primates[42], sheep[43-46], pigs[47], and rodents[6, 48, 49]. A discussion specific to those experimental animals and their CV systems will follow.

Developmental Timeline for Cardiac Growth

When studying developmental programming of experimental animals, the developmental timeline of the heart deserves consideration. Hearts of different species do not develop on the same timeline as humans making the generalization of findings difficult. For example, human and sheep cardiomyocytes complete their endowment and progress from mononucleated to binucleated during the latter portion of the 3rd trimester [~week 36 for humans][50]. Following cyto- and karyokinesis, human and sheep cardiomyocytes begin to hypertrophy [increase in cross-sectional area] to meet the demands of extrauterine life [increase contractile force] within the first 6 weeks of postnatal life[50]. In contrast, mice are considered altricial species, being born when their organs are relatively immature, the cardiac development of a mouse occurs in the postnatal environment, such that cardiomyocyte endowment occurs from PN1-10, and the hypertrophy phase is from PN11-21[44, 50, 51]. In the developing mouse, PN1-10 is considered the last part of the third trimester in humans, and PN11-21 is around the first 6 weeks after birth in humans[4, 49]. About 70-80% of all IUGR observed in humans occurs in the latter part of the third trimester[52, 53], therefore this window of development in mice has clinical relevance for humans. As a surrogate for adulthood, PN80 in mice approximately corresponds to 50 years of age[44, 54].

Large Experimental Animals

Although, non-human primates are the gold standard for animal to human comparisons, they only account for 0.5% of all current biomedical research[55]. Scientists only use non-human primates when no other research model can provide the required information[55]. Only one study to date, conducted by Kuo *et. al.* has used an IUGR baboon model [30% global caloric reduction of pregnant mothers]. Researchers reported impaired diastolic and cardiac function in the IUGR offspring [n=16; 5.7±1.4 years old – human equivalent = ~25 years old] similar to normal healthy controls of a geriatric cohort [n=12; 15.9±2.6 years old], which led to their conclusion that IUGR increases the incidence of CVD[42].

The use of sheep as an experimental animal is more common but only accounts for less than 8% of all biomedical research. Sheep tend to be cited more in fetal development studies due to the advancement of successful survival rates of *in vivo* surgical techniques such as umbilicoplacental embolization inducing IUGR[56]. As a large animal model, sheep hold many similarities to humans, such as resting heart rate and blood pressure[43, 44]. Sheep are also approved as a pre-clinical animal model for CV research, however the infrastructure necessary for large animal husbandry has minimized the use of this experimental animal in biomedical research[56]. Sheep also lack the well-defined and reproducible genotype and phenotypical data available to researchers when compared to mice. Nevertheless, research groups within the DOHaD field have used sheep as an experimental animal to induce growth restriction[43-46, 57-61].

Louey *et. al.* showed that IUGR sheep have reduced heart growth through inhibition of cardiomyocyte development by about 70% when compared to healthy controls[46]. Thornburg *et. al.* showed growth restriction leads to cardiac reprogramming with reductions in heart size, and structure[4, 46], with smaller coronary arteries[62], vascular stiffness[60], fewer cardiomyocytes[44, 48, 50],

and endothelial dysfunction[63-65]. Current research by Morrison *et. al.* showed that maternal undernutrition in late gestation causes cardiac hypertrophy increasing insulin growth factor signaling [IGF2/IGF2R] and collagen deposition [COL1A1] in the right ventricle of the fetal sheep heart[66].

The use of swine as an experimental animal model in biomedical research has become more prominent over the last twenty years due to the many anatomic and physiologic similarities between pigs and humans[67, 68]. However, the use of swine in the DOHaD cardiac literature is less robust. Columbus *et. al.* using a restricted protein [RP] diet in 21 day old piglets revealed a 15.6% reduction in heart weight when compared to a high protein group [n=14-16; HP: 28.7±1.2g, RP: 24.2±1.1g, $p < 0.05$][69]. A major finding from this swine study was the reduction of tissue protein synthesis in all skeletal muscles analyzed in the RP compared to the HP [High Protein] group, however cardiac tissue protein synthesis was not reported[69]. In relation to cardiac function, Bauer *et. al.* showed that SV, Q, MAP, & TPR of newborn [13-25 hours old] IUGR piglets [n=15] was similar to normal weight piglets [n=15], while only heart rate was slightly increased [$p<0.05$] in the IUGR piglets[70]. This study only collected data on newly born piglets and reported minor cardiac differences using retrograde cannulation of the LV between normal weight and IUGR piglets, perhaps echo-electrocardiography in early life and again in adulthood would have exposed greater differences between groups.

Most large animal research involving growth restriction is focused on IUGR, while growth restriction in postnatal development has used smaller animals for experimental research. As such, growth restriction of rodents, specifically during the postnatal window will be discussed.

Small Experimental Animals

Rats and mice belong to the same taxonomic order [Rodentia] and family [Muridae][71]. The use of rodents [*Mus musculus* and *Rattus norvegicus*] account for approximately 90% of all biomedical research, while the mouse alone accounts for ~59% of all laboratory animals used[72]. Typically, behavioral research uses rats where cognition and learning are variables of interest, and genetic studies use mice[71]. Since DOHaD proposes hypotheses across the lifespan it is necessary to use a model that has an accelerated aging timeline compared to humans [average life expectancy; mouse: ~1.5-2 years vs. rat: ~2.5-3 years][73]. Mice are easily accessible, cost-effective, and have 99% of the same DNA as humans, while rats have only ~95% similarity[72, 74]. Additionally, inbred mouse strains are genetically homologous to one another, which reduces genetic variance. Mice also have a much larger reproducible genotype and phenotype database available to researchers, when compared to rats.

Of the rodent growth restriction research available, much of the research is on delayed/impaired cardiomyocyte development. Drenckhahn *et. al.* as well as others, have shown that growth restriction changes rat and mouse cardiac morphology and cardiomyocyte proliferation causing the heart to develop in a more circular and less spherical shape, with more mononucleated cardiomyocytes[48, 50, 51, 75, 76].

Furthermore, Ferguson *et. al.* showed that postnatal growth restriction, reduced cardiac size and function[48]. In this study, the growth restricted mouse group had resting diastolic impairment from a decrease in heart size through differences in cardiomyocyte nucleation[48]. The binucleated cardiomyocytes that experienced postnatal growth restriction showed impaired Ca^{2+} flux with more spontaneous Ca^{2+} spikes when stimulated with isoproterenol. This finding suggests that postnatally growth restricted mouse hearts may have an increased risk of cardiac

arrhythmias in adulthood. Ferguson *et. al.* also determined that the exercise capacity of the growth restricted females was impaired through reductions in total work [joules], maximal work [joules/min], and VO_{2max} [mL/min]. Following this study, Pendergrast *et. al.* established that growth restriction [IUGR and Postnatal] reduced LV mass with diminished anterior and posterior wall thicknesses, while reductions in stroke volume were isolated to the postnatally growth restricted mouse hearts[77].

Growth Restriction and Cardiac Metabolism

Wang *et. al*. showed IUGR was associated with increased expression of GLUT-1 in sheep hearts, suggesting increased reliance on cardiac glucose metabolism[61]. Wang *et. al.*, demonstrated that when Akt is phosphorylated there are adverse effects on cardiac insulin growth factors [Igf] and angiotensin I receptors [At_1][78]. These modifications stimulate cardiomyocyte apoptosis and a reversal of cardiac metabolism back to a fetal phenotype, where glucose and lactate are the primary substrates for energy production [ATP]. This mechanism, commonly seen in heart failure patients, is an insufficient attempt to use glycolysis, generate contractile force, and maintain systolic pressure. Wang *et. al.* postulated this metabolic reversal may impair pyruvate conversion and diminish ATP production from glucose, through the inhibition of pyruvate dehydrogenase[61]. Continuing, researchers stated the metabolic reversal leads to the increased risk of adult CVD in persons born with low birth weight, possibly through an increased reliance on glycolysis as opposed to fatty acid oxidation [FAO] in the heart. Although this mechanism seems biologically plausible, Wang *et. al.* never measured mitochondrial respiration or enzymes associated with glycolysis or FAO cycles. Additionally, only IUGR groups were studied without consideration to the postnatal environment, therefore a gap in the DOHaD cardiac literature exists.

To our knowledge, only one paper has implemented an *in-utero* nutritive model to examine cardiac metabolism through high resolution respirometry in growth restricted mice[79]. Beauchamp *et. al.* showed the adverse influence of a low-calorie diet [50% caloric reduction] during gestation on adult offspring with impairments to cardiac energy metabolism and hypothesized that this may have long-term consequences for CV function and disease in adulthood. The study reported reductions in FAO in the presence of octanoylcarnitine in adulthood but did not obtain respirometry data during early development. Impaired FAO metabolism in the heart is commonly associated with cardiac impairments, cardiomyopathies, and even heart failure[80-86].

The study conducted by Beauchamp *et. al.* was innovative; however, it has limitations. Firstly, only female mice were used and sex differences between control and growth restricted mice remain unknown when using HRR. Secondly, the nutritive model used to induce growth restriction by reducing kcals to the pregnant dams is substandard to an isocaloric LP diet, and does not significantly alter fetal nutritional status[87]. By choosing the substrate of octanoylcarnitine for FAO, Beauchamp *et. al.* disregarded literature stating HRR experimentation should use palmitoylcarnitine+malate when investigating FAO to prevent feedforward inhibition[83, 88, 89]. Continuing, Beauchamp *et. al.* used whole cell, left ventricular cardiac tissue homogenate standardized to citrate synthase, rather than using isolated purified mitochondria[90-93]. The use of isolated organelles is generally favored over intact cells for the study of molecular mechanisms, since there is no interference from cytosolic factors[94]. Therefore, it remains unknown if isolated mitochondria have reduced respirometry rates in the postnatally growth restricted mouse heart.

Beauchamp *et. al.* speculated that the observed differences in respiration may be due to the functional activity of the ETC complexes, since the ETC protein abundance was unchanged between controls and in-utero undernourished groups. Future work should fuel isolated cardiac mitochondria with substrates targeting specific complexes of the ETC and measure JO_2 through HRR instrumentation. Additionally, since Beauchamp *et. al.* only used adult offspring [PN98] of IUGR dams for HRR, the time-course of metabolic impairment from early life growth restriction is largely unknown. Future research should also take measurements during development [PN22] and adulthood [PN80] to make comparisons between groups across the lifespan.

In conclusion, growth restriction is detrimental in humans and experimental animals. Most of the research has been conducted using animal models of IUGR rather than postnatal growth restriction. Additionally, implementing an experimental research design to cause growth restriction cannot be ethically justified for human participants. The use of laboratory animals, especially mice, allow for novel insights into the developmental programming of CVD through the aging process[72, 73]. Mechanistic work in the gestational environment has mostly been accomplished, but little has been done using postnatal exposures of growth restriction. Therefore, the influence of postnatal growth restriction on key components [electrical activity, proteome, and metabolism] of cardiac function is necessary to lay the foundation for evidence-based practices to counteract CVD.

Literature Supporting Methodology Used in this Dissertation

To satisfy the overall objective of this dissertation, methods were used to study the effects of postnatal growth restriction on three key components to cardiac function. Firstly, the electrical conductance system which allows for the heart to contract as a functional syncytium. The aim of this study was to determine if postnatal growth restriction induces cardiac

arrhythmogenesis at rest and/or when pharmacologically stressed with dobutamine in adulthood. We hypothesized that arrhythmias will be present in the mice exposed to postnatal growth restriction, but not un-restricted controls. Secondly, an altered cardiac proteome from postnatal growth restriction may lead to functional impairments. The aim of this study was to determine proteomic differences caused by postnatal growth restriction, with a hypothesis that the restricted mice will exhibit key proteomic differences from controls, leading to impaired cardiac function in adulthood. Lastly, altered cardiac metabolism in IUGR leads to an increased risk for CVD, therefore evaluation during the postnatal environment is needed. The goal of this study was to determine if cardiac mitochondria of the postnatally growth restricted mice are impaired during juvenile development [22 days old] and adulthood [80 days old]. We hypothesize that the postnatally growth restricted mitochondria will have substrate specific reductions in oxygen flux at both time points.

DOHaD researchers have established methods to achieve intrauterine and/or postnatal growth restriction using the above-mentioned experimental animals. As such, these developmental windows and their differing methodologies will be discussed in further detail. After which, a discussion specific to the methods used in this dissertation will occur.

Intrauterine Growth Restriction [IUGR]

Methods used to induce placental insufficiency and subsequently IUGR vary considerably, including genetic models of impaired placental function[95], uteroplacental embolization[57], and the most common placental artery ligation[96, 97]. Briefly, during placental artery ligation, the animal is placed under anesthesia until unresponsive, and then an incision made to the abdominal wall. Next, a silastic tube or suture is placed around the uterine artery forming a cuff which reduces or occludes blood flow and presumably nutrition to the fetus[97].

This methodology has been shown to reduce birth weights and growth rates of the fetus, as well as impair the development of several organs including the brain, liver, lungs, kidney, and the heart[97].

Although effective, limitations exist when using this method with small animals including the invasive nature of surgery[98], increased risk of fetal loss[96], and a fetal hypoxic environment. The hypoxic environment causes reduced oxygen delivery and hemodynamic compromise[99]. Placental arterial ligation modifies animal physiology differently from postnatal growth restriction and leaves a knowledge gap in the literature since researchers are unable to control for the effects of hypoxemia[6, 46, 48, 59]. Therefore, determination of how undernutrition alters cardiac structure and function leading to impairments is unclear when using this method.

Postnatal Growth Restriction

Evidence shows humans and animals experiencing postnatal undernutrition causing growth restriction during developmental in early life have an increased risk of developing CVD into adulthood[1-5, 7, 11, 13, 15, 19, 20, 31, 32, 100, 101]. However, much of the mechanistic work leading to CVD from postnatal growth restriction has not been completed. The neglect of the postnatal environment is surprising since much of the early epidemiological DOHaD literature analyzed weights at one year of age and studied infants who were separated from their primary caregivers after birth.

There are several methods to induce postnatal growth restriction including litter size manipulation[102], separation of dams and pups[103], nipple ligation[104], caloric restriction[79], and feeding dams a low protein [LP] diet[6, 48, 49]. In 1978, Crnic *et. al.* conducted a study comparing all five of the above methods. They concluded that maternal and fetal nutritional status was only affected in the methods using a LP diet[87]. Briefly, when using the low protein diet to induce

postnatal growth restriction typically dams are allowed free access [*ad libitum*] to a diet which is similar to the normal control diet [20% protein] except that all but 8% of the casein is substituted for cornstarch[6]. Dams consuming the LP diet produced ~15-20% less milk; therefore, pups suckling from these dams become growth restricted. Furthermore, the control diet [3853.9 kcal] and LP diet [3867.5 kcal] should be isocaloric and contain the same amount of soybean oil as the only source of fat. The isocaloric LP diet is a reliable technique to induce growth restriction during postnatal development[87, 102, 103, 105, 106].

Electrocardiography

Augustus D. Waller first pioneered the electrocardiogram [ECG] in 1887, and then in 1903, Willem Einthoven used the ECG to identify heart conditions[107-109]. Today, the ECG is one of the most prevalent diagnostic instruments in CV medicine[108]. ECG monitoring allows for the evaluation and origin of all electrical activity in the heart. Researchers and physicians can use the ECG to diagnose and treat arrhythmias, infarctions, electrolyte imbalances, and even drug toxicity[107].

ECG in rodents was first implemented by Dr. Alberto Golbarg in 1968 and today is a commonly used experimental method in CV research[110, 111]. There are several different methods to capture an ECG of the rodent heart [tethered ECG, implanted ECG, or pulse oximetry], however the non-invasive ECG system is advantageous for short term monitoring of several mice, and preferred when pharmacological interventions are used[112]. Based upon this rationale, the non-invasive ECG method is ideal for this dissertation. Briefly, the non-invasive ECG allows an anesthetized mouse to be placed upon a heated platform, embedded with paw-sized electrodes, capturing leads I, II, and III. The electrical signals are recorded for no longer than 10

minutes and then stored for offline analysis using arrhythmia waveform detection software, such as EMKA [Paris, France].

To our knowledge no researchers have implemented the use of ECG in the postnatally growth restricted mouse heart to analyze cardiac function and possible arrhythmogenesis. This is unexpected since the ECG is commonly used in other biomedical fields to describe global CV function[111, 113-115]. By implementing the use of ECG technology in this dissertation, we will be able to determine if postnatal growth restriction increases the occurrence of cardiac arrhythmias at rest or when pharmaceutically "stressed" with dobutamine in adult mice.

Two-Dimensional Differential in Gel Electrophoresis [2D DIGE]

2D DIGE coupled with mass spectroscopy is a reliable and valid technique to identify global proteomic differences[116, 117]. Established in 1975 by Klose *et. al.*[118], 2D DIGE remains a valid technique to study the proteome of a biological system[119, 120]. The results from 2D DIGE can provide the mechanistic groundwork to develop evidence-based practices to treat chronic diseases, including CVD. Thus, 2D DIGE analysis can reveal the signaling pathways associated with postnatal growth restriction that may have previously been unobserved in the DOHaD literature.

When compared to a standard polyacrylamide gel electrophoresis [PAGE], 2D DIGE has greater quantitative capacity, reproducibility, and accuracy of detecting differential protein abundance[121]. Briefly, the 2D DIGE system fluorescently labels experimental samples and allows for the separation of up to three fluorescently labeled protein samples [Cy2, Cy3, and Cy5]. Control samples are labeled with Cy3, experimental/treated proteins samples are labeled with Cy5, and a pool of all samples are labeled with Cy2. The Cy2 labeled samples act as an internal standard whereby all gels can be normalized, resulting in reproducible comparisons of

protein abundance between all gels[122]. This method of fluorescently labeling samples is frequently mentioned in the literature as the "three-dye" methodology of 2D DIGE[123].

Following the separation of fluorescently labeled proteins, gels are scanned, viewed, and differences in protein abundance along with the magnitude of abundance [average ratio] is quantified. Briefly, numerical data for individual spots detected through DeCyder Software are automatically calculated and compared based upon the volume [sum of pixel intensity], area [spot radius covered], peak height [pixel value at the X, Y position of the spot], and slope of the protein spot [gradient associated with the 3D attributes of a spot map pair]. The differential spots on the gels are robotically picked and then proteolytically digested in recombinant porcine trypsin [serine protease]. After the spots are removed and dissolved, they are dried in an Eppendorf tube via Speed-Vac. Peptides are then sequenced and identified through a process called nanoscale liquid chromatography coupled to tandem mass spectrometry [nano LC-MS/MS][124]. This technique has become a necessary tool in the proteomic field, and has benefits over traditional mass spectrometry[124], especially in circumstances yielding low sample volume, such as a juvenile growth restricted mouse heart [PN21]. Following protein identification through nano LC-MS/MS, verification of detection is completed through bioinformatics software such as Scaffold [Proteome Software, Portland, OR].

Following protein identification further analysis is required. REACTOME is an open source, open access, manually curated, and peer-reviewed pathway database. It contains biological pathways including metabolism, signaling, transcription, apoptosis, and CVD etiology [125]. The database operates as a record of biological processes and as a device for determining functional relationships between proteins[125, 126]. There is a plethora of biomedical research that has used REACTOME for the elucidation of mechanisms associated with human disease,

including identifying biomarkers for cancer[127], renal disease[128], type II diabetes[129], and cardiac remodeling[130].

The STRING database [version 10.5] is used in proteomic literature as an instrument used to acquire a network of protein-protein interactions [PPI] [131-134]. STRING literature includes research on skeletal muscle[135], breast cancer[136], Alzheimer's disease[137], and coronary artery disease[138]. STRING includes known and predicted PPI's and was created by the Swiss Institute of Bioinformatics and the Novo Nordisk Foundation Center for Protein Research. The interaction networks from STRING are a useful output for a thorough understanding of the functional actions from identified proteins, and is capable of elucidating proteins for the development of mechanisms leading to disease[139]. Building a network of PPI's through STRING improves the elucidation of identified proteins from a global proteomic screening of the heart, such as 2D DIGE[131-134, 140].

Previous genetic and proteomic literature have used REACTOME and STRING databases together for the development of pathological disease mechanisms[141, 142]. Literature combining the two bioinformatics software include areas such as ischemic cardiomyopathy[143], hepatocellular carcinoma[144], and amyotrophic lateral sclerosis[145].

In summary, 2D DIGE coupled with nano LC-MS/MS followed with bioinformatics can identify differences in global proteomic abundance between samples. By using this methodology, it will help elucidate the proteins within the postnatally growth restricted heart that may impair cardiac function leading to CVD.

High-Resolution Respirometry [HRR]

Mitochondria fulfill several essential roles in energy metabolism, apoptosis signaling, and emission of reactive oxygen species [ROS] [91, 93, 146-151]. Impaired mitochondrial function is an underlying disease mechanism associated with many pathological states, including CVD[79, 83, 88, 89, 146, 148, 152-160].

The measurement of oxygen consumption in isolated mitochondrial samples was first established by Chance *et. al.* over 60 years ago[161, 162]. However, from 1994 to 2001, Gnaiger *et. al.* developed a more advanced, and reliable technique for respirometry experimentation [Oroboros Instruments, Innsbruck, Austria; Oxygraph 2k-HRR]. Today, the O2k HRR methodology to measure mitochondrial function is published in more than 1,700 peer reviewed journal articles and is considered the gold standard for respirometry experimentation. High-resolution respirometry [HRR] allows for quantitative evaluation of oxidative phosphorylation [OxPhos] using intact whole cell lysate or isolated mitochondria[163, 164]. The commonly referred to "oxygraph", uses an amperometric sensor to determine the oxygen consumption and concentration of samples in a 2 mL closed chamber in real-time. To assess mitochondrial function, substrates are injected into the closed chambers of the oxygraph targeting various complexes in the electron transport chain [ETC] and oxygen flux [JO_2] is detected and calculated using DATLAB software [Oroboros Instruments, Innsbruck, Austria].

The O2k HRR system has many advantages over previously used polarographic oxygen electrode devices, including the ability to detect respiratory rates in low-density mitochondrial samples [0.01 mg of mitochondrial protein]. Additionally, the O2k HRR system has two chambers alongside each other, making it ideal for the comparison of CON and PUN mitochondrial samples. However, mitochondrial function will deteriorate over time and

researchers should keep samples on ice using only freshly isolated mitochondria for about 6-8 hours.

In summary, by using the O2k HRR technology, we will be able to determine if postnatal growth restriction impairs mitochondrial function in the heart leading to CVD in adulthood. Additionally, by fueling cardiac mitochondria with various substrates, we will be able to determine the capacity and efficiency of OxPhos when electrons are diverted to different complexes of the growth restricted ETC.

Conclusion

The DOHaD hypothesis has evolved from early epidemiological correlations into a respected area of experimental research. The DOHaD research community can mitigate mortality rates from chronic disease that started in the perinatal environment. Previous literature is apparent; an adverse gestational environment causes negative physiological adaptations that endure across the lifespan causing several chronic diseases, including CVD. However, there are minimal evidence-based practices to counteract CVD progression from postnatal growth restriction, mainly due to the lack of information on the actual causes of heart disease during this developmental window. Impairments to cardiac function increase the risk for CVD[24, 165, 166]; therefore, determining how postnatal growth restriction influences cardiac function is of sound scientific basis. To address the overall aim regarding cardiac function and the gaps in the DOHaD literature outlined above, three hypothesis driven investigations were conducted to elucidate differences in the electrical activity, the cardiac proteome, and metabolic profile of the postnatally growth restricted heart. In order to gain novel insight, it is also essential to use an experimental animal model, such as the mouse, which has an accelerated aging phenotype compared to humans[73].

In conclusion, cardiac function is under-researched in the postnatally growth restricted window of development and deserves more attention through targeted CV research. Based upon the rationale presented, we propose that by determining how postnatal growth restriction alters cardiac function in the mouse heart, not only will significant knowledge gaps in the DOHaD literature become satisfied, but evidence based practices can be developed in the future to reduce mortality rates from postnatal growth restriction.

CHAPTER 3: POSTNATAL UNDERNUTRITION IN MICE CAUSES CARDIAC ARRHYTHMOGENESIS WHICH IS EXACERBATED WHEN PHARMACOLOGICALLY STRESSED

This chapter is a published scientific manuscript.

Visker JR, Ferguson DP. Journal of Developmental Origins of Health and Disease. 2018 August; 9[4]: 417-424

Abstract

Growth restriction caused by postnatal undernutrition increases risk for cardiovascular disease in adulthood with the potential to induce arrhythmogenesis. Thus, the purpose was to determine if undernutrition during development produced arrhythmias at rest and when stressed with dobutamine in adulthood. Mouse dams were fed [CON: 20% protein], or low protein [LP: 8%] diet prior to mating. A cross-fostering model was used where pups nursed by dams fed LP diet in early [EUN; Postnatal day [PN1]-10], late [LUN; PN11-21], and whole [PUN; 1-21] phases of postnatal life. Weaned pups were switched to CON diets for the remainder of the study [PN80]. At PN80, body composition [MRI], and quantitative ECG measurements were obtained under 1% isoflurane anesthesia. After baseline ECG, an IP injection [1.5µg/g body weight] of dobutamine was administered and ECG repeated. Undernutrition significantly [$P<0.05$] reduced body weight in LUN [22.68±0.88g] and PUN [19.96±0.32g] but not in CON [25.05±0.96g] and EUN [25.28±.9207g]. Fat-mass decreased in all groups compared to controls [CON: 8.00±1.2g, EUN: 6.32±0.65g, LUN: 5.11±1.1g, PUN: 3.90±0.25g]. Lean mass was only significantly reduced in PUN [CON: 17.99±.26g, EUN: 17.78±.39g, LUN: 17.34±.33g, PUN: 15.85±.28g]. Absolute heart-weights were significantly less from CON, with PUN having the smallest. ECG showed LUN had occurrences of atrial fibrillation; EUN had increases of 1st degree AV block upon stimulation, and PUN had increased risk for ventricular depolarization arrhythmias. CON did not display arrhythmias. Undernutrition in early life resulted in ventricular arrhythmias under stressed conditions, but undernutrition occurring in later postnatal life there is increased incidence of atrial arrhythmias.

Keywords: **Cardiovascular Arrhythmias, Developmental Origins of Health and Disease, Developmental Programming**

Introduction

Cardiovascular disease is one of the leading causes of death in the United States and incidence rates have been increasing throughout the past decade[167]. The literature has routinely showed that cardiovascular disease is a result of genetic predisposition, lack of physical activity engagement and a diet high in saturated fats[2, 4, 11, 31]. However, an emerging risk factor for cardiovascular impairment is growth restriction caused by early life nutrition. Professor David Barker championed the Developmental Origins of Health and Disease Hypothesis, which states that a brief period of malnutrition or growth restriction in early life will increase the likelihood of cardiovascular disease in adulthood[1, 2, 4, 11, 31, 168]. Yearly, 15 million babies worldwide will be born prematurely and/or experience growth delays due to poor postnatal nutrition. In fact, over 7,000,000 deaths per year is attributed to cardiovascular disease as a result of a suboptimal nutritional environment in early life. Yet, this topic is surprisingly under-researched in terms of mechanisms associated with cardiovascular disease development as a result of early life undernutrition[169].

Evidence has shown that those who suffered from undernutrition in the early formative years have modified cardiovascular development. This phenotype is represented in humans, mice, rats, sheep, pigs and cows[2, 4, 5, 11, 31, 101]. Mice that are undernourished early [EUN] in development [PN1 to PN11] exhibit less cardiomyocyte number and with the majority being mononucleated cardiomyocytes. While those undernourished later [LUN, PN11 to PN21] in life show the effects of impaired cardiomyocyte hypertrophy[4, 44, 46, 47, 54]. Thus, suboptimal nutrition during these different time points could have differential effects on function of the heart. Specifically, any adverse conditions experienced in the postnatal environment that lead to

cardiac reprogramming on heart size, heart structure, or Ca^{2+} management[44, 116, 170, 171] may be associated with increased likelihood of cardiac arrhythmias[8, 46, 172, 173].

The use of an electrocardiogram [ECG] as an imaging tool for cardiac impairment has been widely used in the clinical and research setting, with recent advancements leading to the development of ECGs designed to be used in a murine model[114, 174, 175]. Recent evidence from our lab and others[51, 176] has suggested that cardiac impairment as a result of early life undernutrition is quiescent during rest and pathological during times of stress. Thus, in order to evaluate cardiac health as a result of early life nutrition the heart must be evaluated during rest and when stressed. Dobutamine is a common adrenergic agent used to increase cardiac output[177-180]. Dobutamine acts on the Beta 1 receptors of the sympathetic nervous system to stimulate an increase in stroke volume by causing an inotropic effect on the heart, with a secondary response to increase heart rate and blood pressure[177, 179, 180]. A growing use for Dobutamine administration has been in the use of Pharmacological Stress Echocardiography [PSE] to observe cardiac function and diagnose CV disease[177, 179]. Pharmacological stress testing is an alternative method to dynamic exercise testing that when combined with noninvasive imaging allows for the detection of myocardial impairment[181]. Thus, we used pharmacological stress testing coupled with ECG analysis in mice that were undernourished during the early, late and whole period of postnatal development as a means to determine if early life nutrition predisposes mice for cardiac arrhythmogenesis.

Methods

All experiments were conducted according to the recommendations of the Guide for Care and Use of Laboratory Animals and were approved by the Institutional Animal Care and Use

Committee at Michigan State University. All animals were housed in the vivarium on wood-chip bedding in a single room maintained at 21°C with a 12 h light/dark cycle.

Nutritive Model

To induce postnatal undernutrition, we used methods previously described[49]. Briefly, second and third parity FVB [FVB/N; Charles River Laboratories, Wilmington, MA, USA] mouse dams were fed either a semi-purified control diet [20% protein; Research Diets, New Brunswick, NJ, USA] based on AIN93G, or a low-protein [LP] isocaloric diet [8% protein] beginning 1 week before mating. Table 3.1 displays the composition of the diets. These diets are casein, cornstarch and soybean oil and have been validated for rodent use during gestation, lactation, and early postnatal life. For a detailed review on the theoretical frame work for diet composition readers are directed to the work by Reeves *et al*, 1993[182]. Mating was timed by introducing males for a 24 h period; only pups born within the same 24 h period [postnatal day 0, PN0] were studied. On PN1 all pups born to dams on the control diet were pooled, and redistributed to one of two experimental groups: [1] *Control [CON]:* pups born to and suckled by well-nourished control dams and weaned to a control diet at weaning [PN21]; n = 16; [2] *Postnatal Undernutrition [PUN]:* pups born to well-nourished dams and suckled by dams fed the LP diet, then fed the control diet at weaning [PN21]. Mouse dams that are fed a low protein diet produce 15-20% less milk thus pups nursed by low protein dams will experience a global nutrient deficit and possibly a slightly greater deficit in protein intake[87, 103, 105, 106, 183, 184, 185]. In order to distinguish cardiac differences at different states of postnatal life we used a cross fostering model at PN10 to segregated postnatal undernutrition to the early phase of undernutrition [EUN; PN1-10; n=14 litters] and late phase of undernutrition [LUN; PN11-21; n=15 litters]. As displayed in Figure 3.1, at PN10 a sub cohort pups suckled to control dams

Table 3.1: Composition of control [CON] and low protein [LP] diets.

Diet	**Protein[gm]**	**Fat[gm]**	**Carbohydrate[gm]**	**Fiber[gm]**
CON	196.6	70	609.4	50
LP	80.6	70	728.8	60
	Protein[gm%]	**Fat[gm%]**	**Carbohydrate[gm%]**	**Fiber[gm%]**
CON	19.7	7	60.9	5
LP	8.1	7	73.1	6
	Protein[kcal]	**Fat[kcal]**	**Carbohydrate[kcal]**	**Total[kcal]**
CON	786.4	630	2437.5	3853.9
LP	322.2	630	2915.3	3867.5
	Protein[kcal%]	**Fat[kcal%]**	**Carbohydrate[kcal%]**	**Total[kcal%]**
CON	20	16	63	100
LP	8	16	75	100

Diets were casein and cornstarch based with soybean oil as the only source of fat. LP diet was achieved by replacing casein with additional cornstarch. The two diets contained the same amount of oil [70g], and the fatty acid profile [weight percentage of total fat] consists of palmitic [10.3], oleic [22.8], linoleic [51], and linolenic [6.8] acids.

were cross fostered to dams fed the low protein diet *[LUN]*. Additionally, at PN10 a sub cohort of pups suckled to dams fed the low protein diet were cross fostered to dams fed the control diet *[EUN]*. At PN21 all pups [CON, PUN, EUN, and LUN] were weaned and fed the control diet until electrocardiogram [ECG] measurement at PN80. Thus, at the time of measurement all mice were consuming a non-restrictive diet.

Each dam received seven pups [2–3 males and 4–5 females] and individual pups within a litter were identified with a unique tattoo. Females were only evaluated in this study, as work from our lab has shown that males did not display cardiac impairment as measured by treadmill testing, echocardiography and calcium flux of isolated cardiomyocytes and therefore it was hypothesized that they would not display cardiac arrhythmias[117]. Pups were allocated so that on

PN1, average pup weight for all groups was the same. Litter size was maintained constant throughout lactation by introducing 'donor' pups of similar bodyweight and age to replace any deaths; donor pups were not studied.

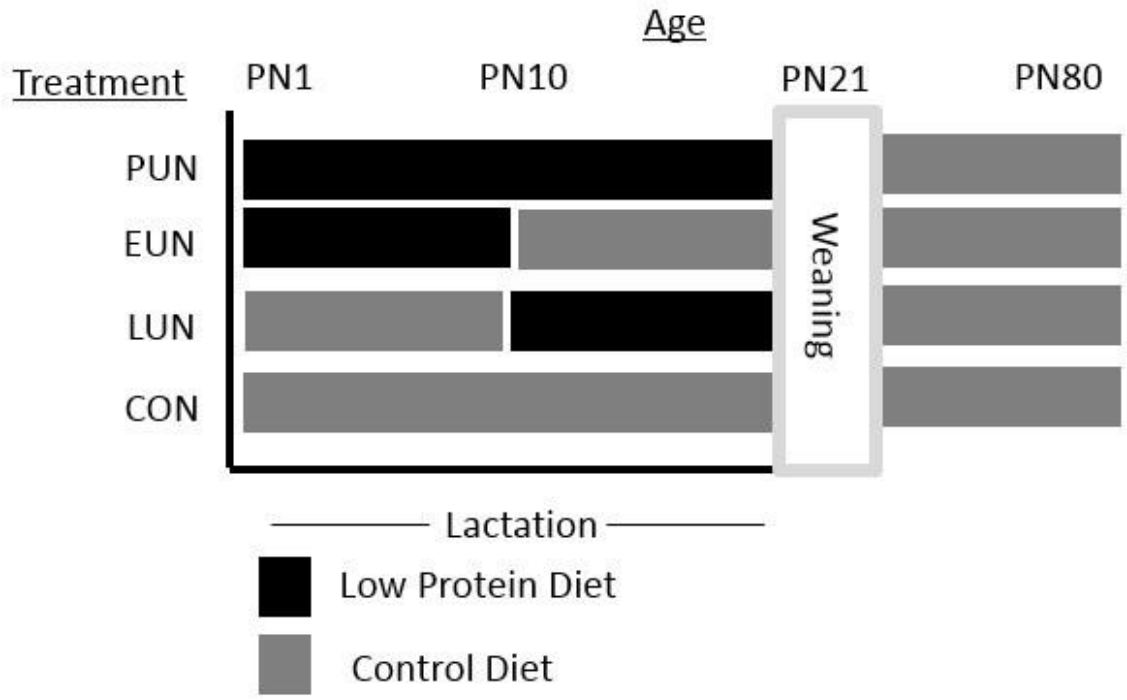

Figure 3.1: Cross-Fostering Model for Early Life Nutrition. Control Diet=20% protein, Low Protein Diet=8% protein. Both diets are isocaloric. Postnatal Undernutrition [PUN] refers to mice suckled to dams fed the LP diet from PN1-PN21. Early Phase of Undernutrition [EUN] refers to mice suckled to dams fed the LP diet from PN1-10, and then pups were cross fostered to dams fed the control diet from PN11-PN21. Late Phase of Undernutrition [LUN] refers to mice suckled to dams fed the CON diet from PN1-10; then cross fostered to dams fed the LP from PN11-PN21. Control Group [CON] refers to mice suckled to dams fed the CON diet PN1-21. At PN21 all pups were weaned from dams and fed the control diet.

Body Composition

At PN80 mice were weighed then fat mass and lean mass were measured by Quantitative Magnetic Resonance [EchoMRI, Houston, TX, USA][49]. Body composition was determined using the supplied software. Mice were then evaluated for cardiac function via electrocardiogram.

Electrocardiogram [ECG]

All tests were done with mice placed under 1% isoflurane anesthesia, with the mice on an ECG/heated board [EMKA, Paris, France] and the limbs taped to the four electrodes. Leads I, II, & III recordings were obtained for 5 minutes. The mouse was then administered an intraperitoneal injection of dobutamine [1.5 µg/g BW; Hospira, Lake Forest, IL, USA] and the measurements were repeated.

Electrocardiogram parameters that were obtained were heart rate [beats·min^{-1}], R-R interval [milliseconds], QRS duration [millisecond], ST Deflection [Volts], and QT duration [millisecond]. Only parameters found to be within established ranges were analyzed[113]. Shape based software [EMKA, Paris, France] was used to detect any change in morphology and presence of arrhythmia. These parameters have been indicated and validated in studies previously analyzing various heart diseases[43, 186, 187].

After completion of the studies, the mice were allowed to recover for 24 hours after which they were euthanized, and the hearts were dissected quantitatively and weighed. Heart weights are reported as absolute weight and as normalized for body surface area as calculated using Meeh's Formula[188].

Body Surface Area =9.662 x [body weight, g] $^{0.667}$

Evaluation of estrous cycle

A validated visual method to evaluate the stage of the estrous cycle was implemented as previously described[189]. Briefly, each mouse was held by the tail with the forepaws resting on a cage lid. Vaginal openings were then visually inspected and classified based on previous literature for stage of estrous cycle. Mice used in the study were within the follicular phase with low circulating estrogen levels.

Statistics

All data was analyzed in JMP v7.0 [SAS, Carey, NC]. Body composition and heart weight was analyzed by a One-way ANOVA with the main effects being diet [CON, EUN, LUN, and PUN].

Electrocardiogram parameters were analyzed with a two-way ANOVA with the main effects being diet [CON, EUN, LUN, and PUN] and treatment [Baseline or Dobutamine] and a Tukey's HSD post hoc test. An alpha level of 0.05 was set *a priori*.

Results

Body Composition and Heart Weight

Our nutritive model successfully induced growth restriction [Figure 3.2], as evident by a reduction [$P<0.05$] in body weight, in the PUN [19.96±0.32g] and LUN [22.68±0.88g] groups as compared to controls [25.05±0.96g] and EUN [25.28±0.92g]. In addition to having the lowest absolute weight the PUN mice had a significant [$P<0.05$] reduction in lean mass [15.85±0.28g] as compared to CON, EUN, and LUN. There was no difference in lean mass between CON [17.99±0.26g], EUN [17.78±0.39g], and LUN [17.34±0.33g]. Fat mass was greatest in the CON [8.00±1.2g] group followed by EUN [6.32±0.65g], LUN [5.11±1.1g], & PUN [3.90±0.25g], each group was significantly different [$P<0.05$] from the other.

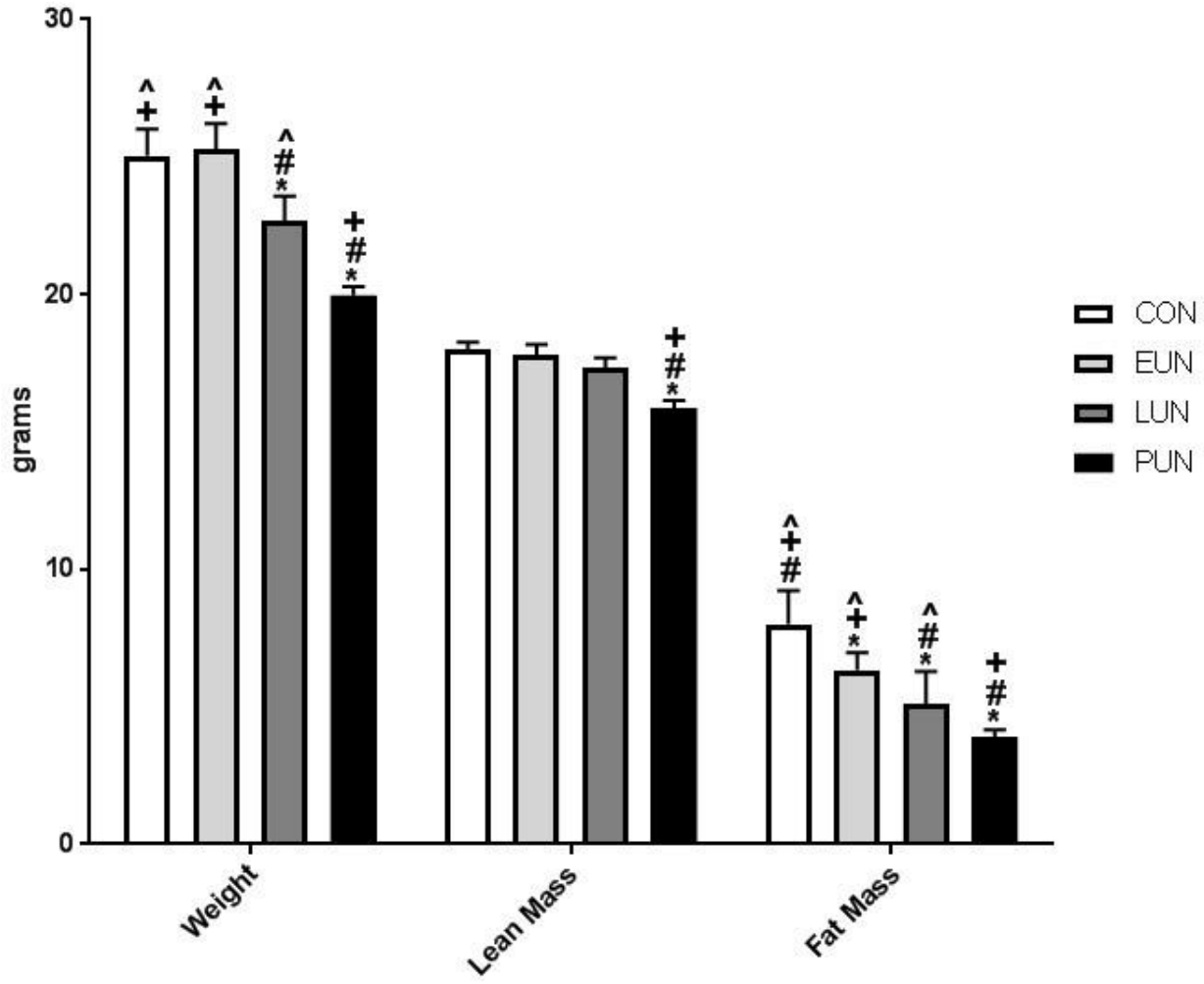

Figure 3.2: Body Weight and Composition at PN80. Mice were undernourished during early [EUN], late [LUN], and throughout [PUN] lactation phase alongside the control [CON] group. Weight was significantly decreased in the LUN, & PUN groups compared to CON, & EUN. Lean Mass was significantly decreased in the PUN group only. Fat mass was significantly different between all groups. *: significantly different from control; #: significantly different from EUN; +: significantly different from LUN; ^: significantly different from PUN. $P<0.05$ values are mean ± SE.

The absolute heart weight of the CON group [0.118±0.005 g] was significantly [$P<0.001$] higher than the EUN [0.103±0.002 g], LUN [0.103±0.004 g], and the PUN group [0.094±0.001 g]; with the PUN group being significantly less than the three other groups. There was no difference between the EUN and LUN absolute heart weights [Figure 3.3B].

When comparing heart weight [standardized to body surface area], amongst the four nutritive groups the only significant decrease in heart weight was the EUN group [1.288±.0.031kg/cm^2] as compared to CON [1.405±0.089kg/cm^2], LUN [1.350±0.040kg/cm^2] and PUN [1.342±0.031kg/cm^2] [P<0.05, Figure 3.3A].

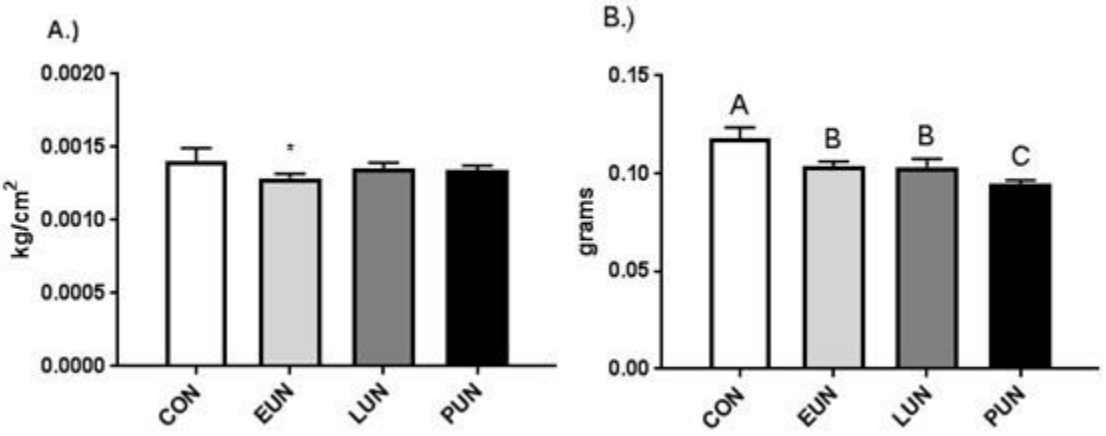

Figure 3.3: Heart Weight at PN80 [standardized and absolute]. A.] Heart Weight [standardized to body surface area]: Mice were undernourished during early [EUN], late [LUN], and throughout [PUN] lactation alongside the control [CON] group. *: The EUN group had a significantly decreased heart weight as compared to the CON group [P<0.05, values are mean ± SE]. **B.] Absolute Heart Weight:** The control group had a higher heart weight than the other treatment groups with the PUN group being significantly less than the CON, EUN and LUN group [P <0.001]. The EUN and LUN groups were not significantly different from each other [values are mean ± SE; different letters indicate significant difference].

Electrocardiogram [ECG]

Table 3.2 displays the results obtained from the ECG analysis for mice that were undernourished during critical periods of development along with the response to dobutamine treatment.

Table 3.2: Electrocardiogram parameters for mice that were undernourished during the early, late, and whole phase of lactation along with a control group with and without stimulation of Dobutamine.

Group	Treatment	Heart Rate [BPM]	R R Interval [ms]	QRS Duration [ms]	S T Deflection [V]	Q T Duration [ms]
CON	Baseline	534.3 ± 68.7	114.1 ± 15.5	34.5 ± 2.4	-0.085± 0.1	62.4 ± 4.2
	Dobutamine	488.7 ± 30.4*	123.2 ± 7.8*	37.7 ± 3.5*	-0.085 ± 0.04	70.3 ± 5.3*
EUN	Baseline	556.9 ± 29.4	108.1 ± 6.2	32.0 ± 2.6	-0.062 ± 0.05	60.2 ± 5.6
	Dobutamine	501.6 ± 34.6*	120.4 ± 8.6*	36.9 ± 2.5*	-0.088 ± 0.07	72.8 ± 3.5*
LUN	Baseline	551.6 ± 59.5	110.1 ± 12.7	31.0 ± 2.9	-0.09 ± 0.06	62.8 ± 5.1
	Dobutamine	526.3 ± 54.3*	115.2 ± 19.3*	35.3 ± 4.2*	-0.12 ± 0.04	77.2 ± 5.3*
PUN	Baseline	534.8 ± 68.4	114.2 ± 15.2	33.0 ± 3.4	-0.081 ± 0.07	64.7 ± 6.4
	Dobutamine	528.3 ± 18.2	113.7 ± 4.0*	39.1 ± 3.4*	-0.11 ± 0.04	80.1 ± 6.3*

ECG parameters obtained from Lead II on CON, PUN, EUN, and LUN groups at Baseline and following Dobutamine treatment. * denotes a significant [P<0.05] change from baseline measurement to dobutamine treatment.

Baseline Measurements:

The heart rate [HR] of the CON group was 534.3±68.7 beats·min ^{1}. The EUN group displayed HR values of 556.9±29.4 beats·min^{-1}, while the PUN and LUN baseline groups HR was 534.8±68.4 beats·min^{-1} and 551.6±59.5 beats·min^{-1}, respectively. There was no difference [P>0.05] in baseline HR values between the groups. As RR interval is closely associated with heart rate there was also no difference in RR intervals [P>0.05] between the groups [CON RR interval 114.1±15.5 ms; EUN 108.1±6.2 ms; LUN 125.0±15.2 ms; PUN 114.2±15.2 ms].

Electrical function of the ventricles at baseline showed that there was no difference [P>0.05] in QRS duration between the four groups [CON 34.5±2.4 ms; EUN 32.0±2.6 ms, LUN 31.0±2.9 ms; PUN 33.0±3.4 ms]. There was no significant [P>0.05] difference in QT Duration between any of the groups at baseline [CON QT duration 62.4±4.2 ms; EUN 60.2±5.6; ms; LUN 62.8±5.1 ms; PUN 64.7±6.4 ms]. Additionally, ST Deflection at baseline was not significantly different [P>0.05] between the diet groups [CON -0.085±0.1 V; EUN -0.062±0.05 V; LUN -0.090±0.06; PUN -0.081±0.07].

Dobutamine Treatment:

Heart rate [HR] had a blunted decrease [P=0.0132] in the PUN group with dobutamine treatment as compared to the other groups with a -1.2% change from baseline as compared to an -8.5% change in the CON mice, -9.9% change in the EUN, and -4.6% change in the LUN. Corresponding to the heart rate the RR interval response with dobutamine treatment significantly increased [P<0.001] in all groups. The PUN group had a 38% change in RR interval from baseline [120.9±25.9 ms] to dobutamine stimulation [166.9±22.6 ms]. In comparison, the CON group had 11% change from baseline [123.9±6.1 ms] to dobutamine stimulation [137.6±5.4 ms]. Treatment with dobutamine also significantly increased the QRS duration [P<0.001] for all groups. The PUN group had an 18.48% change from baseline [33.0±3.4 ms] to dobutamine stimulation [39.1±3.4 ms]. In opposition, the CON group had 9.2% change from baseline [34.5±2.4 ms] to dobutamine stimulation [37.7±3.5 ms]. The EUN and LUN groups recorded 15.3% [32.0±2.6 ms at baseline to 36.9±2.5 ms with dobutamine] and 13.8% change [31.0±2.9 ms at baseline to 35.3±4.2 ms with dobutamine] in QRS duration, respectively. As shown in Figure 3.4 a trending interaction effect [P=0.09] showed the PUN group had the longest QRS

duration [39.1±3.4 ms], as compared to the other groups [CON 37.7±3.5 ms; EUN 36.9±2.5 ms; LUN 35.3±4.2].

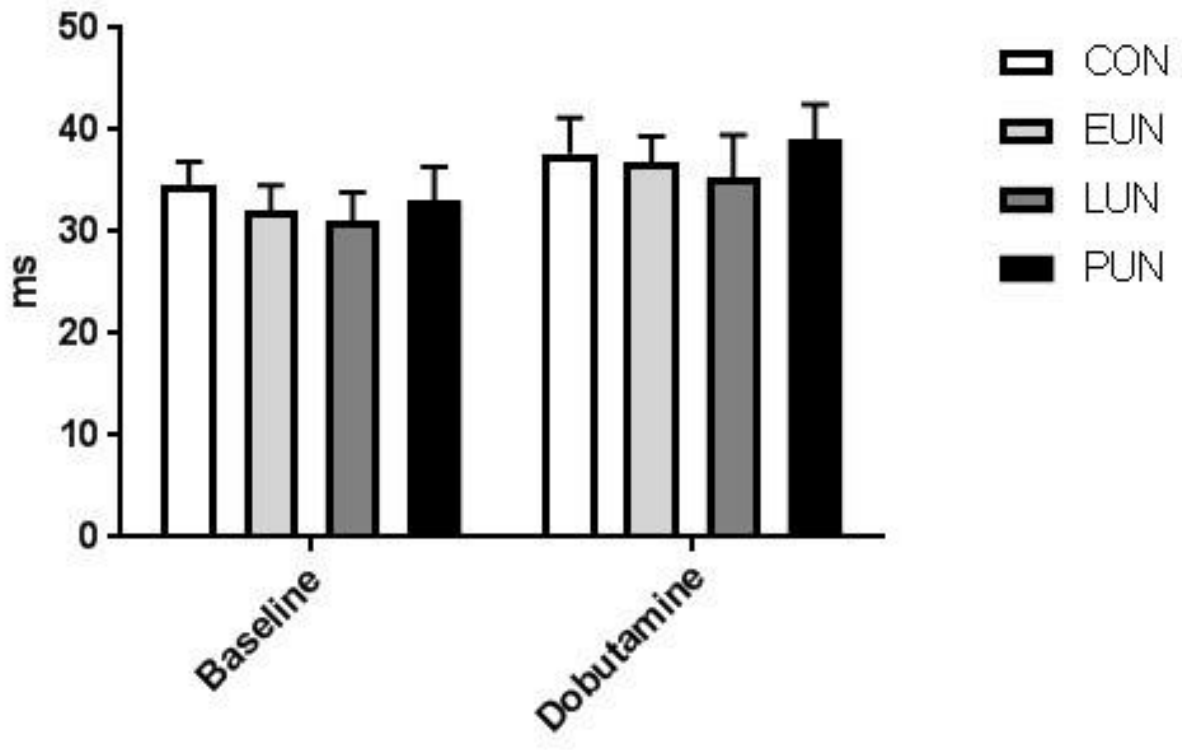

Figure 3.4: QRS duration from the ECG at baseline and with administration of dobutamine. A trend [P=0.09] for increased QRS duration was observed in the PUN group following dobutamine stimulation.

Dobutamine treatment had a significant [P=0.01] effect on QT duration [Figure 3.5] with the PUN [80.1±6.3 ms] and LUN [77.2±5.3 ms] groups having a longer QT duration as compared to CON [70.3±5.3 ms] and EUN [72.8±3.5 ms] groups with dobutamine treatment. There was no difference in ST deflection following dobutamine treatment [P>0.05].

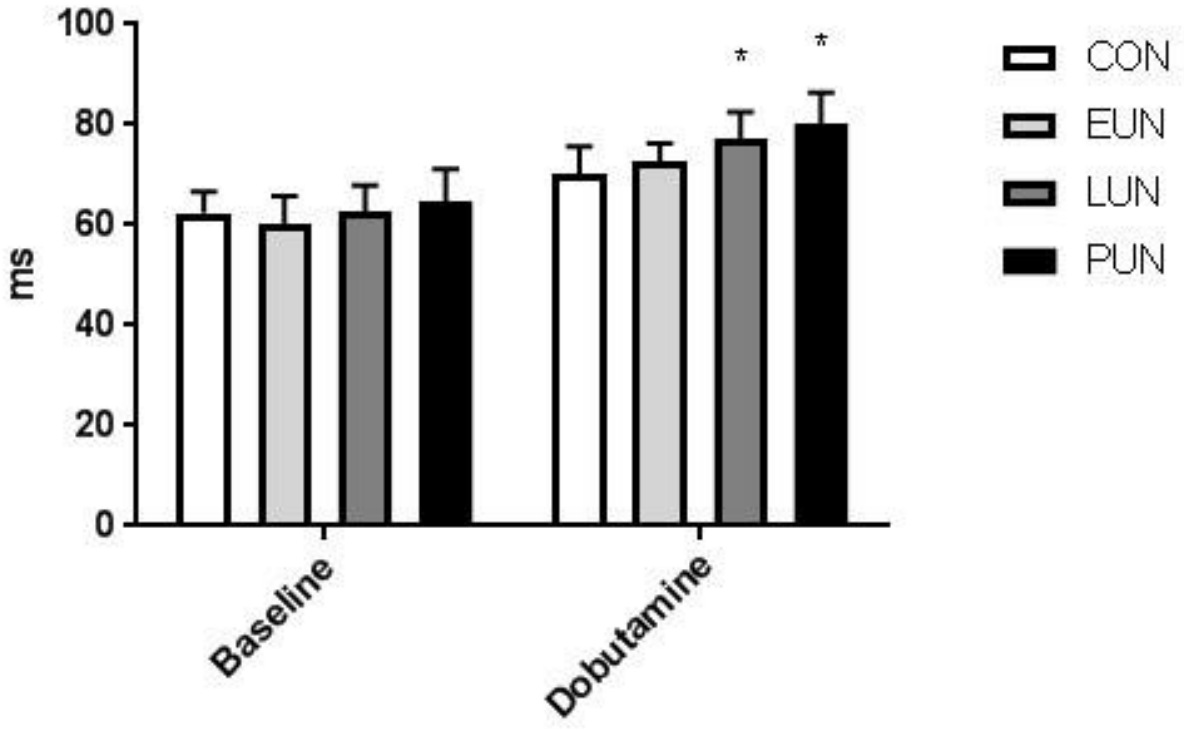

Figure 3.5: QT duration from the ECG at baseline and following administration of dobutamine. *Significant [P=0.01] difference in QT duration in PUN and LUN groups following dobutamine stimulation as compared to the CON and EUN group.

Shape Based Arrhythmia Detection:

There were three types of arrhythmias detected [Wide QRS Complex [25.0% of PUN Baseline, and 87.5% of PUN + Dobutamine], 1st degree AV Block [12.5% of EUN Baseline and 12.5% EUN + Dobutamine], and atrial flutter [EUN Baseline = 62.5%, EUN +Dobutamine = 25.0%, LUN Baseline = 62.5%, LUN + Dobutamine = 62.5%, PUN Baseline = 50.0%, and PUN + Dobutamine = 25.0%]. The control group did not present any arrhythmias at baseline or with dobutamine stimulation [Figure 3.6].

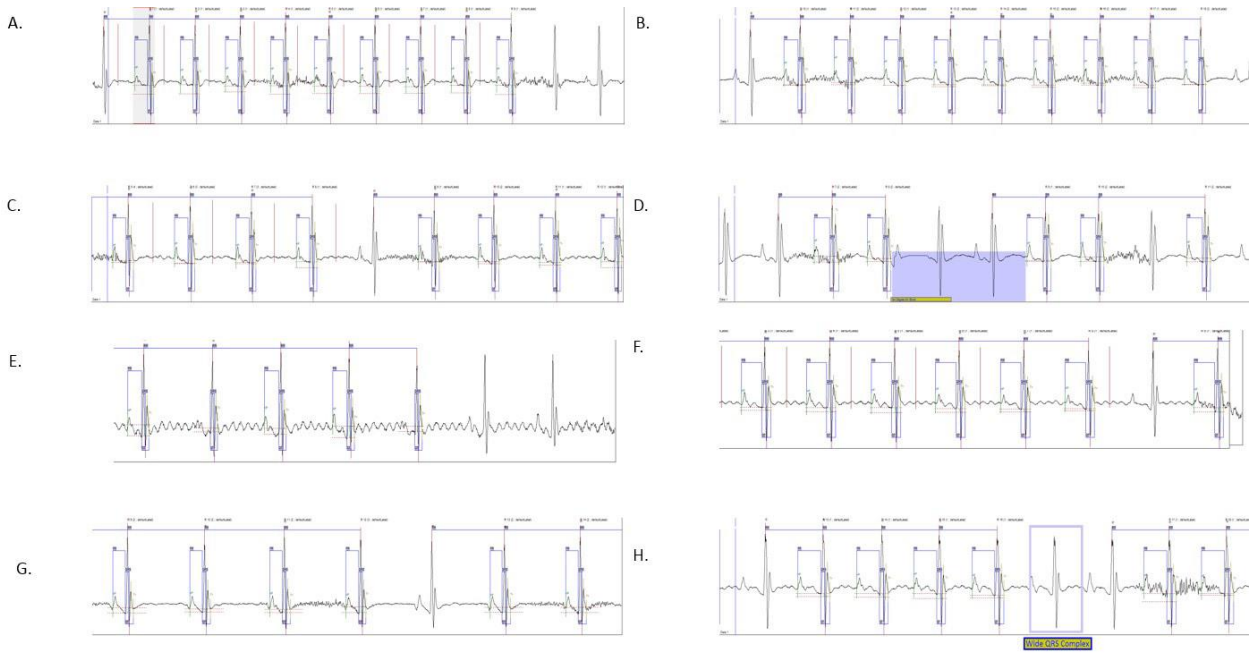

Figure 3.6: ECG rhythm strips collected from EMKA Technologies Software. A. CON group baseline measurement, with normal sinus rhythm. **B.** CON group + dobutamine treatment, no arrhythmias detected. **C.** EUN group baseline measurement, normal sinus rhythm with minimal artifact. **D.** EUN group + dobutamine treatment, software detection of 1st degree AV Block. **E.** LUN group baseline measurement reveals atrial flutter. **F.** LUN group + dobutamine treatment reveals atrial flutter. **G.** PUN group baseline measurement, no arrhythmias detected. **H.** PUN group + dobutamine treatment, Wide QRS complex detection.

Discussion

The Developmental Origins of Health and Disease [DOHaD] hypothesis states that growth restriction in neonatal life permanently effects the body's structure and function, in ways that may lead to chronic disease in adult life[1, 2, 11, 31]. Professor David Barker first championed this hypothesis and the resulting influence on cardiovascular disease over thirty years ago. Since then the literature has documented the effect of neonatal nutrition on growth rate, organ size, body composition, along with clinical relevance on insulin sensitivity and hypertension[5, 101, 190]. However, there is limited information on how undernutrition during various windows of postnatal life influences cardiac function. Thus, the purpose of this study was to determine if early life undernutrition during key windows of development produced alterations in the

depolarization and repolarization phases of the heart as measured by an ECG. Furthermore, we assessed the electrical activity of heart at rest and when pharmacologically stressed with dobutamine, to determine if cardiac functional impairment was quiescent when the mouse was not in a stressed state.

We evaluated three time points of postnatal undernutrition along with a control group. The EUN group experienced an initial deficit in nutrition from PN1-PN11, the LUN group undergoing undernutrition from PN11-PN21, and lastly, the PUN group enduring the lengthiest undernourishment period from PN1-PN21, while the CON group did not experience undernutrition. Following the period of undernutrition, the mice were nutritionally rehabilitated.

PN1-PN11 [EUN] is the cardiomyocyte proliferative phase of developmental in mice where mononucleated cells divide in order to increase cardiomyocyte number[46, 50]. During this period the electrical conductance system is continuing to mature as well[46, 50]. At the end of this period [PN7-10] cardiomyocytes undergo nuclear but not cellular division resulting in binucleated cardiomyocytes[46, 50]. The period of PN11-PN21 [LUN] is considered to be the hypertrophy phase of the cardiomyocytes, where the cells increase cross sectional area in order to produce contractile force to overcome afterload experienced by extra-uterine life[50]. Thus, any nutritional insult, during these periods of development will have a lifelong effect, on the structure and function of the heart.

Postnatal growth failure occurs in a considerable majority of extremely low birth weight infants[9, 106, 183]. Suboptimal nutrition during early life development has been shown to alter body composition including lean mass and increased adiposity[191]. Our nutritive model [Figure 3.1] produced changes in fat and lean mass dependent on the window of development. LUN and PUN mice weighed less than CON and EUN, indicating that EUN mice experienced catch up

growth, however the increase in body mass at PN80 was primarily due to an increase in fat mass [Figure 3.2]. The LUN group did not have increased fat deposition but displayed similar lean mass to the CON and EUN groups. The PUN group displayed a reduction in lean mass and fat mass as compared to the other groups. The PUN's inability to experience lean mass catch up growth could be due to a reduction in myogenic stem cell frequency[191]and a reduction in ribosomal abundance[49]. The combination of these impairments would reduce muscle protein synthesis and reduce lean mass over the life span.

One aspect to the clinical significance of developmental programming is that in addition to a reduction in body mass there can be organ specific growth restriction[192], as evident by the fact that the longer the nutrient restriction the smaller the absolute heart rate at PN80 [Figure 3B], however, when standardizing heart weight to body size the EUN group only displayed a significant impairment in heart weight [Figure 3.3A]. During PN1-10, when EUN was restricted, cardiomyocytes are proliferating thus undernutrition during that time period will reduce cell number and impair growth which cannot be recovered in the later phases of development with cardiomyocyte hypertrophy[51, 176].

As the reduction in heart mass was a result of cardiomyocyte impairment it was hypothesized that there would be an associated functional impairment, which could manifest in the atria and the ventricles.

Atrial Impairment:

Under adrenergic stimulation the EUN group developed 1st degree AV block representing a slow conduction velocity in the electrical impulse being sent from the sinoatrial node to the atrioventricular node. Previous studies using a murine model have shown that 1st degree AV

block will progress into 2nd degree AV block and left ventricular hypertrophy if hypertension is present[193]. The DOHaD literature has consistently shown that early life undernutrition leads to an increased incidence of hypertension[1, 2, 4, 11, 31]

When undernutrition was isolated to the hypertrophy phase of postnatal development [LUN] the ECG analysis revealed atrial flutter at rest and under beta adrenergic stimulation. Atrial flutter is a condition in which the electrical and contractile properties of the atria are impaired and disorganized[194]. Previous literature has hypothesized that atrial flutter and fibrillation are caused by remodeling of the cardiac tissue, causing the cells to become frail and fibrotic[195], with histological analysis of hearts from mice subjected to early life growth restriction having an increase in fibrotic tissue[51, 176], while we did not perform histological analysis on these hearts the manifestation of atrial flutter could be a result of fibrotic tissue present. The development of atrial flutter if gone untreated can potentially lead to an increased risk of atrial fibrillation and stroke due to the increased risk of blood clot formation in the atria[196-200]. It has been well documented in the literature that early life growth restriction increases the risk for stroke[47]. While the etiology of stroke risk from fetal origins may be independent of atrial fibrillation the fact that early life undernutrition also increases the risk of atrial flutter and fibrillation there is a further increase in the risk of stroke for individuals exposed to early life growth restriction.

It was observed in a small proportion of the EUN [3 mice] and PUN [2 mice] that with an injection of dobutamine there was atrial flutter withdrawal. A possible explanation for this is the dobutamine stimulation prolonged the refractory period and slowed the conduction velocity thus preventing re-entry back into atrial flutter, acting as an anti-arrhythmic drug[201].

Ventricular Impairment:

Ventricular arrhythmias are generally accepted to have more clinical significance than atrial, due to the increased mortality risk[202]. The PUN group presented with a healthy ECG tracing at baseline, however when stressed with dobutamine the PUN group displayed a widened QRS complex which represents a prolonged ventricular depolarization. We hypothesize that undernutrition in the late phase [PN11-21] of cardiomyocyte development impaired ventricular conduction as both the PUN and LUN groups had significantly longer QT durations when stimulated with dobutamine indicating a lengthened ventricular repolarization.

We did potentially observe a clinical condition in our PUN and LUN mice, termed long QT syndrome [Figure 3.5]. The pathology of long QT syndrome is characterized by impairment in ventricular repolarization leading to sudden cardiac death. The long QT syndrome is a family of arrhythmic disorders caused by dysfunction in one of 13 different ion channel complex proteins, including calcium, sodium, and potassium channels[203]. During the hypertrophy phase of cardiomyocyte development the sarcoplasmic reticulum matures in order to optimize calcium flux during depolarization[204], thus early life nutrition during this phase could increase the risk of sudden cardiac death syndrome.

In conclusion, these findings suggest that undernourishment during the various phases [EUN, LUN, and PUN] of cardiomyocyte development causes functional and structural impairment. Most notably functional impairment only arose when the heart was stressed. Furthermore, our data indicates that undernutrition during these distinct windows of development results in specific arrhythmias present in adulthood. It was hypothesized that any arrhythmias present in the PUN group would be a combination of arrhythmias present in the EUN and LUN group. As this was not observed in our data, perhaps there is a mechanistic cascade associated

with timing of re-feed that result in the PUN group being different from EUN and LUN and not simply a combination of the two.

Acknowledgements: The authors wish to thank Dr. Daniel Columbus from the Prairie Swine Research Center.

Disclosures: None

CHAPTER 4: POSTNATAL GROWTH RESTRICTION IN MICE ALTERS CARDIAC PROTEIN ABUNDANCE LEADING TO IMPAIRMENT IN ADULTHOOD.

Abstract

Postnatal growth restriction increases the risk for cardiovascular disease in adulthood, yet there is minimal mechanistic rationale for the observed pathology. The purpose of this study was to identify proteomic differences between postnatally growth restricted and unrestricted mice, and propose potential mechanisms related to cardiac impairment in adulthood. FVB mouse dams were fed a control [CON: 20% protein], or a low protein [LP: 8% protein] isocaloric diet 2 weeks before mating. LP dams produce 15-20% less milk inducing growth restriction. At birth postnatal [PN1], pups born to dams fed the CON diet were cross fostered to LP dams [PUN; postnatally undernourished] or a different CON dam [control]. At PN21, a sub-cohort of CON [n=3 males; n=3 females] and PUN [n=3 males; n=3 females] mice were euthanized and their heart proteome analyzed by two-dimensional differential in-gel electrophoresis [2D DIGE] and mass spectroscopy. Western blotting and silver nitrate staining was used as confirmation for 2D DIGE findings. Remaining littermates [CON; n=4 males; n=4 females and PUN; n=4 males; n=4 females] were weaned to the CON diet. At PN77, echocardiography and Doppler blood flow analysis measured cardiac function. At PN80, mice were euthanized, and hearts removed for western blotting to determine if proteomic differences at PN21 persisted into adulthood. 2D DIGE revealed a significant reduction in 12 possible proteins from 6 of 2,187 gel spots. 2D DIGE indicated PUN mice had a reduction in Prdx6, Ttn, Arhga29, Cdkn1c [$p57^{kip2}$], Sltm, Xpo5, Patj, Col1a1, Setd2, Col4a5, Col3a1, and Dnah1 relative to CON mice. $p57^{kip2}$, Ttn, and collagen proteins were confirmed with western blotting and silver nitrate staining, respectfully. At PN77, PUN mice had impaired diastolic and global cardiac function. At PN80, western blots of $p57^{kip2}$ showed that protein abundance was recuperated from PN21. However, PN80 silver nitrate staining of large molecular weight proteins [Ttn, and Collagen fibers] was reduced in growth restricted hearts. Therefore, growth restriction reduces cardiac protein abundance at

PN21 leading to cardiac impairment in adulthood indicating that programing in early life has lasting consequences.

Introduction

Growth restriction caused by early life undernutrition increases the incidence of non-communicable chronic disease in adulthood[1, 2, 4, 5, 11, 13, 31, 32, 100, 101]. In particular, early life growth restriction increases the risk of cardiovascular [CV] disease in adulthood by 47%[1, 2, 11, 27, 31, 32]. Alarmingly, even if growth is recuperated through re-feeding a healthy diet, CV morbidity remains indicating that nutritional status at key developmental windows programs cardiac function across the lifespan[2, 4, 6, 11, 31]. The clinical significance of developmental programming is evident by the fact that over 7 million CV deaths occur in adults who have suffered growth restriction, with an associated healthcare cost of $42.5 billion[2].

While there is considerable evidence on CV pathology due to intrauterine growth restriction[44, 52, 53, 205], there is far less on the dysfunction caused by postnatal growth restriction. From the evidence available, postnatal growth restriction in the mouse impairs cardiac function due to a greater amount of mononucleated cardiomyocytes[4, 48], impaired calcium flux[48], stiffer ventricles leading to diastolic dysfunction[4], and increased cardiac arrhythmias[6] compared to non-growth restricted controls.

Despite the known CV pathology, there is limited information on the molecular mechanisms responsible for functional impairment, which hinders the development of therapeutic countermeasures to offset cardiac impairment. Two-dimensional differential in-gel electrophoresis [2D DIGE] coupled with mass spectroscopy is a reliable and valid technique to identify differences in global proteomic abundance allowing for the proposal of physiological

mechanisms[116, 117]. As such, we implemented a nutritive model to induce postnatal growth restriction in mice[6, 49] and exposed a cohort of mice to 2D DIGE and mass spectrometry to identify differences in cardiac protein abundance [confirmed with western blot, or silver nitrate staining]. We then used validated bioinformatic software to construct mechanistic pathways describing how postnatal growth restriction influences cardiac development and function. The remaining cohort of mice were weaned to a healthy control diet until adulthood. At PN77, echocardiography and Doppler blood flow analysis assessed cardiac function. At PN80, western blotting and silver nitrate staining measured protein abundance in adulthood to see if the protein signatures at PN21 were recovered or persisted into adulthood.

Methods

All experiments were conducted in accordance with the Guide for the Care and Use of Laboratory Animals and were approved by the Institutional Animal Care and Use Committee at Michigan State University. Animals were housed in a climate-controlled vivarium, in a single room maintained at 21°C with a 12-hour light/dark cycle, on wood-chip bedding, and provided food *ad libitum*.

Nutritive Model

Postnatal growth restriction was induced using diet manipulation[49] [Figure 4.1]. Briefly, third parity FVB [Charles River Laboratories, Wilmington, MA, USA] dams were fed a semi-purified control diet [20% protein; Research Diets, New Brunswick, NJ, USA] based on AIN93G, or a low-protein [LP; 8% protein] isocaloric diet two weeks prior to mating [the composition of the diets has previously been described[6]]. To ensure all pups were born the same age, breeding was conducted by placing one male in a female cage for only 24-hours. At

postnatal day [PN] 1, all pups born to females fed the LP diet were euthanized. Pups born to control fed dams were combined and distributed to either: *1] Control Group [CON]:* pups born to a control dam then cross-fostered to a different control dam; *2] Postnatal Undernutrition Group [PUN]:* pups born to a control dam then cross-fostered to a LP fed dam. Dams that consume a LP diet produce 15-20% less milk compared to controls[87, 103, 105, 106, 183, 184], resulting in pups having an 18% reduction in caloric consumption and undergoing postnatal growth restriction[87, 103, 105, 106, 183, 184].

All experimental litters were standardized to equal size, sex ratio, and body mass. Each dam received 8 pups [4 males, 4 females] and individual pups within a litter were given a tattoo identification. Litter size was maintained during lactation with the addition of donor pups of comparable age to replace any natural deaths; donor pups were not studied. At PN21, a sub-cohort [CON; n=3 males, n=3 females and PUN; n=3 males, n=3 females] was placed under 1% isoflurane anesthesia and euthanized via cervical dislocation. Hearts were then analyzed by 2D DIGE, and proteins were confirmed with western blot or silver nitrate staining. The remaining littermates [CON; n=4 males; n=3 females and PUN; n=4 males, n=5 females] were weaned, and fed the control diet until PN80. Thus, growth restriction was isolated to a developmental window of postnatal life [PN1-PN21]. Body mass was measured bi-weekly from PN1-PN28, and then weekly from PN28-PN80 using a calibrated small animal weighing scale [Ohaus Corporation, Parsippany, NJ; CS Series]. At PN77, cardiac function was analyzed via echocardiography and Doppler blood flow analysis. Mice recovered for 2 days, then at PN80 were euthanized as described above. Hearts were removed, weighed and stored in a -80°C freezer for western blotting and silver nitrate staining to determine if proteomic differences persisted or were

recovered in adulthood. Heart mass is reported as absolute and standardized to body surface area, using Meeh's formula[188]:

Body surface area = 9.662 x [body weight] $^{0.667}$

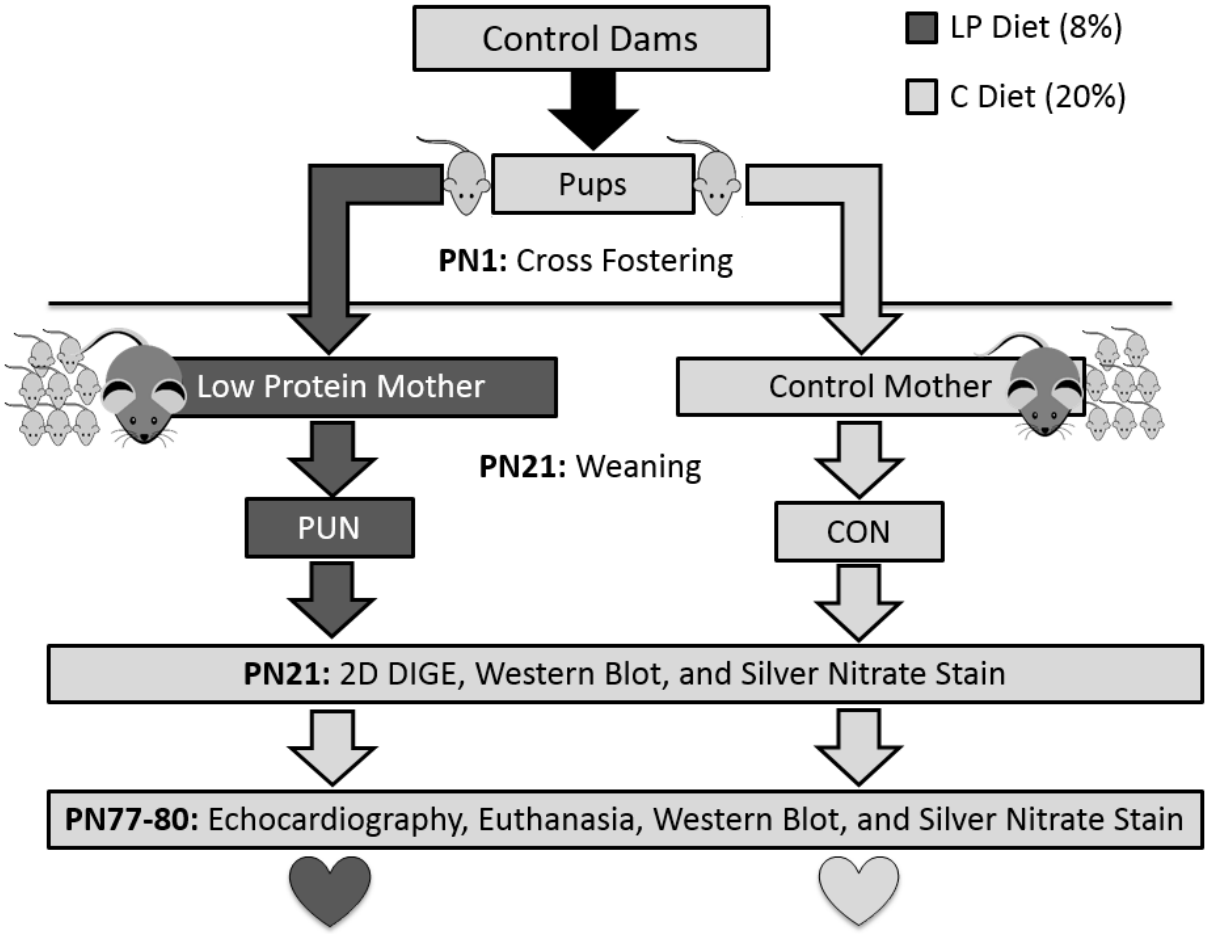

Figure 4.1: Method for Growth Restriction. Two weeks prior to mating, dams were fed either a control Diet [20% protein] or isocaloric low protein Diet [8% protein]. At birth, pups born to LP dams were sacrificed, while CON pups were cross fostered to either control fed dams [CON group] or low protein fed dams [PUN group]. At PN21, mice were weaned, a sub cohort were euthanized, and hearts collected for 2D DIGE, Western Blotting, and Silver Nitrate Staining [CON; n=3 males; n=3 females and PUN; n=3 males; n=3 females]. Postnatal growth restriction was isolated to the developmental window of PN1-21 as the remaining mice were fed the control diet from PN21-PN80. At PN77, cardiac function was evaluated by echocardiography [CON; n=4 males; n=3 females and PUN; n=4 males, n=5 females]. Mice were given 2 days of

Figure 4.1 (cont'd).

recovery, then at PN80 were euthanized and hearts extracted for Western Blotting, and Silver Nitrate Staining [CON; n=4 males; n=4 females and PUN; n=4 males; n=4 females].

The standardization to body surface area allows for comparison of cardiac function between mice of different sizes[188, 206]. Tibia length was measured as a surrogate for body composition and lean tissue growth using digital Vernier calipers [General Tools, Secaucus, NJ] [207].

2D DIGE

2D DIGE and protein identification with mass spectroscopy followed procedures previously described[116, 117, 208, 209]. Protein was extracted from PN21 hearts of CON and PUN mice using liquid nitrogen pulverization in a mortar and pestle then dissolved in DIGE labeling buffer [7 M urea, 2 M thiourea, 4% CHAPS, 30 mM Tris, pH 8.5]. Extracted proteins were quantified using Bradford reagents [Pierce Chemical Company, Dallas, TX] with a BSA standard. Samples were randomized and fluorescently labeled by reacting 40 µg of cardiac protein and 200 pmol of either Cy3 or Cy5 CyDye DIGE Fluors [GE Healthcare, Chicago, IL]. One Cy3- and one Cy5-labeled sample were loaded on a single gel, along with the Cy2-labeled pooled samples of CON and PUN. The pooled, Cy2-labeled samples act as an internal normalization standard, which allowed each protein spot to be semi-quantitatively compared within each gel and amongst all gels. Proteins were iso-electrically focused on 24 cm IPG DryStrips [pH 4-7; GE Healthcare] using an IPGPhor [GE Healthcare] with the following protocol: 500 V for 1 hour followed by a linear gradient to 1,000 V over the span of one hour. A linear gradient to 8,000 V until a total of ~60,000 volt●hour was reached. The focused strips were equilibrated in two steps: 1] 15 min in SDS equilibration buffer I [6 M urea, 2% SDS, 30% glycerol, 50 mM Tris, pH 8.8, 0.01% bromophenol blue, and 10 $mg \cdot ml^{-1}$ DTT] followed by 2] 15

min with equilibration buffer II in which the DTT was substituted by 25 $mg \cdot ml^{-1}$ iodoacetamide. The equilibrated IPG strips were positioned on top of 12% polyacrylamide SDS slab gels and covered with 1% low-melt agarose and run in a DALT 6 system [GE Healthcare; 10°C] at 1 W per gel until the dye front reached the bottom of the gels[210].

Multiplexed gel images were acquired using a Typhoon Trio [GE Healthcare], and viewed using ImageQuant software [GE Healthcare, version 8.1]. Images were loaded into DeCyder software [GE Healthcare, version 6.5] and differences in protein abundance [$p<0.05$] along with the magnitude of abundance [average ratio] were quantified. Average ratio was derived from the normalized spot volume standardized against the internal standard, thus providing the degree of abundant change between identified proteins. Gels used for spot picking were fixed in 10% methanol and 7.5% acetic acid overnight.

Spots displaying significant changes [$p<0.05$] in abundance between growth restricted [PUN] and control [CON] mice [Figure 4.2] were robotically picked and digested [Ettan Picker and Digestor; GE Healthcare] with recombinant porcine trypsin from the gels [Promega, Madison, WI] as explained previously[211]. Spots with a p-value greater than 0.05 but less than 0.075 were also picked and identified [Table 4.1], to provide potential hypothesis driven investigations. Extracted tryptic peptides were dried by Speed-Vac, sequenced and identified by nano-LC/MS/MS on an LTQ XL [Thermo-Finnigan, San Jose, CA] using the MASCOT and X! Tandem search engines. The MASCOT program [v2.2] searched the *Mus musculus* proteome in the NCBInr database using the following limitations and allowances for protein identification: 1] one missed cleavage by trypsin; 2] monoisotopic peptide masses; 3] peptide mass tolerance of 1.2 Da; 4] fragment mass tolerance of 0.8 Da. Additionally, oxidation of methionine [variable modification] and carbamidomethylation [fixed modification] of cysteine were allowed by

MASCOT in the protein identification. Proteins were required to have a minimum of three matching peptides to form the identification. Protein identifications were then verified by Scaffold [Proteome Software, Portland, OR].

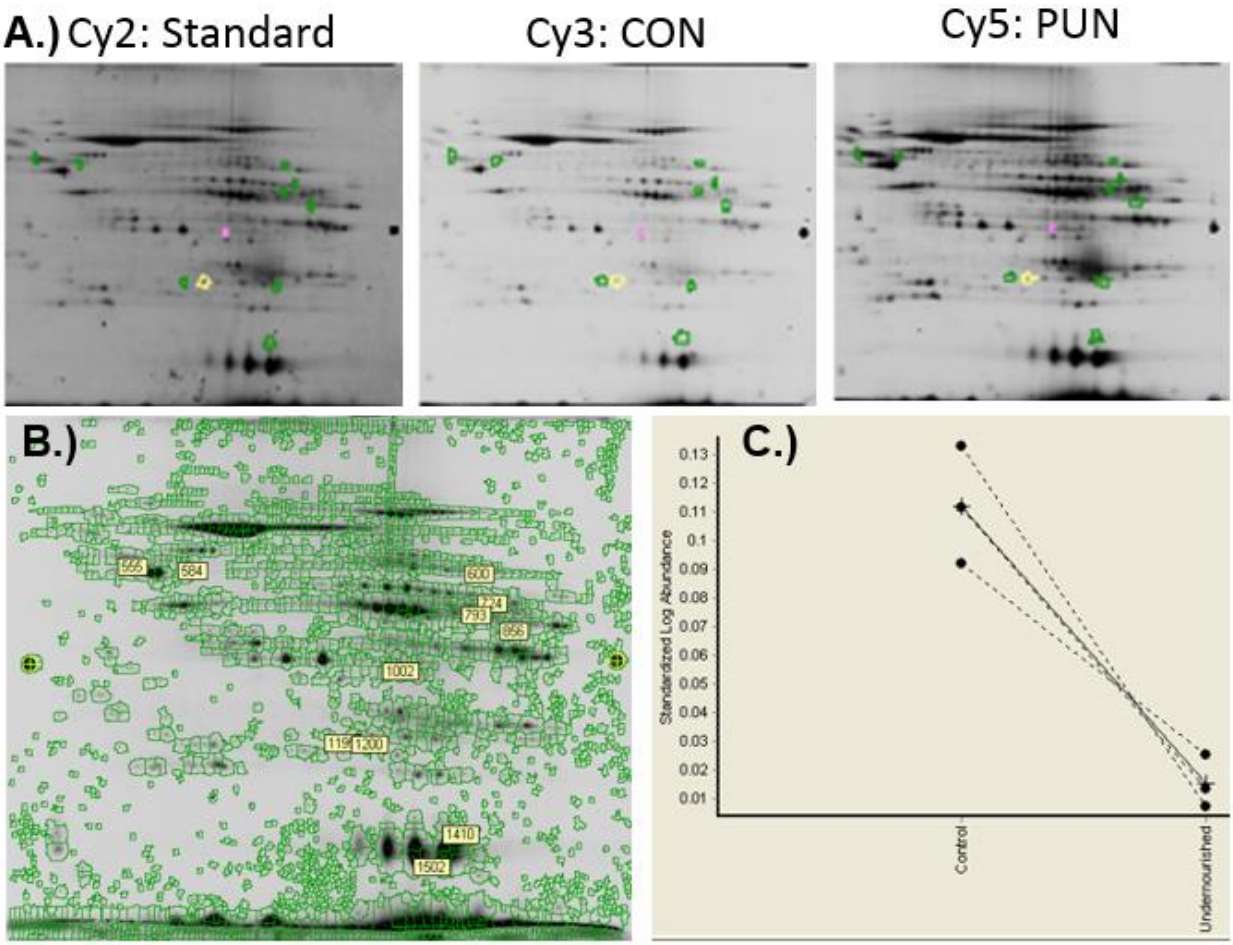

Figure 4.2: Representative image from DeCyder software: **A.]** 6 gels were CyDye-labeled through 2D DIGE three-dye methodology. **B.]** 2,187 total spots were detected and analyzed. Of the total spots, 6 spots were determined to have differential abundance and were robotically picked for digestion; illustrated by the green, yellow, and pink circles in panel A. Each protein spot was assigned a master number, shown as a yellow number tag. **C.]** The graphical view from the DeCyder software shows the standardized log abundance between the CON and PUN of the protein spot that has been selected [yellow circle, panel A]. This protein spot was identified with a master number #1200 [p value = 0.0042, Avg. Ratio = -1.22].

Western Blot

Cdkn1c [$p57^{kip2}$] was identified as a protein of interest by 2D-DIGE [see results] and abundance was confirmed through western blotting at PN21, and again at PN80 to determine if the protein signature persisted into adulthood.

The blotting technique consisted of protein extraction by tissue homogenization with liquid nitrogen in a mortar and pestle, and solubilized in lysis buffer [1% CHAPS, Tris pH 7.5, cOmplete protease inhibitor cocktail tablet, and ddH_2O]. The solution was then centrifuged for 15 minutes at 13,000 x g, where the supernatant and pellet were separated. Quantification of protein concentration was completed using a Bradford Assay[212] in a micro-plate reader [BioRad, iMark, Hercules, CA] with a BSA standard. Proteins were incubated in Laemmli buffer[213] and separated using a self-prepared 9% acrylamide gel via SDS-PAGE. Proteins were then transferred to polyvinylidene difluoride [PVDF] membranes [VWR, Radnor, PA] and blocked for 1 hour in proteomic grade non-fat dried milk. Primary antibodies were used at the manufacturer's recommendations [Cell Signaling, Danvers, MA; Gapdh Rabbit *mAb*, 1:1,000; and Abcam, Cambridge, UK; $p57^{kip2}$, ab75974], then standardized to Gapdh [au; arbitrary units] to ensure equal loading of proteins on SDS-PAGE. Membranes were incubated in a secondary horseradish peroxidase antibody [Abcam, Cambridge, UK; Goat Anti-Rabbit IgG HRP, ab6721] in a 1:2500 ratio for 1 hour. Development and detection of blots was completed using the Kodak Image Station 2000R [Kodak, Hempstead, UK]. Blots were quantified by densitometry software [Carestream Molecular Imaging, Woodbridge, CT].

Silver Nitrate Stain

In addition to Cdkn1c [$p57^{kip2}$], Titin [Ttn], and Collagen fibers [Col1a1, Col3a1, and Col4a5] were identified as proteins of interest [see results] via 2D DIGE and their abundance was confirmed with silver nitrate staining of SDS PAGE.

For confirmation of the relative change in abundance between samples of Ttn and collagen protein, the protocol by Zhu *et. al.* for SDS gel electrophoresis was used, as western blotting does not yield reliable results for Ttn[214, 215] and collagen proteins have reduced specificity of antibody binding[215-217]. Samples were prepared with protease inhibitors [Roche, Basel Switzerland; cOmplete Protease Inhibitor Cocktail] in 4X-SDS sample buffer [1 M Tris-HCl pH 6.8, 1.0 g SDS, 0.8 ml 0.1% Bromophenol Blue, 4 ml Glycerol, 2 ml 14.3 M β-mercaptoethanol, and ddH_2O] and heated at 45°C for 7 minutes. CON or PUN protein [2 µg] were loaded into the wells of a hand-cast, macro-porous 6% SDS-polyacrylamide gel for electrophoretic separation at 30mA for 2.5 hours. Throughout electrophoresis, gels were chilled with a water coolant system maintained at 2-10°C. The gels were soaked in fixative [10% acetic acid, 30% ethanol, 70% ddH_2O] solution for one hour, then the fixative was discarded and replaced to allow gels to be fixed overnight. The next day, gels were rinsed with 20% ethanol solution for 20 minutes, followed by rinsing with ultrapure water for 10 minutes. Gels were then sensitized [0.02% sodium thiosulfate, 99.98% ddH_2O] for one minute and rinsed again [3 times for 20 seconds each] in ultrapure water. Silver nitrate solution [0.2% silver nitrate, 99.8% ddH_2O] was applied to gels for 45 minutes. Gels were rinsed with ultrapure water for 10 seconds and then placed into the developing solution [3% sodium carbonate, 0.025% formaldehyde, placed into 25 mL of sensitizer solution] for 8 minutes, followed by the stop solution [5% Tris,

2.5% acetic acid, 92.5% ddH_2O] for 15 minutes. Gels were then imaged and inspected for high molecular weight proteins [140-245 kDa][218].

Generation of a Potential Mechanism by which Postnatal Growth Restriction Influences Cardiac Impairment

Following 2D DIGE and a secondary confirmatory technique, potential mechanisms were generated using REACTOME[125, 126] and STRING[131-133, 140] software. 2D DIGE protein gene codes were entered into REACTOME to recognize pathways related to the identified proteins. The following functions within REACTOME were used: 1] *Description*: summarizes the protein in the pathway browser such as input/output molecules, catalysts, regulators, and references with supporting evidence; 2] *Structure*: details the 3D structure from the Protein Data Bank; 3] *Gene expression*: expression information from the Gene Expression Atlas [Cambridgeshire, UK]. The software then analyzes all of the identified pathways through a] *entity p-value*; the probability that the overlap between the query and the pathway has occurred by chance, b] *entities false discovery rate*; probability corrected for multiple comparisons, and c] *reaction ratios*; the total reactions in the pathway divided by the total number of reactions for the entire species tissue selected [heart].

STRING [version 10.5] was used to obtain a network of protein-protein interactions [PPI] and has been used in previous proteomic research[131-134]. The database uses five different sources to quantitatively integrate known and predicted PPI's including genomic context predictions, high-throughput lab experiments, conserved co-expression, text-mining and previous knowledge in databases. An adjustable modification to only allow the highest confidence score was made [0.900] in the STRING settings, thus reducing false discovery rates. The network allows for understanding functional activities of the proteins identified from 2D DIGE[139]. Previous genetic

and proteomic literature have used REACTOME and STRING together for the development of pathological disease mechanisms[141, 142].

Echocardiography

Structural and functional parameters of the heart as a result of postnatal growth restriction were assessed by echocardiography [Vevo 770 ultrasound, with 30MHz transducer, Visualsonics, Toronto, Canada] in adulthood as previously described[219]. At PN77, mice were maintained under 1% isoflurane anesthesia on a heated board with their limbs restrained. Measurements were performed in 2D and M-modes with images taken in the short axis at the level of the papillary muscles and used to determine LV systolic and diastolic dimensions. Mitral and aortic blood flow velocities were measured by Doppler from the apical view [10 MHz pulsed Doppler probe with real time Doppler spectrum analyzer, Indus Instruments, Webster, TX, USA]. Recordings were saved for offline analysis and were completed with the observer blinded to the diet group.

Statistics

A linear model compared growth curves between the CON and PUN groups [JMP V12.0 Sass, Cary, NC]. Two-way ANOVAs were used with the main effects of diet [CON vs. PUN] and sex [male vs. female] to compare heart mass [absolute or standardized], tibia length, and western blot protein abundance. An ANCOVA was used to analyze echocardiography parameters with heart rate and body surface areas as covariates. An α level of 0.05 was set *a priori* and if necessary, a Tukey's HSD post hoc test was used for multiple comparisons. The 2D DIGE statistical differences [$p<0.05$] in spot intensity used DeCyder Software as previously described[208, 209]. Briefly, numerical data for individual spots detected through DeCyder Software

are automatically calculated and compared based upon the volume [sum of pixel intensity], area [spot radius covered], peak height [pixel value at the X, Y position of the spot], and slope of the protein spot [gradient associated with the 3D attributes of a spot map pair]. REACTOME and STRING software both had α levels manually changed to 0.05 to reduce false discovery rates.

Results

Growth

PN1-21

Postnatal growth restriction significantly [$p<0.0001$] decreased growth rate from PN1-21 [PUN; males: 0.318±0.017 grams·day^{-1} and females: 0.314±0.016 grams·day^{-1}] when compared with the CON group [males: 0.534±0.013 grams·day^{-1} and females: 0.516±0.022 grams·day^{-1}], with no sex effect present [Figure 4.3A]. Final PN21 body mass of PUN mice [males: 8.6±0.731 g and females: 8.3±0.518 g] were significantly less [$p<0.0001$] than the CON mice [males: 12.7±0.331 and females: 12.1±1.132 g; Figure 4.3C], with no sex effect.

PN22-80

Postnatal growth restriction significantly [$p=0.005$] decreased the growth rate from PN22-80 [PUN; males: 0.1404±0.036 grams·day^{-1} and females: 0.0829±0.026 grams·day^{-1}] when compared with the CON growth rate [males: 0.1381±0.033 grams·day^{-1} and females: 0.1130±0.025 grams·day^{-1}] [Figure 4.3B]. The CON group had a significantly higher body mass compared to the PUN group after re-feeding that persisted over the course of the study [Figure 4.3C], resulting in the PUN mice having a decreased [$p=0.0001$] final body mass [PUN; males: 22.36±1.79 g and females: 19.00±0.98 g] when compared to the CON group [males: 26.50±1.27

g and females: 22.45±1.31 g]. There was a significant sex effect [p=0.0002] with males being larger than females at PN80.

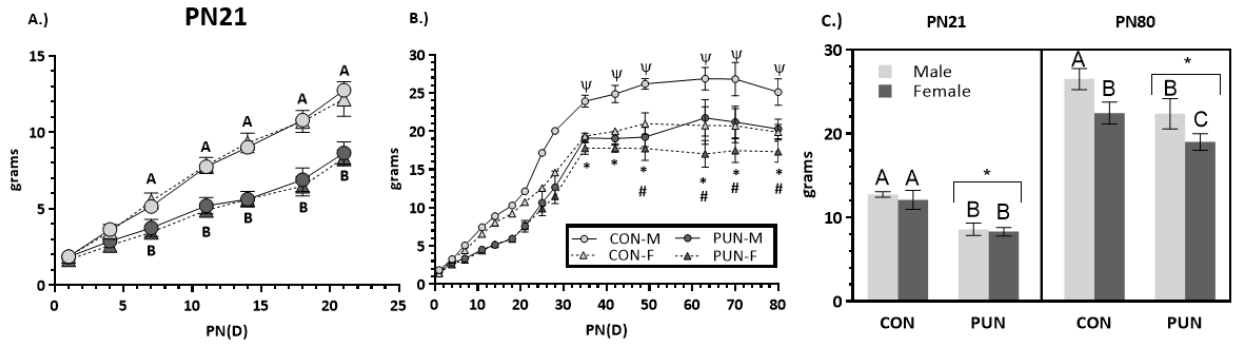

Figure 4.3: Effects of Postnatal Growth Restriction on Body Mass: A.] PN1-PN21: Growth restriction significantly [p<0.0001] decreased the growth rate of the PUN mice when compared with the CON group, there was no sex effect. **B.] Growth curve from PN22-PN80:** Growth restriction significantly [p<0.0001] decreased body mass at several time points [PN35, 42, 49, 63 and 70] in the PUN group. The CON male mass was significantly [p<0.0001] larger than all other groups. There was no significant [p=0.9665] difference between the CON females and PUN males. Ψ significantly different from all other groups; *significantly different from CON males; #significantly different from CON females; ^significantly different from PUN females. **C.] Final Body Mass [PN21 and PN80]:** PN21-PUN mass was significantly less [p<0.0001] than the CON group, with no sex effect. PN80-PUN mass was significantly [p=0.0001] reduced compared to the CON group. Females were significantly [p=0.0002] less than males at PN80. Comparison of PUN males to CON females was non-significant [p=0.9996]. *significantly different from CON group. Values are Mean ± SD. A linear model [panel A & B] and Two-way ANOVA with a Tukey HSD multiple comparison test [panel C] were used for statistical analyses. Levels within the figure not connected by the same letter [A, B, or C] represent statistical significance [p<0.05].

Heart Mass and Tibia Length

PN21

Absolute heart mass [Figure 4.4A] of the PUN group [males: 0.0686±0.006 g and females: 0.0590±0.005 g] was significantly [p=0.0140] less than the CON group [males:

0.0783±0.006 g and females: 0.0760±0.010 g], with no sex effect present. When heart mass was standardized to body surface area [Figure 4.4B], no significant [p=0.3305] differences were found between groups [PUN; males: 0.0016±0.0001 kg/cm^2 and females: 0.0014±0.0002 kg/cm^2] vs. [CON; males: 0.0014±0.0001 kg/cm^2 and females: 0.0014±0.0001kg/cm^2].

Postnatal growth restriction significantly [p=0.0019] reduced tibia lengths [PUN; males: 13.710±0.114 mm; females: 13.147±0.632 mm, Figure 4.4C] when compared to the CON group [males: 15.520±1.197 mm and females: 14.968±0.249 mm], with no sex effect present.

PN80

At PN80, there were no significant [p=0.9914] differences in absolute heart mass [Figure 4.4A] between the PUN group [male: 0.1170±0.020 g and female: 0.1251±0.028 g] and CON group [male: 0.1262±0.033 g and female: 0.1346±0.027 g]. When hearts were standardized to body surface area [Figure 4.4B], there were no significant [p=0.9534] differences between groups [PUN male: 0.0015±0.0002 kg/cm^2 and PUN female: 0.0017±0.0003 kg/cm^2; CON male: 0.0015±0.0004 kg/cm^2 and CON female: 0.0017±0.0003 kg/cm^2].

Tibias of the PUN group [male: 17.176±0.285 mm; female: 17.671±0.272 mm] were significantly smaller [p=0.0008, Figure 4.4C] than the CON group [male: 18.573±0.497 mm; female: 18.152±0.144 mm]. Post-hoc analysis revealed that the PUN males [p=0.0018] and females [p=0.0143] were only significantly different from the CON males not CON females. The PUN males were, however, trending towards being significantly smaller [p=0.0502] than the CON females.

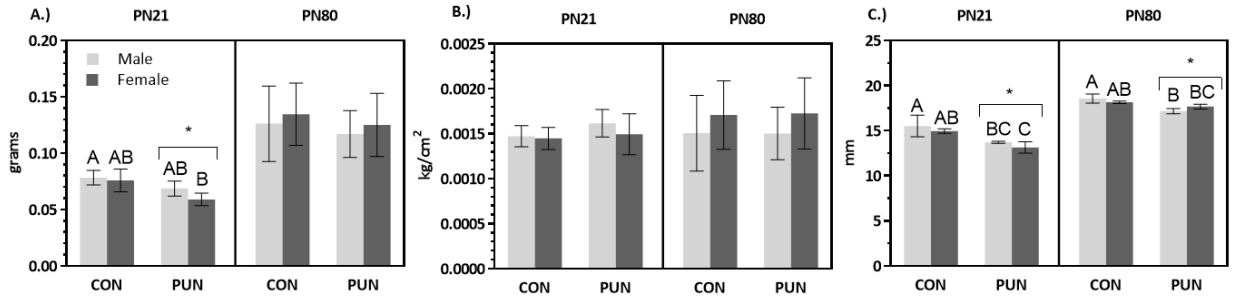

Figure 4.4: Effects of Postnatal Growth Restriction on Heart Mass and Tibia Length A.] Absolute Heart Mass [PN21 and PN80]: The PN21-PUN group was significantly less [p=0.0140] than the CON group, with no sex effect. The PN80-PUN group was not significantly [p=0.9914] different from the CON group, along with no sex effect. **B.] Standardized Heart Mass [PN21 and PN80]:** There is no significant difference at PN21 [p=0.3305] between the PUN group and the CON group, and no sex effect present. At PN80, no significant difference [p=0.9534] was observed between the PUN group and the CON group, and there was no sex effect. **C.] Tibia Length [PN21 and PN80]:** Postnatal growth restriction significantly reduced tibia lengths in the PUN group compared to the CON group at PN21 [p=0.0019] and PN80 [p=0.0008], with no sex effect present at PN21. At PN80 the tibias of PUN males [p=0.0018] and females [p=0.0143] were significantly smaller than the CON males. Values are Mean ± SD. Levels within the figure not connected by the same letter [A, B, or C] represent statistical significance [$p<0.05$]. *, significantly different from CON group. Two-way ANOVA's with a Tukey HSD multiple comparison test were used.

2D DIGE

A total of 2,187 spots were detected and analyzed in 6 CyDye-labeled gels. From this, 6 spots were picked with 30 possible proteins identified from nano-LC/MS/MS to have differential abundance between the CON and PUN hearts, with no sex effects. 12 proteins had a p-value < 0.05, while 18 proteins had a p-value between 0.05-0.075 [Table 4.1]. The 12 significantly identified proteins all had less protein abundance in the PUN group compared to the CON group. The individual proteins from 2D DIGE were associated with extracellular matrix organization/muscle contraction [21.5% lower abundance of Ttn, Collagen Type I α 1 Chain, Collagen Type III α 1 Chain, and Collagen Type IV α 5 Chain], cell cycling/signal transduction [20% lower abundance of $p57^{kip2}$, Exportin 5, and Rho GTPase Activating Protein], and metabolism [25.42% lower abundance of Peroxiredoxin 6, SAFB-like transcription modulator].

Table 4.1: Differential protein abundance between control [CON] and growth restricted [PUN] mice.

Protein	*p*	*Average Ratio*	No. of Identified Peptides	% Sequence Coverage	*Expressed in [CON/PUN]*	*Physiological Category [REACTOME]*
Peroxiredoxin 6 [Prdx6]	0.0042	-1.22	6	32%	CON	Metabolism, Cellular Signaling
Titin [Ttn]	0.019	-1.2	4	0%	CON	Muscle Organization
Rho GTPase Activating Protein 29 [Arhga29]	0.019	-1.2	4	1%	CON	Signal Transduction
Cyclin Dependent Kinase Inhibitor 1C-p57^{kip2} [Cdkn1c]	0.019	-1.2	3	16%	CON	Cell Cycle
SAFB-like Transcription Modulator [Sltm]	0.019	-1.2	3	2%	CON	Metabolism
Exportin 5 [Xpo5]	0.019	-1.2	3	1%	CON	Cell Cycle, Signal Transduction
Crumbs Cell Polarity Complex Component [Patj]	0.019	-1.2	3	3%	CON	Cell-Cell Communication
Collagen Type I α 1 [Col1a1]	0.019	-1.2	3	3%	CON	Extracellular Matrix
Histone-Lysine N-Methyltransferase [Setd2]	0.019	-1.2	9	0%	CON	Gene-Expression [Transcription]
Collagen Type IV α 5 [Col4a5]	0.019	-1.2	5	5%	CON	Extracellular Matrix

Table 4.1 (cont'd).

Collagen Type III α 1 [Col3a1]	0.019	-1.2	9	14%	CON	Extracellular Matrix
Dynein Axonemal Heavy Chain 1 [Dnah1]	0.019	-1.2	4	0%	CON	Protein Transportation [Motor]
Aldolase, Fructose-Bisphosphate A [Aldoa]	0.064	-1.26	20	62%	CON	Metabolism [fatty acid oxidation]
Acetyl-CoA Acetyltransferase 1 [Acat1]	0.064	-1.26	17	54%	CON	Metabolism [fatty acid oxidation]
Acetyl-CoA Acyltransferase 2 [Acaa2]	0.064	-1.26	13	48%	CON	Metabolism [fatty acid oxidation]
Aspartate Aminotransferase [Got1]	0.064	-1.26	12	30%	CON	Metabolism [biosynthesis proteins]
Microtubule Associated Protein 6 [Map6]	0.064	-1.26	6	12%	CON	Extracellular Matrix
Leucine Rich Repeats and Ig-like Domains 3 [Lrig3]	0.064	-1.26	5	6%	CON	Signal Transduction
Acyl-CoA Dehydrogenase Medium Chain [Acadm]	0.064	-1.26	4	13%	CON	Metabolism [fatty acid oxidation]
Aconitase 2 [Aco2]	0.064	-1.26	5	8%	CON	Metabolism [Krebs cycle]
Caveolae Associated Protein 1 [Ptrf]	0.075	1.34	11	42%	PUN	Gene-Expression [transcription]

Table 4.1 (cont'd).

Vitamin D Binding Protein [Gc]	0.075	1.34	14	29%	PUN	Metabolism, Protein Transportation
Hemoglobin Subunit β [Hbb]	0.075	1.34	3	30%	PUN	Transport of Small Molecules
Neuroblast Differentiation-Associated Protein [Ahnak]	0.075	1.34	3	1%	PUN	Structural Protein, Cardiac Ca^{2+} regulation
Heat Shock Protein Family D [Hspd1]	0.075	1.34	4	13%	PUN	Metabolism, Signal Transduction, Cell Cycle
Vimentin [Vim]	0.075	1.34	4	12%	PUN	Programmed Cell Death, Muscle Contraction
Adenomatous Polyposis Coli [Apc]	0.075	1.34	4	0%	PUN	Metabolism, Signal Transduction
ATP Synthase F1 Subunit β [Atp5b]	0.075	1.34	4	11%	PUN	Metabolism [Ox. Phos.]
Potassium Calcium-Activated Channel Subfamily M α1 [Kcnma1]	0.075	1.34	4	3%	PUN	Intracellular Ion Regulation
Fetuin-A [Ahsg]	0.075	1.34	5	16%	PUN	Immune System

Table 4.1 (cont'd).

Protein [gene code], name of identified protein with the associated gene that codes for the protein; *p*, significance of the differential protein abundance from DeCyder software; *Average Ratio*, originated from the normalized spot volume normalized alongside the intra-gel standard provided by DeCyder software analysis, offering a measure of the abundance variances between proteins detected; *No. of Identified Peptides*, the number of peptides recognized from the selected gel spot; *% Sequence Coverage*, the percentage of the number of amino acids found in contrast to the entire number of amino acids in the protein sequence, permitting a confidence interval of 95% that the peptide structure matches the detected protein; *Abundant in [CON/PUN]*, the diet group in which the protein is over-expressed in; *Physiological Category*, the functional pathway the identified protein is associated with. CON [n=3 males; n=3 females] and PUN [n=3 males; n=3 females].

Western Blot

Postnatal growth restriction impairs cardiomyocyte nucleation, leading to functional impairments in adulthood[48], therefore the cell cycle regulator, $p57^{kip2}$, was classified as a protein of interest based on existing literature and significant 2D DIGE results [44, 46, 48, 50, 51, 220].

PN21

In agreement with 2D DIGE and mass spectrometry, the relative protein abundance of $p57^{kip2}$ was significantly [p=0.0071] lower in the PUN group [0.1100±0.0209 au] compared to the CON group [0.1512±0.0212 au, Figure 4.5A]. Therefore, the PUN mouse hearts in this study had a significant, 27.24% reduction in the relative abundance of $p57^{kip2}$ in early life.

PN80

The relative protein abundance of $p57^{kip2}$ in adulthood was recuperated [Figure 4.5A] and showed no significant differences [p=0.3627] between the samples of PUN [0.7017±0.1205 au] and CON [0.6701±0.1042 au] hearts.

Silver Nitrate Stain

Growth restriction alters cardiac morphology[51, 220], stiffens coronary arteries[44, 221], rearranges the extracellular matrix[60], and impairs collagen deposition[66]. Therefore, based on the existing literature and significant 2D DIGE results Ttn and collagen proteins were classified as proteins of interest. Visual inspection of the silver nitrate stained gels for Ttn and collagen protein [Figure 4.5B] showed the PUN mice have less relative protein abundance when compared to the CON mice in the high molecular weight range [140-245 kDa] at PN21 and PN80.

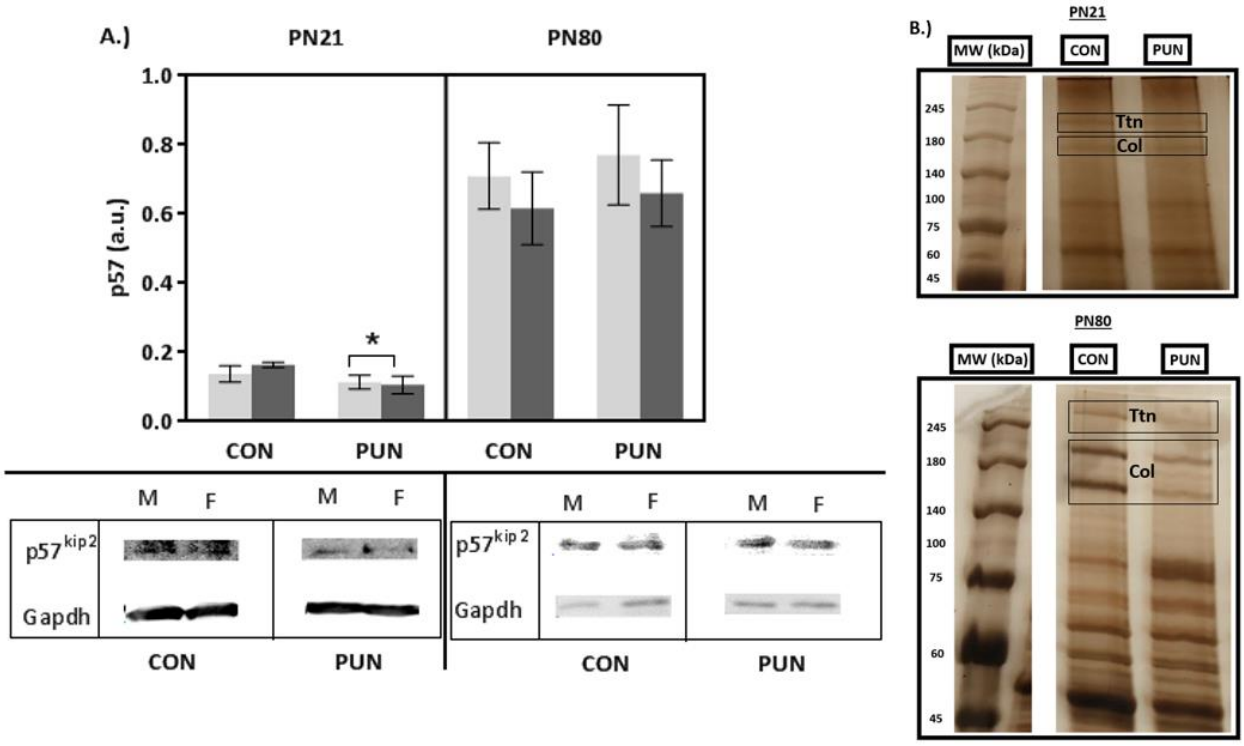

Figure 4.5: Western blot protein abundance of p57^{kip2} and silver nitrate stain of large molecular weight proteins A.] PN21; **p57^{kip2}** PUN abundance is significantly [*; p=0.0071] less than CON. At PN80, no significant differences between diets or sex was seen, as abundance is recuperated [p=0.3627]. Values are Mean ± SD. The blots below the bar graphs are contiguous, representative bands selected from the gels. **B.] Silver Nitrate Stain**; CON and PUN cardiac protein samples [2 µg] were alternatingly loaded onto gels at PN21 and PN80. Upon visual inspection of the large molecular weight bands indicated by the outlined boxes [MW; 140-245 kDa], the CON group show more relative protein abundance at both time-points, confirming 2D

Figure 4.5 (cont'd).

DIGE results and possibly indicating PUN mouse hearts may have less Ttn, and collagen protein. The stain is a contiguous, representative image of CON vs. PUN selected from the gels; however, the reassembly of the molecular weight marker has been added to the left side of the image. For both western blotting and silver nitrate staining the following sample sizes were used: PN21 [CON; n=3 males, n=3 females and PUN; n=3 males, n=3 females] and PN80 [CON; n=4 males, n=4 females and PUN; n=4 males, n=4 females]

Pathway Analysis

Using the REACTOME software, 42 pathways were associated with the five confirmed proteins from 2D DIGE [$p57^{kip2}$, Ttn, Col1a1, Col3a1, Col4a5]. The identified hubs [a combination of interactors, entities, and reactions] included extracellular matrix organization, cell cycle, muscle contraction, signal transduction, developmental biology, immune system, and hemostasis [Figure 4.6].

A.)

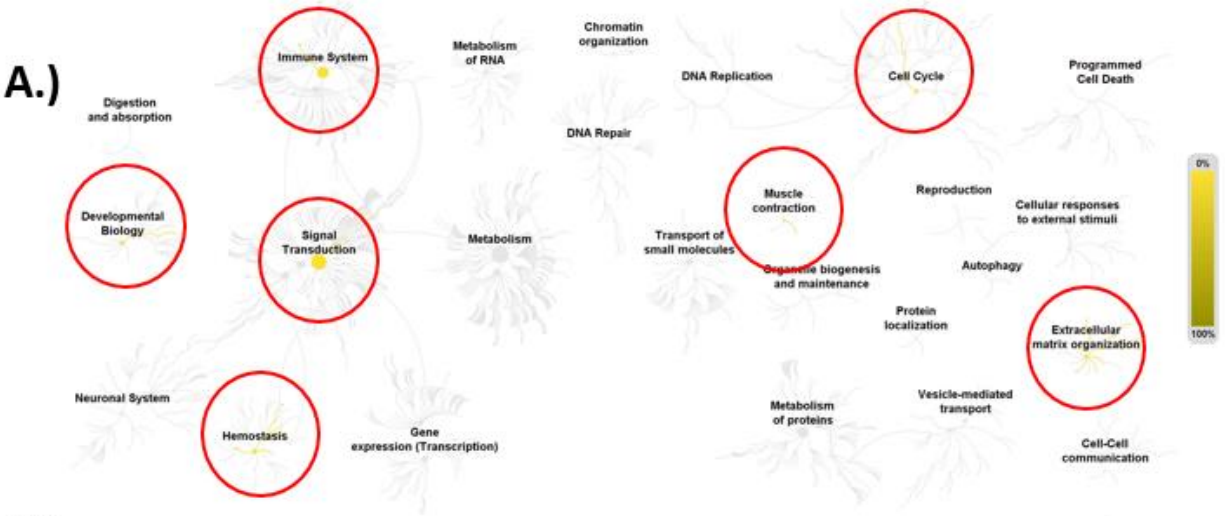

B.)

Mus musculus ()

reactome

Pathway name	Entities				Reactions	
	found	ratio	p-value	FDR*	found	ratio
Non-integrin membrane-ECM interactions	3 / 41	0.004	1.24e-04	0.003	2 / 9	0.001
Collagen chain trimerization	3 / 41	0.004	1.24e-04	0.003	3 / 27	0.003
Collagen degradation	3 / 62	0.006	4.16e-04	0.005	7 / 20	0.003
Assembly of collagen fibrils and other multimeric structures	3 / 68	0.006	5.44e-04	0.005	17 / 26	0.003
Anchoring fibril formation	2 / 16	0.001	6.65e-04	0.005	1 / 4	5.15e-04
Collagen biosynthesis and modifying enzymes	3 / 73	0.007	6.67e-04	0.005	23 / 50	0.006
Integrin cell surface interactions	3 / 82	0.007	9.33e-04	0.006	2 / 44	0.006
NCAM1 interactions	2 / 24	0.002	0.001	0.006	1 / 3	3.86e-04
Crosslinking of collagen fibrils	2 / 25	0.002	0.002	0.006	12 / 13	0.002
Collagen formation	3 / 102	0.009	0.002	0.007	40 / 76	0.01

Figure 4.6: Proposed pathways for cardiac impairment caused by PUN. A.] Pathway network generated by REACTOME [yellow lines: 42 pathways involved]. The most notable pathway hubs [red circles] were extracellular matrix organization, cell cycle, muscle contraction, signal transduction, developmental biology, immune system, and hemostasis. **B.]** Representative image generated by REACTOME of the 10 most relevant pathways sorted by p-value [<0.05] shown in a table.

Interaction Network

Using the STRING software, four networks are presented in Figure 4.7A-D. The network in Figure 4.7A contains the five confirmed 2D DIGE proteins [total nodes/proteins involved] without any software predicted interactions. Col1a1, Col3a1, and Col4a5 represent 3 edges [PPI's between nodes], with an associated PPI enrichment p-value of $2.28e^{-5}$. Figures 4.7B-D have been enriched with software predicted interactors, meaning protein interactions are biologically connected or react with additional proteins not identified from 2D DIGE. The other confirmed 2D DIGE proteins such as Titin [Ttn] and $p57^{kip2}$ [Cdkn1c] can predictably interact with other proteins such as Neb, Tcap, and Cdk2. The p-values for Figures 4.7B-D are $9.67e^{-10}$, $3.08e^{-10}$, and $< 1.0e^{-16}$, respectively, indicating the enriched networks are not random and the observed number of edges is significant. The pathway analysis and the interaction network helped generate potential mechanism leading to cardiac impairment in adulthood from postnatal growth restriction [Figure 4.8].

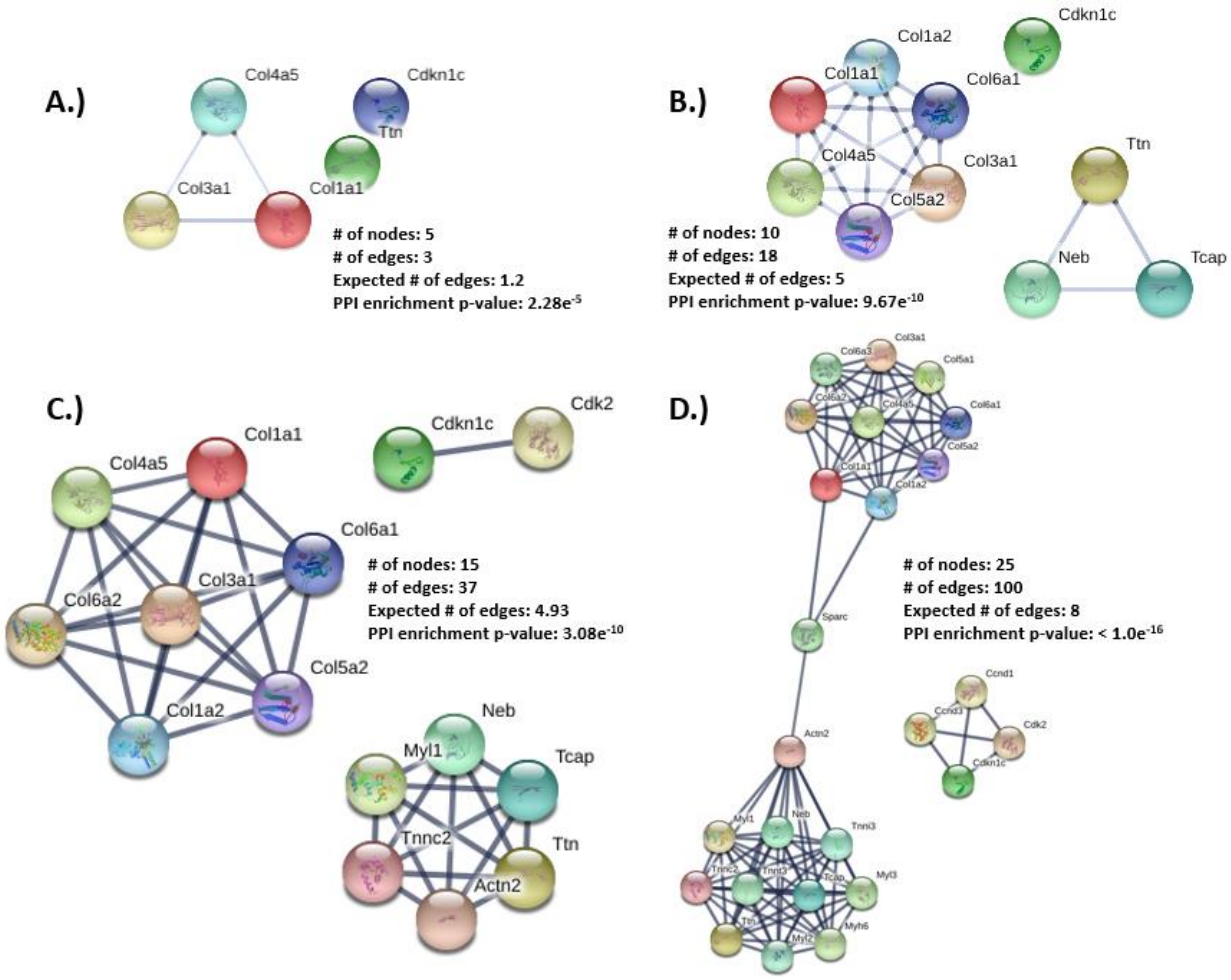

Figure 4.7: The PPI networks constructed by STRING database for the differentially abundant proteins from PUN and CON mouse hearts. The networks consist of the total number of nodes [proteins involved], number of edges [PPI connections amongst nodes], and a PPI enrichment p-value. The *expected number of edges* provides how many edges is anticipated if the nodes were to be selected at random. **A.]** No interactors. **B.]** 5 predicted protein interactors added. **C.]** 10 predicted protein interactors added. **D.]** 20 predicted protein interactors added. The spheres represent the protein and the line thickness represents the PPI associated degree of evidence [combination of gene fusion, gene neighborhood, gene co-occurrence, experimental evidence, text-mining evidence, database evidence, and co-expression evidence]. The information inside of the circle describes the protein structure and the color of the nodes is for visual representation.

Echocardiography

Echocardiography results during adulthood can be viewed in Table 4.2. LV mass was significantly reduced by 12.3% in PUN males and 10.3% in PUN females as compared to CON males and females, respectively [p=0.03]. Despite a reduction in LV mass, there was no difference in systolic function; however, there were significant differences in diastolic function between the groups. The CON females [59.2±2.2 ms] had a longer [p=0.042] ejection time [AET] as compared to the other groups [CON males: 52.3±1.6 ms; PUN males: 51.4 ± 1.6 ms; PUN females: 53.2±1.4 ms]. Blood velocity parameters following atrial contraction [MV A] were significantly higher [p=0.044] in the CON females [448.1±41.6 mm/s^2] as compared to the other groups [CON males: 320.4±30.3 mm/s^2; PUN males: 335.2±29.5 mm/s^2; PUN females: 328.6±27.0 mm/s^2]. This resulted in a statistically different [p=0.045] MV E/A ratio, where the CON females [1.5±0.2] and PUN males [1.6±0.2] had a lower ratio than the CON males [1.9±0.2] and PUN females [2.0±0.1].

There was a significant diet effect influencing isovolumetric contraction and relaxation time. The PUN group [males: 12.7±1.4 ms; females: 11.9±1.3 ms] had a longer [p=0.02] isovolumetric contraction time as compared to the CON group [males: 10.8±1.4 ms; females: 8.6±1.9 ms]. Additionally, the PUN group [males: 18.0±1.1 ms; females: 17.5±0.9 ms] had a longer [p=0.03] isovolumetric relaxation time compared to the control group [males: 15.1±1.1 ms; females: 16.9±1.5 ms].

The alterations in LV mass and diastolic function led to the PUN group having impairments in global cardiac function [Table 4.2]. Stroke volume was significantly reduced [p=0.01] in the PUN group [males: 38.9±2.4µL; females: 36.8±2.1 µL] compared to the CON group [males: 45.7±2.5 µL; females: 43.2±2.8 µL]. This led to a proportional decline [p=0.02] in

cardiac output [CON males: 18.5±1.3 mL·min^{-1}; CON females: 16.9±1.8 mL·min^{-1} vs PUN males: 14.2±1.3 mL·min^{-1}; PUN females: 13.4±2.1 mL·min^{-1}] and myocardial performance index [CON males: 0.49±0.03; CON females: 0.43±0.04 vs PUN males: 0.59±0.03; PUN females: 0.55±0.03].

Table 4.2: Echocardiography between control [CON] and growth restricted [PUN] mice.

	CON		*PUN*		*p-value*		
Parameter	*males*	*females*	*males*	*females*	*Diet*	*Sex*	*Diet*Sex*
Structural							
Heart Rate [beats·min^{-1}]	404.5±29.0	391.3±41.0	365.0±29.0	362.6±25.9	NS	NS	NS
Area, S [mm^2]	12.1±1.1	10.7±1.4	9.4±0.9	9.4±0.9	NS	NS	NS
Area, D [mm^2]	18.7±1.0	16.6±1.5	14.3±1.0	13.6±0.9	NS	NS	NS
LV Mass [mg]	115.7±3.5^{A}	111.5±2.3^{A}	101.4±1.3^{B}	100.0±2.6^{B}	0.03	NS	NS
LV Mass Corrected [mg]	92.5±2.0^{A}	89.3±1.2^{A}	81.1±1.8^{B}	80.0±1.2^{B}	0.04	NS	NS
Systolic Function							
Ejection Fraction [%]	66.2±4.5	67.3±6.2	62.0±4.4	61.7±3.9	NS	NS	NS
Fractional Shortening [%]	36.9±3.3	37.8±4.6	34.2±3.2	33.2±2.9	NS	NS	NS
LVID, S [mm]	2.7±0.2	2.4±0.2	2.8±0.2	2.9±0.2	NS	NS	NS
LVID, D [mm]	4.0±0.2	3.8±0.3	4.2±0.2	4.1±0.2	NS	NS	NS
Diastolic Function							
AET [ms]	52.3±1.6^{A}	59.2±2.2^{B}	51.4±1.6^{A}	53.2±1.4^{A}	-	-	0.042
MVDT [ms]	26.0±4.6	22.0±6.3	21.1±4.4	21.2±4	NS	NS	NS

Table 4.2 (cont'd).

MV A [mm/s^2]	320.4±30.3^{A}	448.1±41.6^{B}	335.2±29.5^{A}	328.6±27.0^{A}	-	-	0.044
MV E [mm/s^2]	598.7±46.0	675.1±63.2	523.4±44.9	641.1±40.4	NS	NS	NS
MV E/A	1.9±0.2^{A}	1.5±0.2^{B}	1.6±0.2^{B}	2.0±0.1^{A}	-	-	0.045
IVCT [ms]	10.8±1.4^{A}	8.6±1.9^{A}	12.7±1.4^{B}	11.9±1.3^{B}	0.02	NS	NS
IVRT [ms]	15.1±1.1^{A}	16.9±1.5^{A}	18.0±1.1^{B}	17.5±0.9^{B}	0.03	NS	NS
Global Function							
Stroke Volume [µl]	45.7±2.5^{A}	43.2±2.8^{A}	38.9±2.4^{B}	36.8±2.1^{B}	0.01	NS	NS
Cardiac Output [ml·min^{-1}]	18.5±1.3^{A}	16.9±1.8^{A}	14.2±1.3^{B}	13.4±1.2^{B}	0.02	NS	NS
Myocardial Performance Index	0.49±0.03^{A}	0.43±0.04^{A}	0.59±0.03^{B}	0.55±0.03^{B}	0.02	NS	NS

LV: left ventricle. S: systole. D: diastole. LVID, S: left ventricle internal diameter [systole]. LVID, D: left ventricle internal diameter [diastole]. AET: ejection time from opening to closing of the aortic valve. MVDT: deceleration time. MV A: blood flow velocity following atrial contraction. MV E: Blood flow velocity during early diastole. MV E/A: Ratio of MV E to MV A. IVCT: left ventricle isovolumetric contraction time. IVRT: Isovolumetric relaxation time. Values are Means ± Standard Error. Difference in superscripted letters across a row indicates statistical significance [$p<0.05$]. [CON; n= 4 males, n= 3 females and PUN; n=4 males, n=5 females]

Discussion

The Developmental Origins of Health and Disease [DOHaD] states growth restriction increases the risk for chronic disease in adulthood[2]. Specifically, low birth and infantile weight at 1-year leads to a 47% increased risk for hypertension and CV disease in adulthood[11, 31]. Using diet manipulation, we showed that body mass across the lifespan of PUN mice were significantly less than controls [Figure 4.3]. Absolute heart mass of PUN mice was significantly less than controls at PN21, but not at PN80, suggesting heart mass was recuperated even though body

mass was reduced [Figure 4.4]. These findings support previous growth restriction research[48, 205], which demonstrate preferential organ development for the heart and brain. The "preferential sparing" of vital organs may come at the expense of peripheral structures such as skeletal muscle and bone, leading to reduced body mass[100].

While heart mass was recuperated from PN21-80, functional impairments existed into adulthood. The PUN group had impairments in LV mass, stroke volume, cardiac output, MPI, and diastolic dysfunction in adulthood. These findings support the existing DOHaD literature, which have shown postnatal growth restriction in mice impairs functional capacity of the heart, calcium flux, and exercise capacity, thus leading to an increased risk for CV disease and mortality in adulthood[6, 42, 44, 46-48, 51, 61, 77, 78, 185, 222-225].

Currently, there is limited information on the molecular mechanisms associated with cardiac impairment from growth restriction. Of the literature present, protein kinase B [*Akt*] and Endothelin-1 [*Edn1*] are shown to be associated with CV impairment caused by early life growth restriction[64, 65, 78]. Our results did not identify differences in protein abundance of these previously identified proteins, possibly due to differences in methodology[2, 4, 8, 9, 32, 46, 49, 59, 168, 191, 205, 223]. Studies showing Akt activation used placental arterial ligation to reduce nourishment to the fetus[65, 226], and Neerhof *et. al.* showed *Edn1* is activated through platelet activating factors in the ischemic intrauterine environment[65]. Thus, methodologies that alter oxygen delivery to the fetus could confound mechanistic results by presenting proteins associated with hypoxemia in addition to growth restriction.

The mice in this experiment were genetically homogeneous, thus any change in protein abundance is due to the 21-day window of postnatal growth restriction. PN1-21 is associated with cardiomyocyte binucleation[44, 46], LV remodeling[51, 61] and increased strength of

contraction[204, 227-229]. The REACTOME analysis revealed pathways [Figure 4.6] in the areas of extracellular matrix organization/muscle contraction, and cell cycling, while the interaction networks from STRING [Figure 4.7A-D] showed significant PPI's from five nodes. These results support existing literature related to growth restriction, showing impaired cardiomyocyte nucleation[4, 46, 47, 58, 230] and cardiac muscle contraction/cell structure[227, 228, 231-235]. From our analysis, we propose a potential molecular mechanism [Figure 4.8] whereby postnatal growth restriction alters the extracellular matrix, cell cycle, and cardiac contraction, which may influence the CV impairment seen in adulthood.

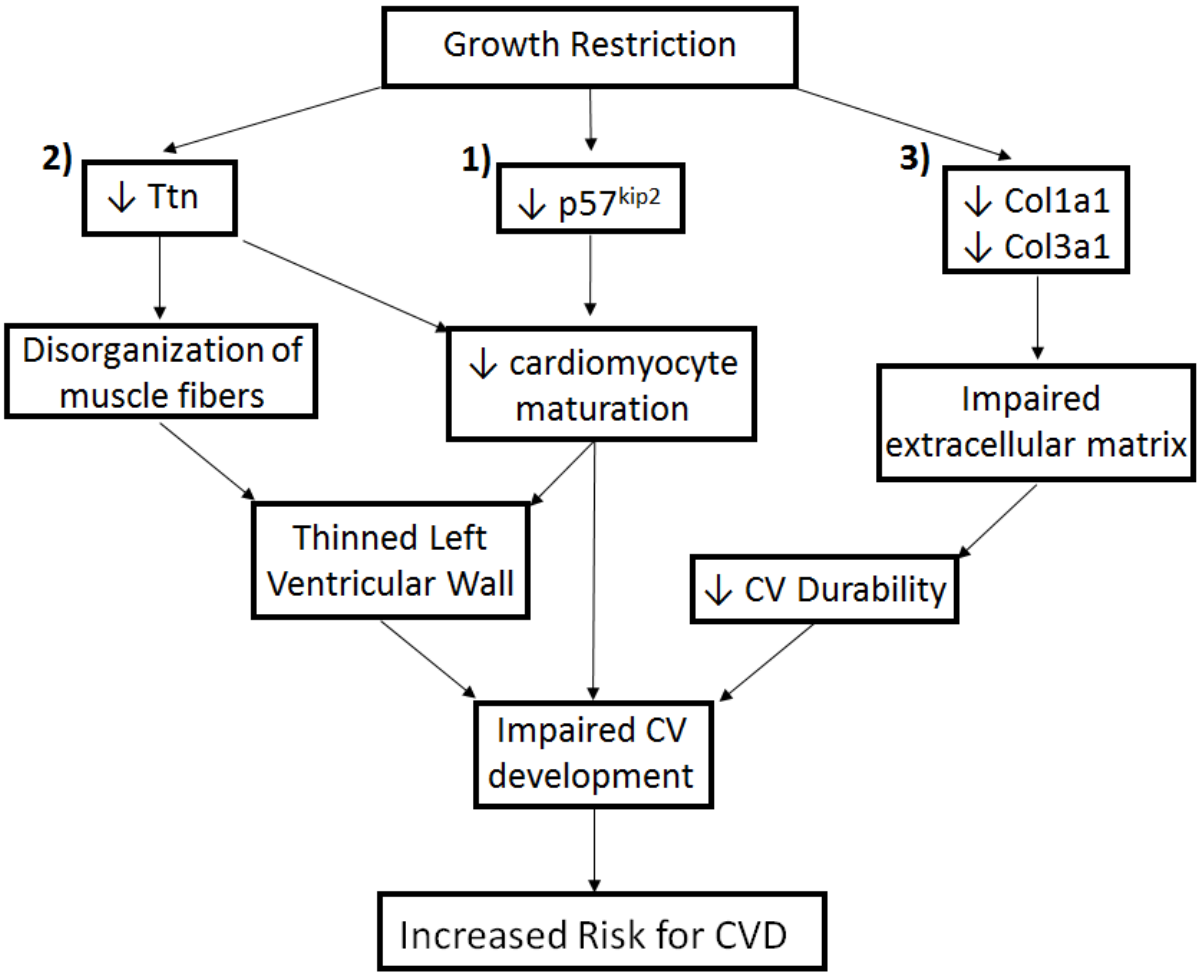

Figure 4.8: Hypothesized schema of how postnatal growth restriction alters extracellular matrix organization, the cell cycle, and contraction. 1] $p57^{kip2}$, is reduced during PN21,

Figure 4.8 (cont'd).

leading to impaired cardiomyocyte maturation and thinning of the LV wall. 2] Reduced Ttn abundance during first 21 days of life also causes a thinning of the LV wall, and disorganization of cardiac muscle fibers, which is not recuperated into adulthood. 3] Reduced collagen fiber networks impairs the extracellular matrix and diminishes CV durability across the lifespan. The convergence of these proteomic alterations in the growth restricted heart increase the risk for CVD in adulthood.

Impaired Extracellular Matrix, Cell Cycle, and Contraction

The PUN mice showed reduced collagen abundance at PN21 and PN80 when compared to the CON mice. Collagen abundance is necessary for proper extracellular matrix organization, cardiac structure, and functional durability across the lifespan[233]. Reduced protein abundance of Col1a1 and Col3a1 using transgenic mice has previously shown cardiac impairment[236]. Additionally, Col1a1 and Col3a1 are used as markers for valvular integrity[235], cardiac fibrosis[234], and connective tissue disease[232]. Therefore, postnatal growth restriction in mice disrupts the abundance of collagen fibers, which may lead to a pathological state from an altered extracellular matrix across the lifespan.

At PN21, our 2D DIGE [p=0.019] and western blot [p=0.007] results showed that $p57^{kip2}$ abundance was significantly less in the PUN mice compared to CON mice. Cyclin dependent kinase inhibitors play a role in cardiomyocyte development by regulating cellular proliferation[58, 230,237]. Haley *et. al.* demonstrated that $p57^{kip2}$ knockout mice undergo increased cellular apoptosis in the heart[238] with altered cellular proliferation[239]. Therefore, the alterations in $p57^{kip2}$ at PN21 may be responsible for the impaired cardiomyocyte binucleation from growth restriction in early life shown previously[44, 46, 48, 50, 51, 75, 240]. In addition to cell cycle regulation, the reduced abundance of $p57^{kip2}$ thins the trabecular layer of the developing heart reducing mass and contractile force [Figure 4.8][241]. While $p57^{kip2}$ was reduced at PN21 it was recovered at PN80 possibly due to the cessation of the cell cycle following cardiomyocyte endowment.[76, 237, 242].

The PUN mice displayed reduced Ttn abundance at PN21 and PN80 compared to the CON mice, indicating that there is a reduction in the costamere responsible for spatial orientation of cardiac muscle fibers[227, 228]. Ttn binds to myosin and operates as a framework for the thick myofilament[243], regulating cardiac muscle force production[244, 245]. Radke *et. al.* showed *N2b* deletion on the gene that encodes for Ttn leads to diastolic dysfunction and cardiac atrophy[228], similar to the pathology seen in our PUN mice [Table 4.2].

Due to the limited reliability of western blotting for Ttn and a reduced specificity of antibodies for collagen proteins, we used silver nitrate staining to confirm the relative protein abundance between our PUN and CON mouse hearts[214-217, 227, 228, 246]. We acknowledge that Ttn and collagen are not the only proteins found in the reported high molecular weight range, but the 2D DIGE combined with nano-LC/MS/MS and our echocardiography results permit Ttn and collagen as proteins of interest.

Conclusion

Postnatal growth restriction during the first 21 days of mouse life reveals cardiac proteomic differences compared to controls. These alterations in protein abundance center on the structural impairments to the extracellular matrix [Col1a1/Col3a1], the regulation of the cardiomyocyte cell cycle [$p57^{kip2}$] and impaired cardiac muscle contraction [Ttn]. These proteomic alterations in the PUN mouse hearts were associated with cardiac impairment in adulthood as evaluated by echocardiography and Doppler blood flow analysis. Future directions should aim to modulate the expression of these identified proteins in order to mitigate cardiac impairment. Furthermore, this investigation only confirmed proteins based on the existing robust literature. The remaining proteins from the 2D DIGE results should be confirmed and their role in cardiac function during early life growth restriction elucidated.

Disclosures

No conflicts of interest, financial or otherwise, are declared by the authors.

Acknowledgments

The authors wish to thank Teresa Krieger-Burke of the In-vivo core at Michigan State University, as well as the undergraduate volunteers in the Neonatal Nutrition and Exercise Research Lab at Michigan State University.

Grants

This project was funded with start-up funds from the Department of Kinesiology at Michigan State University.

CHAPTER 5: POSTNATAL GROWTH RESTRICTION IN MICE ALTERS CARDIAC MITOCHONDRIAL ENERGETICS

Abstract

Postnatal growth restriction leads to cardiovascular disease [CVD] potentially from impairments to cardiac metabolism and oxidative phosphorylation [OxPhos]. The purpose of this investigation was to determine if postnatal growth restriction impairs OxPhos when cardiac mitochondria are fueled with pyruvate+malate [PM], succinate+rotenone [S+R], or palmitoylcarnitine+malate [PCM]. FVB mouse dams were fed a control [CON: 20% protein], or a low-protein [LP: 8% protein] isocaloric diet 2-weeks before mating. LP-dams produce 15-20% less milk thereby pups nursed by LP-dams undergo growth restriction. At birth postnatal [PN1] pups born to dams fed the CON diet were crossed to LP-dams [PUN; postnatally undernourished] or a different CON-dam [control]. At PN21, weaned mice were transferred to the CON-diet. On PN22 and PN80 cardiac mitochondria were isolated via differential centrifugation and functional analysis conducted by measuring oxygen flux [JO_2] and ROS emission [H_2O_2 flux] via high-resolution respirometry [HRR]. Outcome measures of interest were examined by ANOVA to determine the main effects of diet [CON vs. PUN], sex [male vs. female], and age [PN22 vs. PN80] on body mass, heart mass, tibia length, JO_2, and H_2O_2 flux. An α level of 0.05 was set *a priori* and if necessary, a Tukey's HSD post hoc test used. PUN had a significant reduction [p=0.01] across both timepoints in PM-RCR [PN22; males: 7.9±0.7, females: 7.9±0.7 and PN80; males: 8.7±0.6, females: 7.1±1.7] compared to controls [PN22; males: 9.5±0.3, females: 9.0±0.8 and PN80; males: 8.5±1.6, females: 8.5±0.9]. PN80-PCM-LEAK was significantly increased [p=0.02] in the PUN [males: 70.7±9.1 nmol/mg/min and females: 63.2±6.1 nmol/mg/min] compared to the CON [males: 60.3±4.5 nmol/mg/min and females; 57.3±3.2 nmol/mg/min]. During PM-LEAK [p<0.01] & ADP_{max} [p=0.02], at PN22, the PUN-F [LEAK: 119.9±18.8 pmol/mg/min, ADP_{max}: 77.3±22.0 pmol/mg/min] had greater ROS emission than CON-F [LEAK: 97.6±6.3 pmol/mg/min, ADP_{max}: 65.7±8.0 pmol/mg/min], but at

PN80 the PUN-M [LEAK: 123.9±11.4 pmol/mg/min, ADP_{max}: 74.5±7.0 pmol/mg/min] had greater ROS emission than CON-M [LEAK: 101.6±2.7 pmol/mg/min, ADP_{max}: 62.0±4.3 pmol/mg/min]. Postnatal growth restriction reduced RCR, increased LEAK state JO_2, and elevated ROS emission. Thus, postnatal growth restriction reduces OxPhos capacity and increases oxidative stress, which may increase the risk for CVD across the lifespan.

Introduction

Children who are growth restricted have a higher risk of chronic disease in adulthood[31]. Specifically, 7 million CV related deaths occur each year due to growth restriction[6, 8, 27, 247-249]. Therefore, the health outcomes of growth restriction are extremely relevant to the current CV health crisis facing the world today. Growth restriction of mice during the postnatal window of development has shown reduced left ventricular mass, diminished stroke volume and resting diastolic dysfunction through differences in cardiomyocyte nucleation[48, 77]. Additionally, cardiomyocytes that experience postnatal growth restriction show impaired Ca^{2+} flux[48], which increase the risk of cardiac arrhythmias in adulthood[6]. Despite this known pathology, there is minimal research investigating cardiac metabolism of growth restricted hearts. Impairments to mitochondrial function alter cardiac metabolism and lead to the progression of CVD[86]. Therefore, the crucial next step in alleviating CVD risk in the growth restricted population is to determine the metabolic properties of postnatally growth restricted hearts.

For the heart to contract, cardiomyocytes require a constant supply of cellular energy from mitochondria via adenosine triphosphate [ATP][147]. When cardiac mitochondria are fueled by different substrates, they use metabolic pathways that converge on oxidative phosphorylation [OxPhos][250, 251]. The majority of ATP [>95%] in the heart is synthesized through the shuttling of

electrons within protein complexes [CI, II, III, & IV] which comprise the electron transport chain [ETC][148, 154, 161, 252-256].

Substrate utilization in the fetal mammalian heart relies primarily upon glucose and lactate, but quickly transitions to fatty acid oxidation [FAO] in the postnatal environment[257-259]. The mature, non-growth restricted myocardium develops 60-90% of its ATP from FAO, while the influence from carbohydrate metabolism is lesser [10-30%][260, 261]. Cardiac energetics literature has shown that reductions in mitochondrial function with increased oxidative stress leads to cardiac pathology, and metabolic inflexibility[80-84, 86, 158, 262-264]. Impairments to cardiac metabolism of adult female offspring subjected to intrauterine growth restriction have shown reductions in FAO in the presence of octanoylcarnitine[79], but there is no literature regarding the influences of postnatal growth restriction on cardiac metabolism, thus leaving a gap in the literature as postnatal growth restriction is also associated with cardiac impairment[6, 48, 77].

The purpose of this study is to determine the effects of postnatal growth restriction on mitochondrial function *in vitro* through high-resolution respirometry when isolated cardiac mitochondria are fueled with various substrates [carbohydrates, Krebs cycle intermediates, and fatty acids]. Using substrates targeting different metabolic pathways and measuring cardiac mitochondrial respiration together with ROS emission, we determined the role of postnatal growth restriction on cardiac metabolism. We hypothesize that postnatal growth restriction will cause reductions in mitochondrial function during juvenile development, which will persist into adulthood, contributing to the development of CVD.

Methods

All experiments were performed in accordance with the Guide for the Care and Use of Laboratory Animals and were approved by the Institutional Animal Care and Use Committee at Michigan State University. All animals were housed in the vivarium on wood-chip bedding in a well-maintained room at 21°C with a 12 h light/dark cycle.

Nutritive Model

Postnatal growth restriction was induced using diet manipulation [Figure 5.1] as previously described[49]. Briefly, FVB [Charles River Laboratories, Wilmington, MA, USA] third parity dams consumed a semi-purified control diet [20% protein; Research Diets, New Brunswick, NJ, USA] based on AIN93G, or a low-protein [LP] isocaloric diet [8% protein] two weeks prior to breeding [the composition of the research diets has also been explained previously[6]]. Dams that consume a LP diet yield 15-20% less milk compared to controls[87, 103, 105, 106, 183, 184], causing the pups to have an 18% reduction in body mass[87, 103, 105, 106, 183, 184]. Breeding was conducted by placing one male in a female cage for a 24-hour period ensuring all pups born were the same age. At postnatal day [PN] 1, pups born were weighed, sexed, and cross-fostered to produce two experimental groups. Pups born to dams fed the control diet were pooled and distributed to either: *1] Control Group [CON]:* pups born to a control dam then cross fostered to a different control dam; n=10 litters; *2] Postnatal Undernutrition Group [PUN]:* pups born to a control dam then cross fostered to a dam fed the LP diet; n=10 litters. Pups born from LP dams were not used in this study.

Each litter consisted of 8 pups [4 males, 4 females] and individual pups within a litter were given tattoo identification. All litters were made equal size, sex ratio, and starting body

mass. Litter size was preserved throughout lactation by using 'donor' pups of similar age to supplant any fatalities; these pups were not included in this study. At PN22, a sub cohort was placed under 1% isoflurane anesthesia and euthanized via cervical dislocation then hearts were analyzed by high-resolution respirometry [HRR] [see below]. The remaining littermates were placed on the control diet after weaning until PN80. Thus, postnatal growth restriction was isolated to the developmental window throughout lactation [PN1-PN21]. At PN80, mice were euthanized using the same technique described above for PN22. Hearts were removed, weighed and used for mitochondrial isolation in HRR. Heart mass is shown as absolute and standardized to body surface area [BSA], using Meeh's formula[188]:

Body surface area = 9.662 x [body weight] $^{0.667}$.

Body surface area standardization is a method commonly used to compare mice of different body masses[188, 206]. Tibia length was determined using digital Vernier calipers [General Tools, Secaucus, NJ] as a substitute for body composition and lean tissue growth[207].

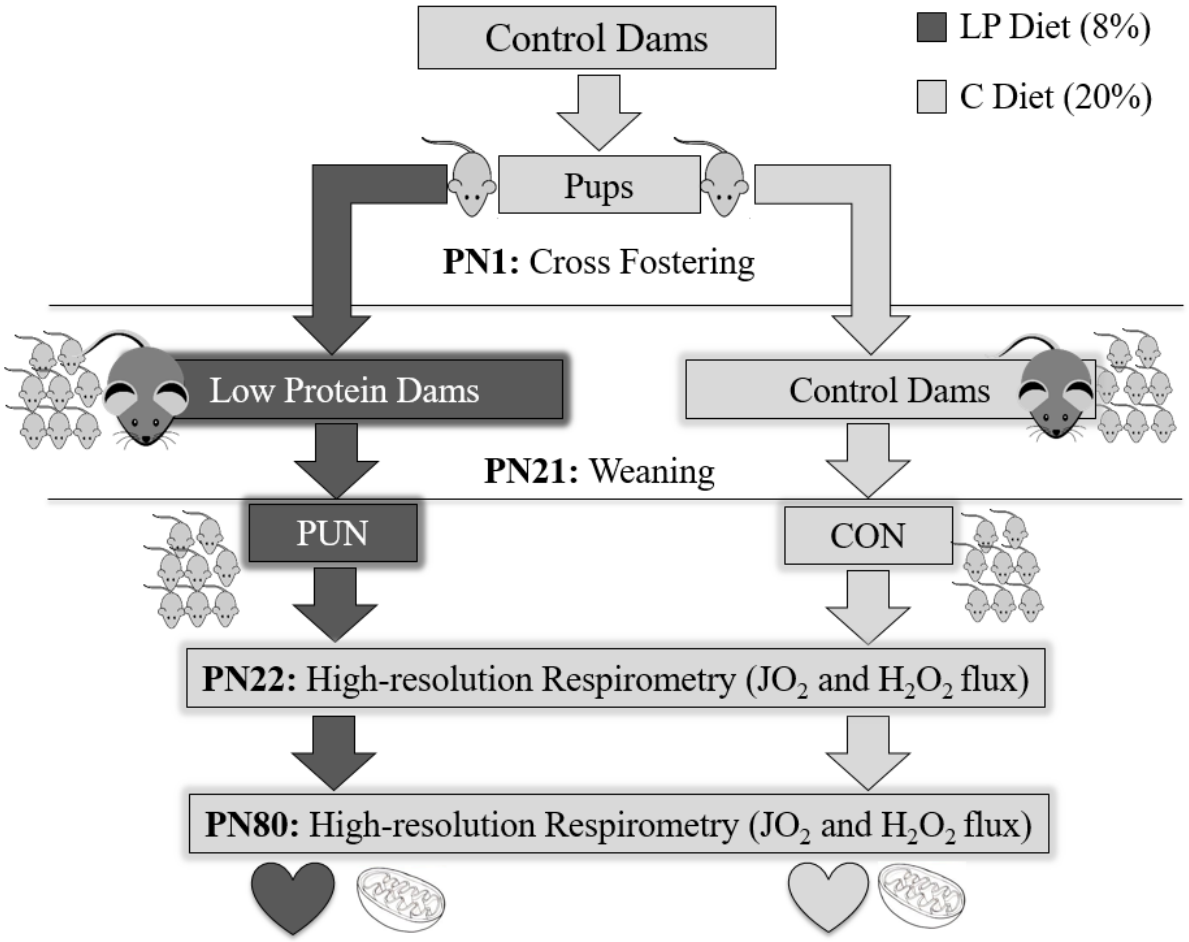

Figure 5.1: Cross-Fostering Methodology for Postnatal Growth Restriction. Two weeks before breeding, dams were given access to control diet [20% protein] or isocaloric low protein diet [8% protein]. CON born pups were pooled and cross-fostered to a different control fed dams [CON group; n=10 litters] or a different low protein fed dam [PUN group; n=10 litters], the pups born to LP dams were not used in this study. At PN21, all mice were weaned to the control diet, thus postnatal growth restriction was isolated to the developmental window of lactation. Following a day of rest, at PN22 [post-weaning], cohorts of mice were euthanized, and hearts were surgically removed. After which, mitochondria were isolated via differential centrifugation for high-resolution respirometry, consisting of JO_2 and H_2O_2 flux measurements. This process was repeated with different mice treated with the exact same cross-fostering method of growth restriction in adulthood at PN80.

Isolation of mitochondria and protein quantification

Cardiac mitochondria was isolated from FVB mouse hearts at 2 developmental ages [PN22 & PN80] through differential centrifugation [all spins were completed at 4°C for 10

minutes] as published previously[250]. Briefly, mice were placed under 1% isoflurane anesthesia, until unresponsive to a physical stimulus. Following cervical dislocation, the heart was surgically removed and rinsed in cold cardioplegic solution [25 mM KCl, 100 mM NaCl, 10 mM dextrose, 25 mM MOPS, and 1 mM EGTA, 0.22 µm sterile filtered at pH 7.5]. Hearts were then washed and minced in cooled isolation buffer [IB; 200 mM mannitol, 50 mM sucrose, 5 mM dibasic potassium phosphate, 5mM MOPS, 1 mM EGTA, and 0.1% BSA at pH 7.15]. After mincing with scissors, the nearly 1 mm^3 sized tissue sections were placed in a 50 mL tube containing 25 mL IB and 0.5 U/mL of protease. The solution was homogenized at 18,000 rpm for 20 seconds with a 110 mm probe Omni homogenizer [Omni Inc., Kennesaw, GA]. Following homogenization, the first spin occurred at a speed of 8,000 x g in a tabletop centrifuge resulting in a pellet. The supernatant was discarded, and the pellet was rinsed and re-suspended via vortex in IB [25 mL] then spun for a second time at a slower speed of 800 x g. Following this spin, the supernatant was placed into a clean 50 mL falcon tube, and the pellet was discarded. A third and final spin of 8,000 x g produced a mitochondrial rich pellet which was always kept on ice and was never used for more than 8 hours. The pellet was then re-constituted in a small volume of IB [10-20 µl]. The BCA assay[265] with bovine serum albumin standards was used for determining total mitochondrial content using a Synergy H1MG plate reader [Biotek, Winooski, VT]. Based upon the total mitochondrial content, all samples were then standardized to a concentration of 30 mg/ml using isolation buffer. Thus, allowing for comparisons across all experimental groups and time points, since the concentration of samples was equal.

High-Resolution Respirometry [HRR]

Respiration flux [JO_2] was measured at 37°C using an Oroboros Oxygraph 2K high-resolution respirometer system [Oroboros Instruments, Innsbruck, Austria]. The oxygraph uses

an amperometric sensor to determine the oxygen consumption and concentration of oxygen in a closed chamber. CON and PUN cardiac mitochondria were injected into the oxygraph machine with oxygenated respiration buffer [5mM ATP, 5 mM dibasic potassium phosphate, 6 mM magnesium chloride, 130 mM potassium chloride, 1 mM EGTA, 20 mM MOPS, and 1% w/v BSA at pH 7.1]. Experimental conditions varied with the presence of 5 mM sodium pyruvate and 1 mM L-malate [PM; carbohydrate; Complex I substrate], 5mM succinate and 1 μM rotenone [S+R; Krebs Cycle Intermediate; Complex II substrate and Complex I-inhibitor], or 25 μM palmitoyl-carnitine and 1 mM L-malate [PCM; fatty acid oxidation]. Ethylene glycol-bis-tetra-acetic acid [EGTA], a calcium-chelating agent was added since previous literature has indicated that calcium overload inhibits isolated mitochondrial respiration, particularly in the presence of PCM[150, 155, 156, 250, 266].

When the isolated cardiac mitochondria were fueled by different substrates [PM, S+R, or PCM], two steady states of JO_2 were recorded [Figure 5.2]. The steady states evaluated have previously been described[150] in increasing order of ATP synthesis as follows: [1] LEAK state[93], where mitochondria respire to maintain resting membrane potential, and [2] ADP stimulated maximal respiration by the addition of 0.5 M ADP where the mitochondria consume oxygen in the ETC for the synthesis of ATP.

Additionally, coinciding with JO_2, reactive oxygen species [ROS] emission was evaluated through a fluorometric measurement of hydrogen peroxide [Amplex® Ultrared, Thermo Fisher, Waltham, MA] as previously described[92]. ROS calibration was performed before data collection by continually adding 0.1 μM H_2O_2 and ROS detection was performed by using 10 μM Amplex® Ultrared, 1 U/mL horse radish peroxidase [HRP], and 5 U/mL superoxide dismutase [SOD] in the chambers. Stable portions of the ROS-H_2O_2 flux were measured and any

noticeable artifact in the recording was excluded. Thus, allowing for a measurement of oxidative stress of isolated mitochondria in the diet groups since ROS emission has been linked to oxidative damage in diseases such as ischemia, diabetes, and athersclerosis[92].

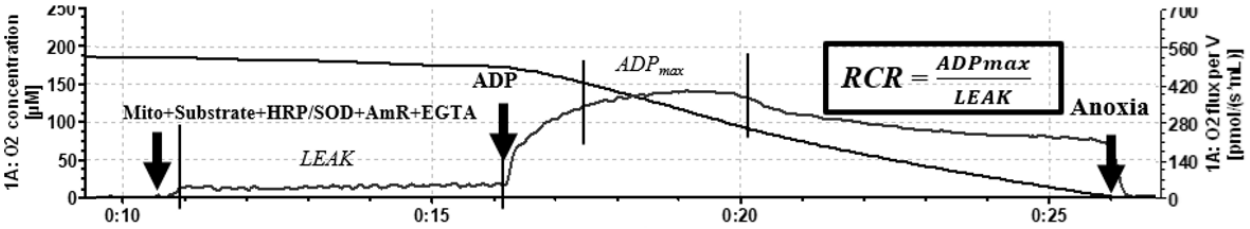

Figure 5.2: Representative Oxygraph recording for JO_2. Various substrates were loaded into the oxygraph chambers [PM, S+R, or PCM]. Next, horse radish peroxidase [HRP] and superoxide dismutase [SOD] were added since the Amplex Ultrared [AmR] to H_2O_2 reaction is catalyzed by HRP and the main species of mitochondrial ROS produced is superoxide anion which is rapidly converted to H_2O_2 by SOD. Then AmR is added as a fluorescent probe for H_2O_2 detection via the O2k-Fluorometer. EGTA, is then added as a calcium-chelating agent. Cardiac mitochondria [CON or PUN; 30 mg/ml] were injected into the chambers for the measurement of LEAK state respirometry [5 minutes]. A bolus of ADP is then added to stimulate mitochondrial respiration until the chamber becomes anoxic. The measurement of respiratory control ratio [RCR] is computed by dividing the maximally stimulated ADP respiration [ADP_{max}] by the LEAK state. The left y-axis is the concentration of oxygen in the chamber [µM], while the right y-axis is the JO_2 flux [pmol/s*mL]. The unit of pmol/[s*mL] is converted into nmol/mg/min. The x-axis is time, as measured in minutes.

Statistics

The Shapiro-Wilk and D'Agostino-Pearson omnibus test were used to verify normality of data. If data were not normally distributed a logarithmic transformation was performed. Following which, a linear model and repeated measures ANOVA were used to compare growth curves between the CON and PUN groups [GraphPad Prism, v7.01, San Diego, CA]. Two-way ANOVAs were used with the main effects of diet [CON vs. PUN] and sex [male vs. female] to compare heart mass [absolute or standardized], and tibia length. An α level of $P<0.05$ was set *a priori* and if necessary, a Tukey's HSD post hoc test was used for multiple comparisons. Three-way ANOVAs were used for JO_2 and H_2O_2 flux measurements with the main effects of diet

[CON vs. PUN], sex [male vs. female], and age [PN22 vs. PN80]. An α level of $P<0.1$ was set *a priori* for the main interaction of Diet*Sex*Age.

Results

Body Mass

PN1-22

Postnatal growth restriction caused significant reductions in body mass starting at PN7 [CON-M; 4.668±0.426 g and CON-F; 4.700±0.485 g vs. PUN-M; 3.500±0.312 g and PUN-F; 3.377±0.359 g, Figure 5.3A] continuing through weaning at PN21 [CON-M; 11.311±1.101 g and CON-F; 11.455±1.114 g vs. PUN-M; 8.159±0.579 and PUN-F; 7.931±0.588 g]. Final body mass at PN22 was also significantly reduced [$p<0.001$] in the PUN mice [males; 8.48±0.792 g and females; 8.43±0.396 g] compared to the CON mice [males; 12.122±1.059 g and females; 12.314±0.580 g]. There were no sex differences between males and females during this window of development [Figure 5.3B].

PN22-80

As seen in Figure 5.3A, postnatal growth restriction significantly [$p<0.0001$] reduced body mass at every weighing throughout the experiment [PN22 to PN80]. Final body mass [Figure 5.3B; PN80] of the postnatally growth restricted mice [males; 25.146±2.176 g and females; 19.257±0.923 g] were significantly reduced [$p<0.001$] when compared to unrestricted controls [males; 29.47±3.321 g and females; 22.518±1.853 g]. There was a significant sex effect [$p<0.001$] starting at PN28 through PN80, where males had greater body mass than females.

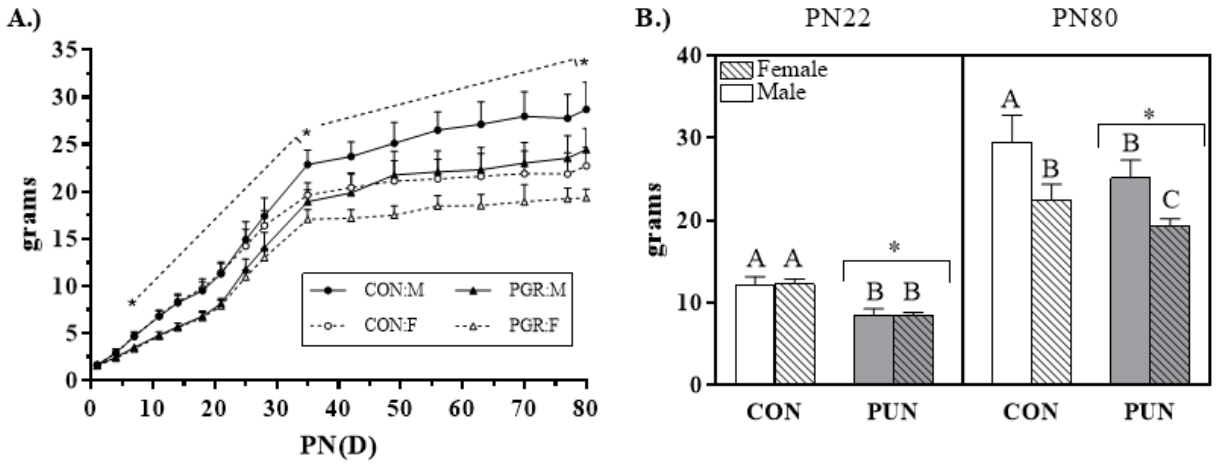

Figure 5.3: Influence of Postnatal Growth Restriction on Body Mass: A.] Growth Curve from PN1-P80; Starting at PN7 through PN22 growth restriction significantly [p<0.001] decreased the body mass of the PUN when compared with the CON group, with no sex effect. At PN25, postnatal growth restriction continued to cause significant [p<0.001] reductions in body mass until PN80. Sex differences started at PN28 and continued until PN80 [p<0.001], with males being larger than females. Repeated measures ANOVA was used in panel A. **B.] Final Body Mass at Respirometry [PN22 and PN80];** Final body mass on the days of PN22 respirometry was significantly reduced [p<0.001] in the PUN when compared with the CON group, with no sex effect. Final body mass on the days of PN80 respirometry was also significantly reduced [p<0.001] in the PUN when compared with the CON group. A sex effect was present at PN80 with males being larger than females [p<0.001]. Two-way ANOVA within each time-point [PN22 or PN80] with a Tukey HSD multiple comparison test were used in panel B. Values are mean±sd. Levels within the figure not connected by the same letter [A, B, or C] represent statistical significance [p<0.05]. *, significantly different from CON group.

Heart Mass & Tibia Length

PN22

Absolute heart mass [Figure 5.4A] of postnatally growth restricted mouse hearts was significantly reduced [p<0.001] at PN22 when compared to CON hearts [CON-M; 0.085±0.005 g and CON-F; 0.079±0.008 g vs. PUN-M; 0.068±0.010 g and PUN-F; 0.062±0.008 g]. There was a significant sex effect [p=0.007], with male heart mass being greater than females.

When heart mass was standardized to body surface area, the significant diet effect disappeared [p=0.68, Figure 5.4B], indicating that hearts were proportional for the size of the

mouse [CON-M; 0.0016±0.0001 kg/cm^2 and CON-F; 0.0015±0.0001 kg/cm^2 vs. PUN-M; 0.0017±0.0001 kg/cm^2 and PUN-F; 0.0015±0.0002 kg/cm^2]. However, the sex effect remained significant [p=0.005], with male hearts having larger standardized heart mass than females.

Postnatal growth restriction significantly reduced [p<0.001] average tibia length [Figure 5.4C] at PN22 in the PUN mice [males; 13.891±1.172 mm and females; 13.220±0.938 mm] when compared to the CON mice [males; 15.203±1.030 mm and females; 14.928±0.782 mm]. There was no significant sex effect on average tibia length during this developmental window [p=0.08].

PN80

Absolute heart mass in adulthood of postnatally growth restricted mouse hearts was significantly reduced [p<0.001] when compared to CON hearts [CON-M; 0.138±0.019 g and CON-F; 0.124±0.016 g vs. PUN-M; 0.117±0.009 g and PUN-F; 0.105±0.007 g]. Again, there was a significant sex effect [p=0.007] with male heart mass being larger than females. At PN80, standardized heart mass was not significant between controls and postnatally growth restricted mice.

Average tibia length in adulthood was significantly reduced [p<0.001] in the postnatally growth restricted mice [PUN-M; 17.698±0.490 mm and PUN-F; 16.854±0.469 mm vs. CON-M; 18.155±0.387 mm and CON-F; 17.735±0.381 mm]. However, post-hoc analysis revealed that tibia length was only significantly reduced in the PUN-F mice as compared to controls [both comparisons; p<0.001]. Additionally, there was a significant sex effect in adulthood [p<0.001], with males having longer tibias than females.

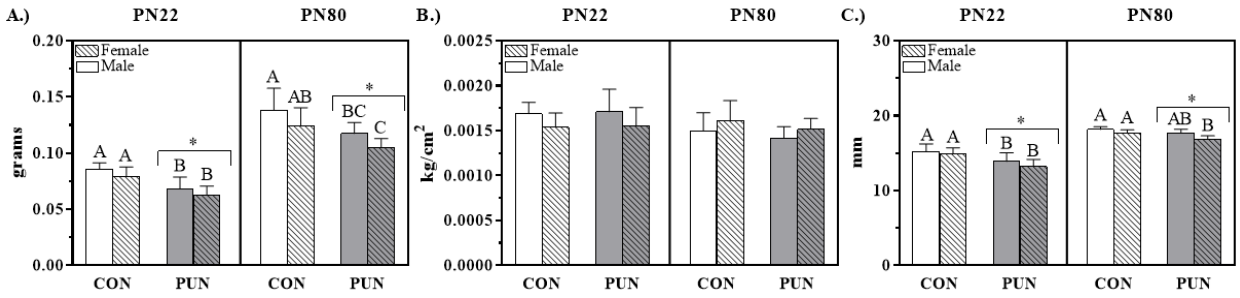

Figure 5.4: Influence of Postnatal Growth Restriction on Heart Mass and Tibia Length. A.] Absolute Heart Mass [PN22 and PN80]: The PN22-PUN hearts were significantly less [$p<0.001$] than the CON group, with a sex effect present [males > females; $p=0.007$]. The PN80-PUN hearts were significantly reduced [$p<0.001$] when compared to CON hearts, with a similar significant sex effect [$p<0.007$]. **B.] Standardized Heart Mass [PN22 and PN80]:** There is no significant difference at PN22 or PN80, and there was no sex effect present. **C.] Tibia Length [PN22 and PN80]:** Postnatal growth restriction significantly reduced [$p<0.001$] average tibia length at PN22 when compared to CON group, with no sex effect present. At PN80, tibias of PUN were significantly less [$p<0.001$] than the CON group, however only PUN-F [$p<0.001$] were significantly reduced from controls through post-hoc analysis. Values are mean±sd. Two-way ANOVA's within each time-point [PN22 or PN80] with the main effects of diet [CON vs. PUN] and sex [Male vs. Female] with a Tukey HSD multiple comparison test were used. Levels within the figure not connected by the same letter [A, B, or C] represent statistical significance [$p<0.05$]. *, significantly different from CON group.

Respirometry [JO_2]

Respirometry results during early life [PN22] and adulthood [PN80] can be viewed in Table 5.1.

Table 5.1: Respirometry [JO_2] between control [CON] and growth restricted [PUN] mice at PN22 & PN80.

	CON				*PUN*				*p-value*						
	males		*females*		*males*		*females*		*Diet*	*Sex*	*Age*	*Diet*Sex*	*Diet*Age*	*Sex*Age*	*Diet*Sex*Age*
PN	*22*	*80*	*22*	*80*	*22*	*80*	*22*	*80*							
	PM [CI]														
LEAK	37.3 ± 5.9	39.5 ± 5.9	40.7 ± 7.5	40.9 ± 3.3	46.1 ± 5.3	40.2 ± 7.0	45.0 ± 7.2	45.3 ± 10.7	.06	.4	.7	.9	.4	.7	.4
ADP	353.8 ± 47.7	328.2 ± 18.0	363.9 ± 47.4	342.9 ± 19.0	367.9 ± 56.9	348.8 ± 42.6	367.9 ± 56.9	309.8 ± 17.6	.7	.5	.1	.1	.9	.9	.7
RCR	9.5 ± 0.3^{A}	8.5 ± 1.6^{A}	9.0 ± 0.8^{A}	8.5 ± 0.9^{A}	7.9 ± 0.7^{B}	8.7 ± 0.6^{B}	7.7 ± 1.2^{B}	7.1 ± 1.7^{B}	**.01**	.1	.4	.4	.2	.6	.2
	S+R [CII]														
LEAK	176.4 ± 5.8	165.2 ± 14.7	173.2 ± 7.2	167.1 ± 16.8	176.2 ± 2.3	193.6 ± 34.9	169.4 ± 18.1	171.0 ± 18.4	.3	.3	.9	.3	.2	.8	.5
ADP	567.0 ± 12.7	505.4 ± 23.2	544.2 ± 45.0	545.2 ± 16.6	552.6 ± 30.7	558.1 ± 23.4	521.4 ± 54.1	513.8 ± 19.2	.7	.2	.2	.06	.2	.3	.1

Table 5.1 (cont'd).

RCR	3.21 ± 0.1	3.1 ± 0.4	3.1 ± 0.1	3.3 ± 0.3	3.1 ± 0.2	2.9 ± 0.4	3.1 ± 0.3	3.0 ± 0.2	.2	.7	.5	.8	.5	.3	.8
	PCM [FAO]														
LEAK	67.9 ± 2.8^{A}	60.3 ± 4.5 ^{B}	67.6 ± 4.5^{A}	57.3 ± 3.2^{B}	65.4 ± 2.9^{AB}	70.7 ± 9.1^{A}	66.4 ± 7.0^{AB}	63.2 ± 6.1^{A}	.1	.2	.06	.7	**.02**	.2	.5
ADP	391.5 ± 13.5^{A}	321.9 ± 46.5^{B}	390.8 ± 31.1^{A}	360.1 ± 24.0^{B}	361.5 ± 27.7^{A}	373.4 ± 65.4^{B}	363.5 ± 38.3^{A}	314.1 ± 25.8^{B}	.3	.7	**.01**	.08	.3	.7	**.07**
RCR	5.8 ± 0.2	5.4 ± 1.1	5.7 ± 0.1	5.9 ± 0.8	5.5 ± 0.2	5.3 ± 0.3	5.5 ± 0.5	5.0 ± 0.6	.06	.8	.3	.3	.5	.7	.4

PM: pyruvate+malate. S+R: succinate+rotenone. PCM: palmitoylcarnitine+malate. CI: complex I. CII: complex II. FAO: fatty acid oxidation. RCR: respiratory control ratio. Values are mean±sd. Units are nmol/mg/min except for RCR, which is a ratio. Three-way ANOVAs with the main effects of diet [CON vs. PUN], sex [Male vs. Female], and age [PN22 vs. PN80] were conducted with a Tukey HSD multiple comparison test if necessary. Levels [A or B] not connected by the same letter represent statistical significance through multiple comparison within that main effect [$p<0.05$]. An α level of $P<0.1$ was set *a priori* for the main interaction of Diet*Sex*Age.

Pyruvate + Malate [Complex I]

Postnatal growth restriction caused a non-significant trend [p=0.06] for increased LEAK across the lifespan between PUN [PN22; males: 46.1±5.3 nmol/mg/min, females; 45.0±7.2 nmol/mg/min and PN80; males: 40.2±7.0 nmol/mg/min, females; 45.3±10.7 nmol/mg/min] and CON [males: 37.3±5.9 nmol/mg/min, females: 40.7±7.5 nmol/mg/min and PN80; males: 39.5±5.9 nmol/mg/min, females: 40.9±3.3 nmol/mg/min].

When mitochondria were stimulated with ADP, there were no significant differences in JO_2 between controls and postnatally growth restricted mitochondria in the presence of PM. However, due to the elevated LEAK mentioned above, a significant 11.54% reduction [p=0.0135] in the respiratory control ratio [RCR] was observed across both timepoints in the PUN [PN22; males: 7.9±0.7, females: 7.7±1.2 and PN80; males: 8.7±0.6, females: 7.1±1.7] when compared to controls [PN22; males: 9.5±0.3, females: 9.0±0.8 and PN80; males: 8.5±1.6, females: 8.5±0.9].

Succinate + Rotenone [Complex II]

Postnatal growth restriction revealed no significant changes of JO_2 flux when using S+R during LEAK, ADP_{max}, or RCR compared to healthy unrestricted controls.

Palmitoylcarnitine + Malate [Fatty Acid Oxidation]

Postnatal growth restriction caused a significant diet*age interaction [p=0.021] with a 13.8% increased PN80-LEAK JO_2 in the PUN [males: 70.7±9.1 nmol/mg/min and females: 63.2±6.1 nmol/mg/min] compared to the CON [males: 60.3±4.5 nmol/mg/min and females; 57.3±3.2 nmol/mg/min]. No significant differences were seen during PN22-LEAK.

During ADP_{max} postnatal growth restriction caused a significant main interaction [p=0.07] of diet*sex*age with the PUN-M at PN22 [361.5±27.7 nmol/mg/min] having lower JO_2 flux than the CON-M [391.5±13.5 nmol/mg/min], but at PN80 the PUN-F [314.4±25.8 nmol/mg/min] had lower JO_2 flux than the CON-F [360.1±24.0 nmol/mg/min].

A significant age effect [p=0.016] was also found during ADP_{max} with PN22-JO_2 flux results being larger than PN80 results.

Postnatal growth restriction showed no significant changes in the RCR compared to controls when using PCM. However, a non-significant trend [p=0.06] revealed the PUN [PN22; males: 5.5±0.2, females: 5.5±0.5 and PN80; males: 5.3±0.3, females: 5.0±0.6] had a 6.5% reduction in RCR when compared to the CON [PN22; males: 5.8±0.2, females: 5.7±0.1 and PN80; males: 5.4±1.1, females: 5.9±0.8]

Reactive Oxygen Species [H_2O_2 flux]

ROS results during early life [PN22] and adulthood [PN80] can be viewed in Figure 5.5.

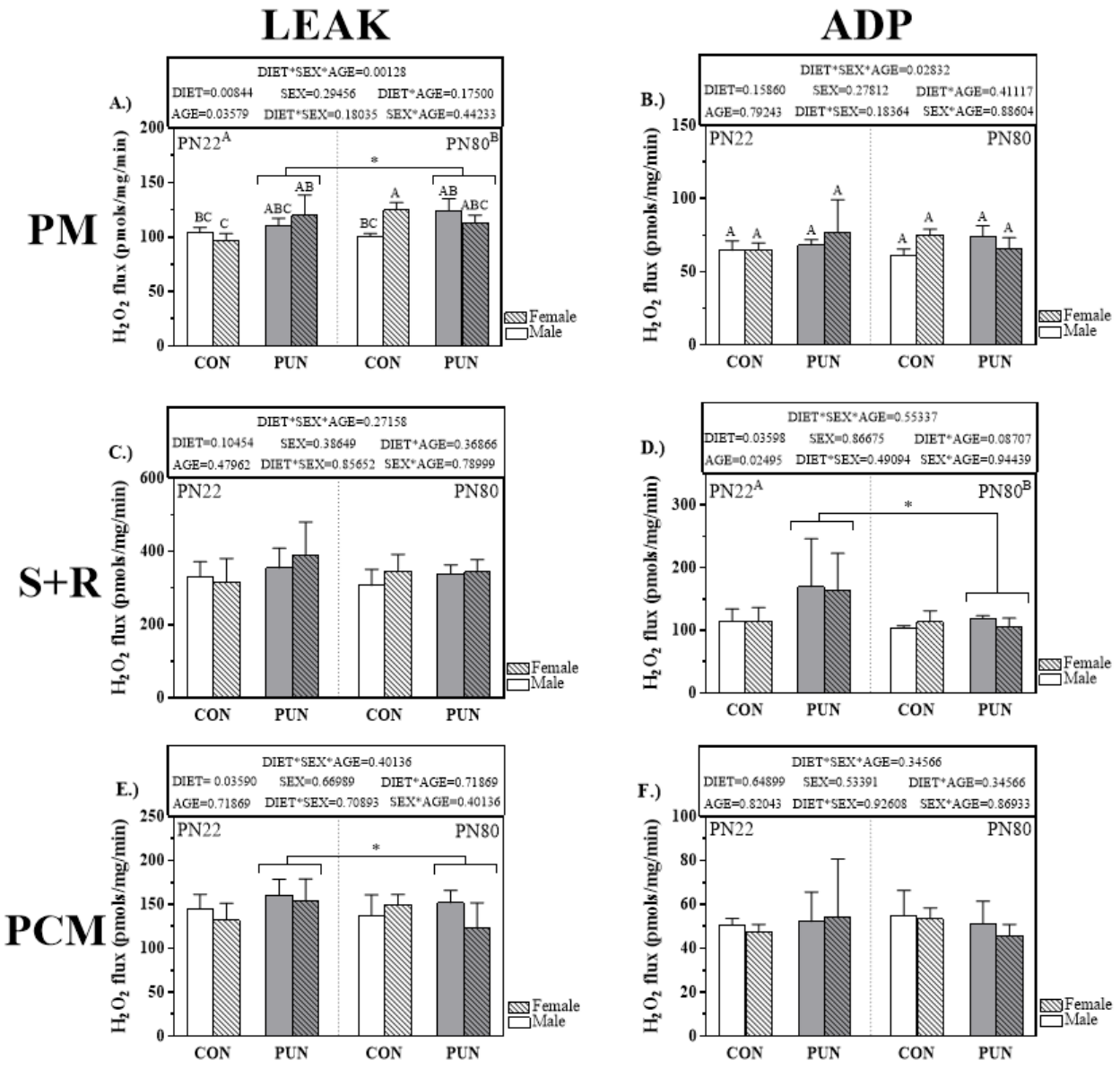

Figure 5.5: The Effects of Postnatal Growth Restriction on Mitochondrial ROS Emission: A.] PM-LEAK [PN22 and PN80]: Postnatal growth restriction caused a significant diet*sex*age interaction on ROS emission with PUN-F having greater H_2O_2 flux than CON-F at PN22, but PUN-M having greater H_2O_2 flux than CON-M at PN80. CON-F had higher H_2O_2 flux than CON-M at PN80. A significant diet effect was found with PUN having higher H_2O_2 flux than CON across the lifespan. Additionally, a significant age effect was found with higher H_2O_2 flux at PN80 vs. PN22. **B.] PM-ADP_{max} [PN22 and PN80]:** Similarly to panel A, postnatal growth restriction caused a significant diet*sex*age interaction on ROS emission with PUN-F having higher H_2O_2 flux than CON-F at PN22 but PUN-M having greater H_2O_2 flux than CON-M at PN80. Multiple comparison revealed no significant differences between any groups. **C.] S+R-LEAK [PN22 and PN80]:** No significant differences. **D.] S+R-ADP_{max} [PN22 and PN80]:** A diet*age interaction was trending [p=0.08] where PUN ROS emission was higher vs.

Figure 5.5 (cont'd).

CON at PN22 but not at PN80. A significant diet effect shows PUN having higher H_2O_2 flux across the lifespan when compared to CON, and a significant age effect was found with higher H_2O_2 flux at PN22 vs. PN80. **E.] PCM-LEAK [PN22 and PN80]:** A significant diet effect shows PUN having higher H_2O_2 flux across the lifespan when compared to CON. **F.] PCM-ADP_{max} [PN22 and PN80]:** No significant differences. Values are mean±sd. Three-way ANOVAs with the main effects of diet [CON vs. PUN], sex [Male vs. Female], and age [PN22 vs. PN80] were conducted with a Tukey HSD multiple comparison test if necessary. Levels within the figure not connected by the same letter [A, B, or C] represent statistical significance [$p<0.05$]. *, represents a significant [$p<0.05$] diet effect between CON and PUN. An α level of $P<0.1$ was set *a priori* for the main interaction of Diet*Sex*Age.

Pyruvate + Malate [Complex I]

Postnatal growth restriction caused a significant diet*sex*age interaction [p=0.00128] in ROS emission [Figure 5.5A] during LEAK state respirometry. At PN22, the PUN-F [119.9±18.8 pmol/mg/min] had greater ROS emission than CON-F [97.1±6.1 pmol/mg/min], but at PN80 the PUN-M [123.9±11.4 pmol/mg/min] had greater ROS emission than CON-M [101.1±2.1 pmol/mg/min]. A significant diet [p=0.00844] effect was also found which revealed PUN [PN22; males: 110.9±6.3 pmol/mg/min, females; 119.9±18.8 pmol/mg/min and PN80; males: 123.9±11.4 pmol/mg/min, females; 112.7±7.4 pmol/mg/min] have greater amounts of ROS emission across both time points vs. CON [PN22; males: 104.0±4.9 pmol/mg/min, females; 97.1±6.1 pmol/mg/min and PN80; males: 101.1±2.1 pmol/mg/min, females; 125.1±6.6 pmol/mg/min]. Lastly, a significant Age [p=0.03579] effect showed PN80-ROS emission was greater than PN22 results.

During ADP_{max}, a significant diet*sex*age interaction [p=0.02832, Figure 5.5B] was seen with ROS emission being elevated at PN22 in the PUN-F [77.3±22.0 pmol/mg/min] compared to the CON-F [65.3±4.5 pmol/mg/min], then at PN80, the PUN-M [74.5±7.0 pmol/mg/min] had

higher ROS emission than CON-M [61.4±4.1 pmol/mg/min]. Post-hoc analysis of this interaction revealed no significant individual comparisons.

Succinate + Rotenone [Complex II]

During LEAK state respirometry in the presence of S+R, there were no significant differences in H_2O_2 flux between groups [Figure 5.5C]. However, during ADP_{max} there was a trend for a Diet*Age interaction [p=0.08, Figure 5.5D] showing higher ROS emission in the PN22-PUN group [males; 169.6±76.3 pmol/mg/min and females; 162.9±59.9 pmol/mg/min] when compared to CON [PN22; males: 114.4±19.7 pmol/mg/min and females; 114.5±21.8 pmol/mg/min and PN80; males: 103.0±4.6 pmol/mg/min and females; 113.5±17.6 pmol/mg/min] and also the PN80-PUN [males: 118.8±4.3 pmol/mg/min and females; 105.3±14.0 pmol/mg/min]. A significant diet effect [p=0.03598] was found with higher ROS emission across both timepoints in the PUN vs. CON. Additionally, a significant age effect [p=0.02495] was found with higher mitochondrial ROS emission during PN22 vs. PN80.

Palmitoylcarnitine + Malate [Fatty Acid Oxidation]

During LEAK respirometry postnatal growth restriction caused a significant diet effect [p=0.03590, Figure 5.5E] with PUN [PN22; males: 160.3±18.4 pmol/mg/min and females; 154.4±24.9 pmol/mg/min and PN80; males: 151.9±13.9 pmol/mg/min and females; 123.5±28.5 pmol/mg/min] having higher ROS emission than CON [PN22; males: 144.9±16.7 pmol/mg/min and females; 132.0±19.6 pmol/mg/min and PN80; males: 137.7±23.5 pmol/mg/min and females; 149.8±11.6 pmol/mg/min], across both timepoints. During ADP_{max} respiration [Figure 5.5F] in the presence of PCM, there were no significant differences [p>0.05] in ROS emission between groups.

Discussion

The Developmental Origins of Health and Disease [DOHaD] literature has shown that growth restriction in early life increases the risk for CVD in adult humans, non-human primates, farm animals and rodents[1, 4, 6, 11, 32, 48, 77, 225, 267]. By altering the diet of nursing mouse dams, we have demonstrated that body mass across the lifespan of PUN mice is significantly reduced compared to unrestricted controls [Figure 5.3] as has been shown previously[6, 48, 77, 225]. Absolute, but not relative heart mass of PUN was significantly less than CON at both PN22 and PN80; indicating hearts were proportional for the size of the animals [Figure 5.4], yet literature reveals cardiac pathology in PUN hearts is present in adulthood[6, 48, 77]. Additionally, in support of previous growth restriction research, tibia lengths of PUN mice were significantly reduced across the lifespan, representing impaired lean tissue growth[49].

Presently, there is minimal information on the influence of postnatal growth restriction in early life on cardiac energetics. Beauchamp *et. al.* showed the adverse effect of a low-calorie diet [50% caloric reduction] during gestation on adult female offspring with impairments to cardiac energy metabolism, and demonstrated that this may have long-term consequences for CV function and disease in adulthood[79]. The study reported reductions in FAO in the presence of only octanoylcarnitine in adulthood, but did not obtain respirometry data with different substrates, males, or during early development. Therefore, we have designed our experiments to characterize cardiac energetics [JO_2 and H_2O_2 flux] of postnatally growth restricted mice [males and females] when isolated mitochondria of different ages [PN22 and PN80] are fueled with carbohydrates [PM], Krebs cycle intermediates [S+R], and fatty acids [PCM].

Respirometry [JO_2] and ROS [H_2O_2]

LEAK respirometry represents the mitochondria respiring to maintain resting membrane potential, and when elevated may indicate a reduced proton motive force [ΔP], or altered mitochondrial membrane potential [$\Delta\Psi$][94]. Based upon our results, the PUN group had a 11.48%, and 13.8% increase in LEAK respirometry when their cardiac mitochondria are fueled with carbohydrates [PM; across the lifespan] or fatty acids [PCM; PN80 only], respectively. Although there is no clinically established threshold, reduced ΔP through elevated LEAK respirometry is related to cardiac disease pathology[94, 268, 269]. Quarrie *et. al.* reported a 2-fold increase during LEAK respirometry in isolated rat mitochondria with ischemic reperfusion injury when compared to non-ischemic controls[270]. The PUN group in this study did not show elevated LEAK as high as reported by Quarrie *et. al.*, however, it did lead to a significant 11.54% reduction in RCR [Table 5.1]. RCR has been cited as the single most useful general measure of mitochondrial function, since it prioritizes the primary activity of mitochondria, which is to idle at low LEAK states but react to ADP by rapidly resynthesizing ATP at maximal rates[94]. Sharov *et. al.* previously showed ~25-30% reduction in RCR in humans with ischemic cardiomyopathy when compared with normal donor hearts[271]. While, Lemieux *et. al.* showed a 12% CI-linked reduction to RCR in human heart disease patients with no or mild heart failure undergoing heart surgery [average age: 64 years old][272]. Therefore, our data are closely aligned with Lemieux *et. al.* and PUN cardiac mitochondria are unable to idle at low LEAK states leading to a reduction in mitochondrial function [↓ RCR], which has been associated with CVD[94, 268, 269, 273].

Corresponding with JO_2 flux impairments, mitochondrial ROS emission was significantly elevated when PUN cardiac mitochondria were fueled with carbohydrates [PM; Figure 5.5A and 5.5B], TCA intermediates [S+R; Figure 5.5D], and fatty acids [PCM; Figure 5.5E]. As

documented previously, mitochondrial ROS emission leads to oxidative damage[274-277], and even minor elevations of ROS emission may indicate mitochondrial dysfunction leading to CVD[94].

Elevations in ROS emission have been shown to impair intracellular calcium flux[276], inducing electrophysiological alterations of cardiomyocytes leading to increased ventricular arrhythmias[277]. Interestingly, this disease pathology closely parallels the cardiac impairments [impaired calcium flux, and wide QRS complexes] seen in postnatally growth restricted mouse hearts in adulthood[6, 48]. Thus, the increased mitochondrial ROS emission that was detected indicates oxidative stress during early life [PN22] and again in adulthood [PN80], which may contribute to the pathogenesis of CVD associated with postnatal growth restriction[264, 273, 278].

Conclusion

Postnatal growth restriction alters cardiac mitochondrial energetics across the lifespan. Based upon the results, impairments in the PUN are mostly Complex-I and FAO dependent alterations when cardiac mitochondria are fueled with PM or PCM. These impairments present through reduced mitochondrial efficiency [↓ RCR: PM; ↓11.54% and PCM; ↓6.5%] via elevated LEAK state respirometry. These deficits may reduce ΔP, and future research should measure mitochondrial membrane potential and uncoupling proteins in the postnatally growth restricted mitochondria. Additionally, PUN mitochondria have significantly elevated ROS emission across the lifespan, indicating oxidative stress in the growth restricted mouse heart. Oxidative stress via heightened mitochondrial ROS emission is present in many CVD mechanisms[24, 147, 264, 273, 278-280]. Collectively, these results indicate impairments to mitochondrial function and cardiac energetics thus increasing the risk for CVD across the lifespan in the postnatally growth restricted mouse heart.

CHAPTER 6: SUMMARY AND CONCLUSIONS

Summary

The purpose of this dissertation was to characterize heart function following early life growth restriction during the postnatal window of development. Investigations were performed to examine electrical conductance, cardiac protein abundance, and energetics of the heart following postnatal growth restriction. Cardiac function was assessed via electrocardiography [ECG] from three periods throughout postnatal growth restriction. A proteomic screening of the postnatally growth restricted mouse heart was conducted and compared with unrestricted healthy control hearts using two-dimensional differential gel electrophoresis [2D DIGE]. Then, a functional measurement of cardiac metabolism was assessed following postnatal growth restriction using high-resolution respirometry [HRR] instrumentation. Below is a summary and conclusion for each chapter of the dissertation.

Postnatal Undernutrition in Mice Causes Cardiac Arrhythmogenesis Which is Exacerbated When Pharmacologically Stressed

Impairments to electrical conductance prevent the heart from contracting as a function syncytium[111, 113, 115]. Ferguson *et. al.* had shown previously that postnatally growth restricted cardiomyocytes had impaired calcium handling with more calcium spikes when stimulated with isoproterenol[48]. As calcium is necessary for cardiac muscle contraction, this finding suggests that mouse hearts subjected to postnatal growth restriction have an increased risk for arrhythmias in adulthood. ECG is a commonly used clinical and diagnostic measure of heart function, however, prior to the first manuscript of this dissertation, there were no studies that assessed the influence of postnatal growth restriction on the electrical activity of the heart.

Mice used in this investigation were exposed to growth restriction during one of three developmental windows; early [EUN; PN1-10], late phase [LUN; PN11-21], and combined

phase [PUN; PN1-21] through diet manipulation [see chapter 3 for details]. ECG parameters were obtained with adult mice [PN80] placed under 1% isoflurane anesthesia. Leads I, II, and III were recorded for 5 minutes, and then an intraperitoneal injection of dobutamine was administered, whereby recordings were repeated. The administration of dobutamine acted on β1 receptors of the sympathetic nervous system and is a commonly used drug to assess cardiac function for those with CVD[177-180].

Results from this study revealed that postnatal growth restriction caused an increased risk for cardiac arrhythmias in adulthood. When growth restricted mice were "stressed" with dobutamine, they presented with an impaired CV system. Specifically, the EUN group had higher occurrences of 1st degree AV block, the LUN group had a higher prevalence of atrial flutter, and PUN had an increased risk for ventricular depolarization arrhythmias [wide QRS complexes]. These results suggest that postnatal growth restriction increased the risk of abnormal electrical activity of the heart which lasted into adulthood. Based upon these results, for the remaining two studies of this dissertation, a cross fostering model was used to produce only combined phase PUN groups [PN1-21], since the most severe cardiac impairment was seen in this group.

Postnatal Growth Restriction in Mice Alters Cardiac Protein Abundance Leading to Impairment in Adulthood

It has been well documented that early life growth restriction alters CV structure and function in adulthood[1, 2, 4, 6, 7, 11, 13, 31, 32]. However, there is inadequate information on the molecular mechanisms responsible for the functional impairment reported. Unfortunately, this impedes the development of evidence-based countermeasures to offset cardiac impairment. 2D

DIGE coupled with mass spectroscopy is a valid method to recognize differences in proteomic abundance, thus allowing for the proposal of mechanisms leading to CVD[116, 117].

Based upon the rationale described in the previous paragraph, we applied diet manipulation to induce postnatal growth restriction [PN1-21] in FVB mice[6, 49]. Then, we subjected a group of mouse hearts to 2D DIGE and mass spectrometry to identify differences in cardiac protein abundance. The remaining mice were weaned to a healthy control diet until adulthood. At PN77, echocardiography and Doppler blood flow analysis evaluated cardiac function. At PN80, western blotting and silver nitrate staining quantified relative protein abundance in adulthood to see if the verified protein signatures at PN21 were recovered or continued into adulthood. Next, we used bioinformatic software to assemble a mechanistic pathway explaining how the 2D DIGE verified proteins influence proteomic abundance and lead to the progression of CVD following postnatal growth restriction.

Results from chapter two of this dissertation, showed an altered cardiac proteome of mice exposed to postnatal growth restriction. Overall, 2D DIGE indicated PUN mice had a reduction in proteins such as Prdx6, Ttn, Arhga29, Cdkn1c [$p57^{kip2}$], Sltm, Xpo5, Patj, Col1a1, Setd2, Col4a5, Col3a1, and Dnah1 relative to CON mice. Based upon previous literature, $p57^{kip2}$, Ttn, and collagen proteins were confirmed with a secondary technique via western blotting and silver nitrate staining, respectfully. At PN77, PUN mice presented with impaired diastolic and global cardiac function. At PN80, western blots of $p57^{kip2}$ showed that protein abundance was recovered from PN21. However, at PN80 a reduction of large molecular weight proteins [Ttn, and Collagen fibers] continued in the adult growth restricted hearts. The hypothesized mechanism that we constructed explains that a reduction of $p57^{kip2}$ at PN21 leads to impaired cardiomyocyte maturation and a thinning of the LV wall. Then, a reduction in Ttn abundance even further thins

the LV wall, and possibly causes disorganization of muscle fiber orientation. Lastly, a reduced collagen fiber network impairs the extracellular matrix and weakens CV durability across the lifespan.

In conclusion of part two, postnatal growth restriction reduces cardiac protein abundance at PN21 leading to cardiac impairment in adulthood, which indicates developmental programing throughout early life has permanent negative health consequences.

Postnatal Growth Restriction in Mice Alters Cardiac Mitochondrial Energetics

Deficits to mitochondrial function modifies cardiac energetics and leads to the development of CVD[86]. Growth restriction leads to CVD possibly from impairments to cardiac metabolism and OxPhos[2, 50, 61, 78, 79, 223]. However, investigations assessing the effect of postnatal growth restriction on cardiac mitochondrial energetics are non-existent. Therefore, the purpose of the final investigation of this dissertation was to determine if postnatal growth restriction impairs cardiac energetics and OxPhos when cardiac mitochondria are fueled with various substrates such as pyruvate+malate [PM], succinate+rotenone [S+R], or palmitoylcarnitine+malate [PCM].

As a result of diet manipulation of mouse dams, we reproducibly generated postnatally growth restricted [PUN] and healthy unrestricted control [CON] mice. Following a day of rest after weaning, on PN22 cardiac mitochondria was isolated via differential centrifugation and a functional analysis of OxPhos was performed by measuring oxygen flux [JO_2] and ROS emission [H_2O_2 flux] via HRR. During HRR, mitochondria were fueled by different substrates targeting the ETC [PM; CI, S+R; CII, and PCM; FAO], and two steady states of JO_2 and H_2O_2 flux were recorded [LEAK and ADP_{max}]. The steady states represent measurements of ATP

synthesis[150]: [1] LEAK state; where mitochondria respire to maintain resting membrane potential[93], and [2] ADP_{max}; addition of ADP causes mitochondria to consume oxygen in the ETC for the synthesis of ATP. At PN80, these measurements were repeated on littermates of the PUN and CON groups. Therefore, we constructed our experiments to characterize cardiac energetics of postnatally growth restricted mouse hearts during early life development [PN22] and in adulthood [PN80], when isolated mitochondria are fueled with different substrates.

Postnatal growth restriction caused elevations in LEAK JO_2 when using PM as a substrate and in adulthood during PCM-LEAK-JO_2 was also increased in the PUN. This result led to a significant reduction in the PM-respiratory control ratio in the PUN mitochondria [↓ 11.54%] when compared to healthy control mice. Previous research has linked an increased LEAK and reductions in RCR to the pathogenesis of CVD[94, 273]. Postnatal growth restriction also caused heightened ROS emission when cardiac mitochondria were fueled with PM, during S+R-ADP_{max}, and during PCM-LEAK. Increased ROS emission indicates oxidative stress and has also been linked to CVD through cellular damage[24, 147, 264, 278-280].

Collectively these results suggest that postnatal growth restriction reduces the Complex I dependent RCR via elevated LEAK state JO_2. Additionally, the heightened ROS emission across the lifespan increases the oxidative stress on the growth restricted heart. Increases in ROS emission have been shown previously to impair intracellular calcium flux[276], triggering electrophysiological variations of cardiomyocytes causing ventricular arrhythmias[277]. This disease pathology closely parallels the cardiac impairments seen by Visker *et. al.* in postnatally growth restricted mouse hearts in adulthood, and throughout this dissertation[6, 48]. The mitochondrial impairments revealed during this project appear to be centered upon Complex I of the ETC and FAO when cardiac mitochondria respire in the presence of PM and PCM.

Mitochondrial impairments to Complex I of the ETC, and FAO have been shown previously in the progression of heart failure, and are associated with CVD[281, 282]. Therefore, postnatal growth restriction causes mitochondrial impairments through a reduced OxPhos capacity, oxidative stress [↑ ROS] which increase the risk for CVD across the lifespan.

Conclusion

The purpose of this dissertation was to characterize heart function following an episode of early life growth restriction during postnatal development. The experimental research conducted successfully satisfies the aims of this dissertation. We have revealed negative alterations to physiology in electrical conductance, cardiac protein abundance, and mitochondrial cardiac energetics following postnatal growth restriction. Additionally, this dissertation addresses existing gaps in the DOHaD literature and lays the foundation for evidence-based practices to be developed to counteract CVD.

Consistent with previous DOHaD literature, the results of this dissertation suggest that postnatal growth restriction has negative health outcomes to cardiac structure and function in adulthood. The novel findings within this dissertation focus upon an increased risk for potentially fatal cardiac arrhythmias, an altered cardiac proteome leading to abnormal heart function, and impaired mitochondrial energetics in the postnatally growth restricted mouse heart. We recommend that future research is directed towards developing non-pharmaceutical interventions such as exercise, targeting the cardiac impairments seen in this dissertation, to improve cardiac function and alleviate financial healthcare costs in the postnatally growth restricted population.

APPENDIX

Western Blot

A] Preparation of gel plates

1. Put the glass plates and Aluminum backing plates [with a 0.75 mm spacer] on a clean surface [like a paper towel].

2. Spray Clean with 100% methanol and Kim-wipe. [PS: they are expensive so don't break.]

-Clean very well!

B] Putting the gel plates on the gel caster unit to create the gel-plate sandwich

1. Insert the spacers [black ones] on the sides of the plates [1 for each side, so 2 for 1 pair of plates]. This must be done carefully until the spacers fixed in place.

2. Insert the gel-plates pair in the gel stand vertically with the glass surface facing you.

-Make sure all edges are flush or it will leak.

-Make it tight, but not too tight

3. Screw the plates with the little grey screws, not too tight but just enough to hold the gel.

4. The gel seal [contained in a small white tube] is used on the corners [edges which face opposite the open surface]. [GELSEAL 5GR TUBE]

-Put some gel across the bottom of the glass and aluminum

5. Parafilm is used as a suspender, and a neatly cut parafilm strip is doubly folded and kept on the surface of the gel caster unit.

6. Put the gel stand in the gel caster and use large black screws clamps on the sides, by turning them and pushing in and up 180 degrees [don't over rotate them].

-Put red clamps on the top of the gel plate and aluminum backing plate.

7. Spray distilled water on the gel – plate surface [in between the 2 plates] to test for leaking.

-Wait a couple of minutes to see if any leaks occur

- "Dr. Larry" procedure to get the water out of the gel caster: hold caster firmly and shake to remove water droplets [do not drop!!!]

C] Preparation of the gel

1. We need to prepare a running gel and a stacking gel.

-Running Gel: aka separating gel, slightly basic [pH = 8.8] with a [higher acrylamide], has narrow pores in the gel

-Stacking Gel: slightly acidic [pH = 6.8] with a lower [acrylamide], has a porous structure

-Smaller proteins travel more easily and rapidly whereas larger proteins will be "stuck" at the top of the gel

Preparation of RUNNING GEL

1. Take a small beaker for making the gel.

2. Pipette 3.3 ml distilled water.

3. Put 4ml of Acrylamide mix [Bis 30 % acrylamide brown bottle].

4. Add 2.5 ml Tris 8.8.

5. Pipette 100µl of 10% Sodium dodecyl sulfate [SDS].

6. Pipette 100µl of 10% Ammonium persulfate solution [APS]→ small test tube.

7. Pipette 4 µl of TEMED.

8. MIX WELL.

9. Squirt this mixture using a pipette in between the gel surface till little more than 3/4th of the plate surface is filled. [Level with the center of the top screw on the gel stand.]

10. If the gel parallax appears to be wavy, it should be flattened using water saturated iso-butanol [2-methylbutane] or "Water Saturated Iso-butanol" on shelf.

-This is a slippery substance, use caution while using pipette

-Fill to top of the gel plate.

11. Wait for the gel to harden up. Takes approximately 15-20 minutes.

-"Dr. Larry" procedure again: hold caster firmly and shake to remove water droplets [do not drop!!!]

12. After the gel is hardened dump the iso-butanol, and wash 3x with distilled water

<u>Preparation of STACKING GEL</u>

Get a small beaker for making the stacking gel.

1. Pipette 3.4 ml of distilled water.

2. Pipette 830 µl of acrylamide mix.

3. Pipette 630 µl of Tris 6.8pH.

4. Pipette 50 µl of SDS.

5. Pipette 50 µl of 10% APS.

6. Pipette 5 µl of TEMED.

Then pipette this gel in between the plates - all the way to the top.

D] Creating the gel WELLS

1. This is done using the small white 10 well comb.

2. Push the comb in between the gel plates neatly.

-Angle the comb and use even pressure to slide it into place [do not break the glass]

-The first well on either side of the gel is not used and will be filled with 1X Sample Buffer [8 Total wells possible for sample/caster]

3. Till then prepare the sample by spinning it on vortex, adding distilled water and 4X Sample buffer [Laemmli buffer] and incubating at 90 C for 12 minutes. The amount you add will be based on the protein concentration of the sample. Remember you must add an equal volume of protein.

-The sample is heated after being diluted in order to denature the proteins. This ensures that the negatively charged amino acids is neutralized & enabling the protein to move from top to bottom when the electrical charge is applied

[traveling from negative to positive on the gel]. Do NOT heat to >100 degrees [the test tube tops will pop off]

-Example: sample heart = [500µg/µl] protein [aim for ~40µg of protein] → 7.5 µl 4X Sample Buffer + 7.5 µl Water + 15µl sample heart [33.33 µg of protein]

4. Pull the combs from gel casters as slowly as possible. Wash it with distilled water three times.

- "Dr. Larry" procedure again: hold caster firmly and shake to remove water droplets [do not drop!!!]

E] Adding the buffer on the gels

After the samples have reached the desired temperature, mix them well on the Mini Spin Centrifuge.

-30 seconds, 5.0 ref

1. Clip the gel-plates to the buffer chamber using the red clamps [longer side facing you].

2. Fill the buffer chamber [bottom to top] with 1X ELECTROBLOT BUFFER [put in fridge to cool].

3. Place the well decal [plastic template] on the glass plate and fill the sample wells.

-Use the P100 pipette from the circular rack and the special elongated loading tips

-Make sure to slowly load the 8 wells→ do not blow the sample everywhere

4. Connect the buffer chamber with the voltage system, at 25mA, constant voltage until the blue protein marker line reaches to the bottom of the gel plates.

-A = Constant, Voltage will auto-adjust to maintain the consistent amps needed

-Can check the time on the voltage system if needed [~60-90 minutes]

F] Transferring proteins [causing proteins to move out of the gel and onto the membrane]

1. Cut the nitrocellulose gel to fit the well decal [plastic template]→ Cut off the stacking gel where the wells are located so it is a square gel. Place the membrane in the Tupperware box. Pour transfer buffer over it.

-Label "TBL" for Top Back Left on the membrane

-Label "1" and "10" on the other side

Now take the glass plates apart gently and lift the spacer out. Using the space cut the BOTTOM LEFT portion of the gel.

2. Lift the gel sheet up and place it delicately in the transfer buffer solution [in the Tupperware case] and rock for few minutes.

3. Rock the membranes and the gel in transfer buffer for 20 minutes.

4. Take the western blot kit buffer case, dip the sponge in transfer buffer, followed by dipping 2 pieces of filter paper in the transfer buffer

5. Place the filter paper on the sponge.

6. Lift the gel and place it on the paper [close to black side]. Avoid air bubbles. Put the membrane on it, followed by 2 pieces of paper and another sponge.

-Sandwich Cassette = Sponge, Filter Paper, Filter Paper, Gel, Membrane, Filter Paper, Filter Paper, Sponge

7. Lock the case and place it vertically in the blotting chamber.

-place the hinges of the cassette facing upwards

-Black to Black & Red to Red

-Gel to the black and Membrane to the red electrodes

-Place the black part of the cassette to the black electrodes

-Place the grey part of the cassette to the red electrodes

G] Blotting the proteins

1. Fill the chamber with transfer buffer and put the case [containing sponge, membrane, and gels sheet].

2. Put a stir bar in the bottom of the chamber so the transfer buffer is mixing while the machine runs. Set the stir bar to 3 and a half.

3. Leave the chamber connected at 100 mA for 2 and half – 3 hours.

H] Staining procedure

1. After 3 hours take out the case from transfer chamber, and gently take the gel sheet out and put it in another Tupperware case containing.

2. Pour blocking buffer [500ml TBS + 25g non-fat dairy milk, powdered + .5ml TWEEN] over it and rock for an hour.

3. Wash membrane 3x for 5 minutes with TBS [TRIS-BUFFERED SALINE, NOT TRANSFER BUFFER SOLUTION]

-Rock on tilt table

I] Application of antibodies

1. If greater then 40ug of protein loaded dilute antibodies in a 1:500[10 ul] ratio. If less, then 40ug loaded uses 1:250[20ul]. [In 5 ml of blocking buffer.]

-Concentrations are manufacturer specific

2. Make pouches using the freezer bag. Seal it from all sides except one and place the gel sheet on it. Pipette the primary antibodies into the pouch.

3. Rock it for few minutes and keep it in the fridge overnight on a rocker.

J] Addition of secondary antibodies [IN THE DARK]

1. After the samples have been incubated in the fridge overnight take the samples out of the pouch and wash 3 times in TBS and rock for 5 minutes each time.

2. Put 5 ml of blocking buffer in the centrifuge tube and secondary antibody [anti—rabbit HRP linked]. If greater then 40ug protein loaded use 1:2000 [2.5 ul] if less, then 40ug loaded use 1:1000 [5 ul].

3. Prepare the freezer bag pouches as above and place the gel sheet on it and pipette out the secondary antibodies. Incubate for 1 hour on the rocker.

4. Take the sample out of the pouch and wash the gel sheets with TBS buffer 3 times for 5 minutes each.

-ECL Reagent A 10 ml + ECL Reagent B 10 ml

-2 minutes on rocker

K] Imaging

1. This will be done on the Kodak Imaging Station IR2000.

2. Put the membrane on plastic sheet and inside the chamber after making sure the room lights are switched off.

Transfer Buffer Solution = 800 ml Water + 100 ml CAPS + 100 ml Methanol

TBS = 750 ml 2X NaCl + 100 ml Tris 7.5

SOLUTIONS/BUFFER RECIPES

5x SDS Sample Buffer

Reagents

SDS

Trizma base

Glycerol

0.04% Bromophenol blue

Procedure

Place a 150 ml beaker on the balance and tare to zero

Weigh 50gm of glycerol into the beaker

Add 70 ml of DI water

Add stir bar

Add 3.78g of Trizma base

Allow all components to dissolve

pH to 6.8 with HCL

Add 30 ml of DI water.

Add 10 gm SDS and stir until dissolved

Add 25 ml 0.04% bromophenol blue; mix well.

Note to make 4x Sample buffer combine 800 ul 5x Sample buffer [above] with 200 ul of beta mercaptoethanol

BCA Protein Assay [Thermo Scientific Protocol]

1. Dilute the BSA Standard
2. Prepare BCA Working Reagent
    a. Combing reagents, A+B at a 50:1 ratio
        i. It will be a light green solution
3. Pipette 25 microliters of each standard or sample into a microplate well
4. Pipette 200 microliters of BCA working reagent into same wells
5. Gently mix the components for 30 seconds
6. Incubate the plate at 37 degrees for 30 minutes
7. Cool the plate at room temperature for 5 minutes
8. Put into the plate reader and measure the absorbance at or near 562nm

BUFFERS

SDS Lysis Buffer [50 mL]

SDS [0.5 g]

Glycerol [5 mL]

β-Mercapto Ethanol [5 mL]

1M Tris, pH 6.8 [2 mL]

Bromophenol Blue [pinch]

Xylene Cyanol

Stain [1 L]

Methanol [150 mL]

Acetic Acid [100 mL]

Coomassie Blue [2 g]

Blot Transfer Buffer [1 L]

Methanol [200 mL]

Glycine [14.4 g]

Tris [3.03 g]

Sample Buffer [100mL]

1M Tris-HCl pH 6.8 [25 mL]

2% SDS [2 g]

Glycerol [10 mL]

1M DTT [2 mL]

Bromophenol Blue [0.01 g]

SDS Running 5X Gel Buffer [5 L] [2 L]

Tris	150 g	60 g
SDS	25 g	10 g
Glycine	720 g	288 g

5X TBS	[1 L]	[2 L]
Tris	24.2 g	48.4 g
NaCl	292.4 g	584.8 g

pH to 7.5

10X Transfer Buffer [1 L]

Tris [24.7 g]

Glycine [112.6 g]

Do not pH the transfer buffer

1X Transfer Buffer [1 L]

10X Transfer Buffer [100 mL]

Methanol [200 mL]

Add methanol to final 1X dilution only

Tris-Saline [1 L]

1M Tris, pH 7.3 [5 mL]

NaCl [8.77 g]

Tris-Saline 0.1% Triton [2 L]

1M Tris, pH 7.2 [5 mL]

1M Tris, pH 7.4 [5 mL]

5M NaCl [60 mL]

Triton X-100 [2 mL]

1X TBS-T [1 L]

TBS [667 mL]

Tween-20 [333 mL]

30% Acrylamide/Bis-Acrylamide [500 mL]

Acrylamide [150 g]

Bis-acrylamide [4 g]

10% [w/v] Ammonium Persulfate [500 mL]

Ammonium persulfate [50 g]

Make 50 mL aliquots. Store at -20°C.

Silver Nitrate Stain

Solutions/Buffers to be made

A] Fixative: Acetic acid 10%, ethanol 30%

- Measure 100 ml glacial acetic acid
- Measure 300 ml ethanol
- Fill to 1000 ml with MilliQ water

B] Rinse: 20% ethanol

C] Sensitizer: 0.02% sodium thiosulfate

- Weigh 0.2 gm sodium thiosulfate
- Dissolve in 1000 ml MilliQ water

D] Silver Nitrate: 0.2% silver nitrate

- Measure 2.0 gm silver nitrate
- Dissolve in 1000 ml MilliQ water

E] Developer: must be prepared fresh [make at step 6 of the SOP]; 3% sodium carbonate, 0.025% formaldehyde, sodium thiosulfate [10 mgm/L]

- Measure 15 gm sodium carbonate
- Measure 25 ml of stock sodium thiosulfate [see step C]
- Measure 125 µl 37% formaldehyde
- Fill to 500 ml with MilliQ water

F] Stop: Tris, acetic acid

- Measure 50 gm Tris base
- Measure 25 ml glacial acetic acid
- Fill to 1000 ml with MilliQ water

Standard Operating Procedure

1. Soak the gel in fixative [see step A] for at least one hour. Then, change the solution for a minimum of another hour; however, overnight is ok.
2. Rinse the gel in rinse solution [see step B] for 20 minutes
3. Rinse the gel in MilliQ water for 10 minutes [minigel] or 20 minutes [13 x 16 cm gel]
4. Soak the gel in sensitizer solution [see step C] for 1 minute

5. Rinse the gel in MilliQ water 3 times for 20 seconds each rinse
6. Soak the gel in silver nitrate solution [see step D] for 45 minutes.
    a. Make the developer at this time!
7. Rinse the gel with MilliQ water for 5-10 seconds
    a. This is a critical step…SECONDS AND NOT MINUTES
8. Soak the gel in the developing solution [see step E] until bands are adequate
    a. 3-4 minutes
        i. DO NOT over-expose or under-expose
9. Soak the gel in stop solution [see step F] for a minimum of 15 minutes, then store in fresh MilliQ water

After the SOP is complete, the gel staining process is complete. It does not require destaining like a coomassie blue stained gel. The bands can then be image and compared.

Mitochondrial Isolation and High-resolution Respirometry

1] Turn ON oxygraphs and clean with de-ionized water

2] Create "new folder", change slope from 40 to 5 with a 3-panel lay-out

3] Turn on plate-reader and centrifuge

4] Take out buffers: RB0 and IB [thawed the night before]

5] Cool dissection tools on ICE: put IB [10 mls] beaker on ice for mincing, put a splash of IB in a 50 ml Falcon tube, put cardioplegic solution in a petri dish for rinshing

6] Place animal in isoflurane chamber until anesthetized, then cervical dislocation and surgically remove the heart

7] Rinse all blood out of heart and trim the fat in the petri dish filled with cardplegic solution

8] Quantitatively weigh the heart

9] Wash cardioplegic solution off of the heart in a small beaker of isolation buffer

10] Mince the heart in isolation buffer

11] Put small minced pieces into 50 ml Falcon tube and fill up to 25 mls

12] Centrifuge on program #1 : 10 minutes at 8,000 x g in 4 degrees C

13] Keep the pellet and discard the supernatant [first wash/rince the pellet with a splace of isolation buffer]

14] Fill the tube with 25 mls of fresh isolation buffer and vigorously vortex to mix the pellet

15] Centrifuge on program #2: 10 minutes at 800 x g in 4 degrees C

16] While solution is centrifuging, cool a serological pippette on ice inside of the plastic wrapping

17] Power pippette the supernatant and discard the pellet, place supernatant into a new 50 ml Falcon tube [DO NOT TOUCH THE PELLET], then fill to 25 mls with fresh isolation buffer

18] Centrifuge on program #3: 10 minutes at 8,000 x g in 4 degrees C

19] Prepare BCA assay kit with standards

20] When centrifuge is complete, discard the supernatant and keep the mitochondrial rich pellett for resuspension in isolation buffer

21] Following resuspension quantify the content of your solution, and standardized the concentration to the desired amount using isolation buffer

After the mitochondrial rich pellet has been resuspended and quantified, you are now ready for O2k respirometry experimentation. Although the experiments of this disseration will

be outline below, the reader is directed to *Mitochondrial and Respiratory Control: an introduction to OxPhos analysis* written by Dr. Erich Gnaiger.

Pyruvate + Malate [with ROS detection]

1.) 14 ul Pyruvate + Malate
2.) 6 ul Horse-radish Peroxidase/Superoxide Dismutase
3.) 2 ul Amplex Ultra-red
    a. DON'T PUT ON ICE
4.) 4 ul EGTA
5.) 5 ul Mitochondrial sample
    a. Wait ~ 5 minutes to capture LEAK State
6.) 2 ul Adenosine Diphosphate

Palmitoylcarnitine + Malate [w/ ROS detection]

1.) 5 ul Palmitoylcarnitine
2.) 8 ul Malate
3.) 6 ul Horse-radish Peroxidase/Superoxide Dismutase
4.) 2 ul Amplex Ultra-red
    a. DON'T PUT ON ICE
5.) 4 ul EGTA
6.) 5 ul Mitochondrial sample
    a. Wait ~ 5 minutes to capture LEAK State
7.) 2 ul Adenosine Diphosphate

Succinate + Rotenone [w/ ROS detection]

1.) 20 ul S

2.) 1 ul Rotenone

3.) 6 ul Horse-radish Peroxidase/Superoxide Dismutase

4.) 2 ul Amplex Ultra-red

    a. DON'T PUT ON ICE

5.) 4 ul EGTA

6.) 5 ul Mitochondrial sample

    a. Wait ~ 2 minutes to capture LEAK State

7.) 2 ul Adenosine Diphosphate

REFERENCES

REFERENCES

1. Barker DJ, Winter PD, Osmond C, Margetts B, Simmonds SJ. Weight in infancy and death from ischaemic heart disease. *Lancet*. 1989 Sep 9;2(8663):577-80

2. Barker DJ. The origins of the developmental origins theory. *J Intern Med.* 2007;261:412-417.

3. Forsén T, Eriksson JG, Tuomilehto J, Teramo K, Osmond C, Barker DJ. Mother's weight in pregnancy and coronary heart disease in a cohort of Finnish men: follow up study. *BMJ.* 1997:Oct 4;315(7112):7837-7840.

4. Thornburg KL. The programming of cardiovascular disease. *J Dev Orig Health Dis.* 2015;6:366-376.

5. Wells JC. Environmental quality, developmental plasticity and the thrifty phenotype: a review of evolutionary models. *Evol Bioinform Online.* 2007;3:109-120.

6. Visker JR, Ferguson DP. Postnatal undernutrition in mice causes cardiac arrhythmogenesis which is exacerbated when pharmacologically stressed. *J Dev Orig Health Dis.* 2018 Aug;9(4):417-424.

7. Eriksson JG, Eriksson JG, Tuomilehto J, Osmond C, Barker DJ. Early growth and coronary heart disease in later life: longitudinal study. *BMJ.* 2001:Apr 21;322(7292):7949-7953.

8. Baum M, Ortiz L, Quan A. Fetal origins of cardiovascular disease. *Curr Opin Pediatr.* 2003;15:166-170.

9. Dusick AM, Poindexter BB, Ehrenkranz RA, Lemons JA. Growth failure in the preterm infant: can we catch up? *Semin Perinatol.* 2003;27:302-310.

10. Osmond C, Kajantie E, Forsen TJ, Eriksson JG, Barker DJ. Infant growth and stroke in adult life: the Helsinki birth cohort study. *Stroke.* 2007:Feb;38(32):264-270.

11. Barker DJ. In utero programming of cardiovascular disease. *Theriogenology.* 2000;53:555-574.

12. Fall CHD, Kumaran K. Metabolic programming in early life in humans. *Philos Trans R Soc Lond B Biol Sci.* 2019:Apr 15; 374(1770):20180123.

13. Barker DJ. Sir Richard Doll Lecture. Developmental origins of chronic disease. *Public Health.* 2012;Mar;:185-189.

14. Naidoo S, Kagura J, Fabian J, Norris SA. Early Life Factors and Longitudinal Blood Pressure Trajectories Are Associated With Elevated Blood Pressure in Early Adulthood. *Hypertension.* 2019:Feb; 73(72):301-309.

15. Stein CE, Fall CH, Kumaran K, Osmond C, Cox V, Barker DJ. Fetal growth and coronary heart disease in south India. *Lancet.* 1996;Nov 9:348(9037):1269-1273.

16. Rich-Edwards JW, Stampfer MJ, Manson JE. Birth weight and risk of cardiovascular disease in a cohort of women followed up since 1976. *BMJ.* 2019:Aug 16;315(7105):7396-7400.

17. Barker DJ, Kajantie E, Eriksson JG. Growth and chronic disease: findings in the Helsinki Birth Cohort. *Ann Hum Biol.* 2009:Sep-Oct;36(35):445-458.

18. McKerracher L, Moffat T, Barker M, Williams D, Sloboda DM. Translating the Developmental Origins of Health and Disease concept to improve the nutritional environment for our next generations: a call for a reflexive, positive, multi-level approach. *J Dev Orig Health Dis.* 2019:Aug;10(14):420-428.

19. Barker DJ, Thornburg KL. The obstetric origins of health for a lifetime. *Clin Obstet Gynecol.* 2013;Sep;511-519.

20. Hales CN, Barker DJ, Clark PM, et. al. Fetal and infant growth and impaired glucose tolerance at age 64. *BMJ.* 1991;Oct 26:1019-1022.

21. Paneth N AF, Stein AD. Early nutritional origins of hypertension: a hypothesis still lacking support. *J Hypertens Suppl.* 1996:Dec; 14(15):S121-129.

22. Paneth N, Ahmed F, Stein AD. Early origin of coronary heart disease (the "Barker hypothesis"). *BMJ.* 1995:Feb 18;310(6977):6411-6412.

23. Hanson M, Gluckman P. Developmental origins of noncommunicable disease: population and public health implications. *Am J Clin Nutr.* 2011;94:1754s-1758s.

24. Blackmore HL, Ozanne SE. Programming of cardiovascular disease across the life-course. *J Mol Cell Cardiol.* 2015;83:122-130.

25. Santini MP, Forte E, Harvey RP, Kovacic JC. Developmental origin and lineage plasticity of endogenous cardiac stem cells. *Development.* 2016;143:1242-1258.

26. Kyle UG, Pichard C. The Dutch Famine of 1944-1945: a pathophysiological model of long-term consequences of wasting disease. *Curr Opin Clin Nutr Metab Care.* 2006;Jul;388-394.

27. Painter RC, Roseboom TJ, Bleker OP. Prenatal exposure to the Dutch famine and disease in later life: an overview. *Reprod Toxicol.* 2005;20:345-352.

28. Ekamper P, van Poppel F, Stein AD, Lumey LH. Independent and additive association of prenatal famine exposure and intermediary life conditions with adult mortality between age 18-63 years. *Soc Sci Med.* 2014:Oct;119:232-239.

29. Lumey LH, Stein AD, Kahn HS, et. al. Cohort profile: the Dutch Hunger Winter families study. *Int J Epidemiol.* 2007:Dec;36(36):1196-1204.

30. Painter RC, de Rooij SR, Bossuyt PM, et. al. Maternal nutrition during gestation and carotid arterial compliance in the adult offspring: the Dutch famine birth cohort. 2007 Mar;25(3):533-40.

31. Barker DJ. The fetal origins of coronary heart disease. *Acta Paediatr Suppl.* 1997;422:78-82.

32. Barker DJ, Osmond C, Golding J, Kuh D, Wadsworth ME. Growth in utero, blood pressure in childhood and adult life, and mortality from cardiovascular disease. 1989 Mar 4;298(6673):564-7.

33. Portrait FRM, van Wingerden TF, Deeg DJH. Early life undernutrition and adult height: The Dutch famine of 1944-45. *Econ Hum Biol.* 2017:Nov;27(Pt B):339-348.

34. Eriksson MRK, Eriksson JG. Early life stress and later health outcomes--findings from the Helsinki Birth Cohort Study. *Am J Hum Biol.* 2014:Mar-Apr;26(22):111-116.

35. Haapanen MJ, Osmond C, et. al. Infant and childhood growth and frailty in old age: the Helsinki Birth Cohort Study. *Aging Clin Exp Res.* 2019:May;31(35):717-721.

36. Tikanmäki M, Tammelin T, Vaarasmaki M. Prenatal determinants of physical activity and cardiorespiratory fitness in adolescence - Northern Finland Birth Cohort 1986 study. *BMC Public Health.* 2017:Apt 20;17(21):346.

37. Jantunen H, Wasenius N, Salonen MK, et. al. Change in physical activity and health-related quality of life in old age - a 10-year follow-up study. *Scand J Med Sci Sports.* 2019:Jun 17. doi:10.111

38. Åström MJ, von Bonsdorff MB, Perala MM, et. al. Glucose regulation and physical performance among older people: the Helsinki Birth Cohort Study. *Acta Diabetol.* 2019:Oct;55(10):1051-1058.

39. Alastalo H, Raikkonon K, Pesonen AK, et. al. Cardiovascular morbidity and mortality in Finnish men and women separated temporarily from their parents in childhood--a life course study. *Psychsom Med.* 2012:Jul-Aug;74(76):583-587.

40. Salonen MK, Kajanti E, Osmond C, et. al. Developmental origins of physical fitness: the Helsinki Birth Cohort Study. *PLoS One.* 2011;6:e22302.

41. Kaseva N, Wehkalampi K, Strang-Karlsson S, et. al. Lower conditioning leisure-time physical activity in young adults born preterm at very low birth weight. *PLoS One.* 2012;7:e32430.

42. Kuo AH, Li C, Li J, et al. Cardiac remodelling in a baboon model of intrauterine growth restriction mimics accelerated ageing. *The Journal of Physiology.* 2017.

43. Zwanenburg A, Jellema RK, Jennekens W, et. al. Heart rate-mediated blood pressure control in preterm fetal sheep under normal and hypoxic-ischemic conditions. *Pediatr Res.* 2013;Apr:420-426.

44. Bubb KJ, Cock ML, Black MJ, et al. Intrauterine growth restriction delays cardiomyocyte maturation and alters coronary artery function in the fetal sheep. *J Physiol.* 2007;578:871-881.

45. Khanal P, Johnsen L, Axel AM, et. al. Long-Term Impacts of Foetal Malnutrition Followed by Early Postnatal Obesity on Fat Distribution Pattern and Metabolic Adaptability in Adult Sheep. 2016 Jun 3;11(6):e0156700.

46. Louey S, Jonker SS, Giraud GD, Thornburg KL. Placental insufficiency decreases cell cycle activity and terminal maturation in fetal sheep cardiomyocytes. *The Journal of physiology.* 2007;580:639-648.

47. Morton M, Tsang H, Hohimer R, et al. Left ventricular size, output, and structure during guinea pig pregnancy. *The American Journal of Physiology.* 1984;246:R40-48.

48. Ferguson DP, Heredia CP, et. al. Postnatal undernutrition alters adult female mouse cardiac structure and function leading to limited exercise capacity. *J Physiol.* 2019;Feb 7.

49. Fiorotto ML, Davis TA, Sosa HA, Villegas-Montoya C, Estrada I, Fleischmann R. Ribosome abundance regulates the recovery of skeletal muscle protein mass upon recuperation from postnatal undernutrition in mice. *J Physiol.* 2014;592:5269-5286.

50. Botting KJ, Wang KC, Padhee M, et al. Early origins of heart disease: low birth weight and determinants of cardiomyocyte endowment. *Clin Exp Pharmacol Physiol.* 2012;39:814-823.

51. Drenckhahn JD, Strasen J, Heinecke, et. al. Impaired myocardial development resulting in neonatal cardiac hypoplasia alters postnatal growth and stress response in the heart. *Cardiovascular Res.* 2015;Apr 1:43-54.

52. Sharma D SS, Farahbakhsh N, Sharma P. Intrauterine growth restriction - part 1. *J Matern Fetal Neonatal Med.* 2016:Dec;29(24):2977-2987.

53. Sharma D SS, Farahbakhsh N, Sharma P. Intrauterine growth restriction - part 2. *J Matern Fetal Neonatal Med.* 2016:Dec;29(24):4037-4048.

54. Black RE, Victoria CG, Walker SP, et. al. Maternal and child undernutrition and overweight in low-income and middle-income countries. *Lancet.* 2013;Aug 3;382:427-451.

55. Friedman H, Ator N, Haigwood N, et. al. The Critical Role of Nonhuman Primates in Medical Research. *Pathog Immun.* Vol 22017:352-365.

56. Camacho P, Fan H, Liu Z, He J-Q. Large Mammalian Animal Models of Heart Disease. *J Cardiovasc Dev Dis*. 2016 Oct 5;3(4). pii: E30

57. Charlton V, Johengen M. Fetal intravenous nutritional supplementation ameliorates the development of embolization-induced growth retardation in sheep. *Pediatr Res.* 1987:Jul;22(21):55-61.

58. Chattergoon NN, Louey S, Stork P, Giraud GD, Thornburg KL. Mid-gestation ovine cardiomyocytes are vulnerable to mitotic suppression by thyroid hormone. *Reprod Sci.* 2012;Jun;642-649.

59. De Blasio MJ, Robinson JS, Owens JA. Placental restriction of fetal growth reduces size at birth and alters postnatal growth, feeding activity, and adiposity in the young lamb. *Am J Physiol Regul Integr Comp Physiol.* 2007;Feb;R875-886.

60. Dodson RB, Rozance PJ, Fleenor BS, et. al. Increased arterial stiffness and extracellular matrix reorganization in intrauterine growth-restricted fetal sheep. *Pediatr Res.* 2013:Feb;73(72):147154.

61. Wang KC, McMillen IC, Duffield JA, Brooks DA, Morrison JL. Alteration of cardiac glucose metabolism in association to low birth weight: experimental evidence in lambs with left ventricular hypertrophy. *Metabolism.* 2013;Nov:1162-1172.

62. Luyckx VA, Brenner BM. Birth weight, malnutrition and kidney-associated outcomes--a global concern. *Nat Rev Nephrol.* 2015:Mar;11(13):135-149.

63. Ward AM, Phillips DI. Fetal programming of stress responses. *Stress.* 2001:Dec;4(4):263-271.

64. Nezar MA, el-Baky AM, Soliman OA, et. al. Endothelin-1 and leptin as markers of intrauterine growth restriction. *Indian J Pediatr.* 2009;May;485-488.

65. Neerhof MG, Synowiec S, Qu XW, Thaete LG. The significance of endothelin in platelet-activating factor-induced fetal growth restriction. *Reprod Sci.* 2012;Nov;1175-1180.

66. Darby JRT, McMillen IC, Morrison JL. Maternal undernutrition in late gestation increases IGF2 signalling molecules and collagen deposition in the right ventricle of the fetal sheep heart. *J Physiol.* 2018:Jun;596(512):2345-2358.

67. Swindle MM, Makin A, Herron AJ, Clubb FJ, Frazier KS. Swine as Models in Biomedical Research and Toxicology Testing. *Vet Pathol.* 2012 Mar;49(2):344-56

68. Almond GW. Research applications using pigs. *Vet Clin North Am Food Anim Pract.* 1996:Nov;12(13):707-716.

69. Columbus DA, Steinhoff-Wagner J, Suryawan A, et. al. Impact of prolonged leucine supplementation on protein synthesis and lean growth in neonatal pigs. *Am J Physiol Endocrinol Metab.* 2015:Sep 15;309(306): E601-610.

70. Bauer R, Walter B, Gaser E, Rosel T, Kluge H, Zweiner U. Cardiovascular function and brain metabolites in normal weight and intrauterine growth restricted newborn piglets--effect of mild hypoxia. *Exp Toxicol Pathol.* 1998:Sep;50(54-56):294-300.

71. Ellenbroek B, Youn J. Rodent models in neuroscience research: is it a rat race? *Dis Model Mech.* Vol 92016:1079-1087.

72. Dutta S, Sengupta, P. Men and mice: Relating their ages. *Life Sci.* 2016:May 1;152:244-248.

73. Vanhooren V, Libert C. The mouse as a model organism in aging research: usefulness, pitfalls and possibilities. *Ageing Res Rev.* 2013:Jan;12(11):18-21.

74. Demetrius L. Aging in mouse and human systems: a comparative study. *Ann N Y Acad Sci.* 2006:May;1067:1066-1082.

75. Ferguson DP. Postnatal undernutrition alters female mouse cardiomyocyte structure and function leading to a permanent impairment in exercise capacity in adulthood. Integrative Biology of Exercise Conference: *APS* 2016:Poster #40.

76. Ponnusamy M, Li PF, Wang K. Understanding cardiomyocyte proliferation: an insight into cell cycle activity. *Cell Mol Life Sci.* 2017;Mar;1019-1034.

77. Pendergrast LA, Leszczynski EC, Visker JR, Triplett AN, Ferguson DP. Early life undernutrition reduces maximum treadmill running capacity in adulthood in mice. *Appl Physiol Nutr Metab.* 2019:Jul 16.

78. Wang KC, Zhang S, McMillen IC, Brooks DA, Morrison JL. Akt signaling as a mediator of cardiac adaptation to low birth weight. *J Endocrinol.* 2017;May:R81-R94.

79. Beauchamp B, Thrush AB, Quizi J, et. al. Undernutrition during pregnancy in mice leads to dysfunctional cardiac muscle respiration in adult offspring. *Biosci Rep.* 2015;Apr 10;:e00200.

80. Bjørndal B, Alteras EK, Lindquist C, Svardal A, Skorve J, Berge RK. Associations between fatty acid oxidation, hepatic mitochondrial function, and plasma acylcarnitine levels in mice. *Nutr Metab.* 2018;Jan 29;15:10.

81. Dávila-Román VG, Herrero P, et. al. Altered myocardial fatty acid and glucose metabolism in idiopathic dilated cardiomyopathy. *J Am Coll Cardiol.* 2002;Jul 17;:271-277.

82. de Brito Alves JL, Toscano AE, da Costa-Silva JH, Vidal H, Leandro CG, Pirola L. Transcriptional response of skeletal muscle to a low protein perinatal diet in rat offspring at different ages: The role of key enzymes of glucose-fatty acid oxidation. *J Nutr Biochem.* 2017;Mar;117-123.

83. Grynberg A, Demaison L. Fatty acid oxidation in the heart. *J Cardiovasc Pharmacol.* 1996;28:S11-17.

84. Hoppel C. The role of carnitine in normal and altered fatty acid metabolism. *Am J Kidney Dis.* 2018;Apr;41:S4-12.

85. Manakov D, Ujcikova H, Pravenec M, Novotny J. Alterations in the cardiac proteome of the spontaneously hypertensive rat induced by transgenic expression of CD36. *J Proteomics.* 2016;145:177-186.

86. Nsiah-Sefaa A, Mckenzie M. Combined defects in oxidative phosphorylation and fatty acid β-oxidation in mitochondrial disease. *Biosci Rep.* 2016;Feb 2;36(2):e00313.

87. Crnic LS, Chase HP. Models of infantile undernutrition in rats: effects on milk. *J Nutr.* 1978;Nov:1755-1760.

88. Brass EP, Hoppel CL. Effect of carnitine on mitochondrial oxidation of palmitoylcarnitine. *Biochem J.* 1980;May 15;188(2):451-458.

89. Ojuka E AB, Bezuidenhout N, et. al. Measurement of β-oxidation capacity of biological samples by respirometry: a review of principles and substrates. *Am J Physiol Endocrinol Metab.* 2016;May 1;E715-723.

90. Djafarzadeh S, Jakob SM. High-resolution Respirometry to Assess Mitochondrial Function in Permeabilized and Intact Cells. *J Vis Exp.* 2017;Feb 8.

91. Lanza I, Nair KS. Functional assessment of isolated mitochondria in vitro. *Methods Enzymol.* 2009;457:349-372.

92. Makrecka-Kuka M, Krumschnabel G, Gnaiger E. High-Resolution Respirometry for Simultaneous Measurement of Oxygen and Hydrogen Peroxide Fluxes in Permeabilized Cells, Tissue Homogenate and Isolated Mitochondria. *Biomolecules.* 2015;Jun 29:1319-1338.

93. Pesta D, Gnaiger E. High-resolution respirometry: OXPHOS protocols for human cells and permeabilized fibers from small biopsies of human muscle. *Methods Mol Biol.* 2012;810:25-58.

94. Brand M, Nicholls, D. Assessing mitochondrial dysfunction in cells. *Biochem J.* Vol 4352011:297-312.

95. Chiossi G, Costantine MM, Tamayo E, Hankins GD, Saade GR, Longo M. Fetal programming of blood pressure in a transgenic mouse model of altered intrauterine environment. *J Physiol.* 2016:Dec 1;594(523):7015-7025.

96. Hunt K, Vatish M. Definitions and reporting of placental insufficiency in biomedical journals: a review of the literature. *Eur J Obstet Gynecol Reprod Biol.* 2016:Oct;205:146-149.

97. Dickinson H, Davies-Tuck M, et. al. Description of a method for inducing fetal growth restriction in the spiny mouse. *J Dev Orig Health Dis.* 2017:Oct;8(5):550-555.

98. Miwa Y, Sladky KK. Small Mammals: Common Surgical Procedures of Rodents, Ferrets, Hedgehogs, and Sugar Gliders. *Vet Clin North Am Exot Anim Pract.* 2016:Jan;19(11):205-244.

99. Nardozza LM, Caetano AC, Zamarian AC, et. al. Fetal growth restriction: current knowledge. *Arch Gynecol Obstet.* 2017:May;295(295):1061-1077.

100. Osmond C, Barker DJ. Fetal, infant, and childhood growth are predictors of coronary heart disease, diabetes, and hypertension in adult men and women. *Environ Health Perspect.* 2000;Jun;108 Suppl:545-553.

101. Fall CH, Barker DJ, Osmond C, Winter PD, Clark PM, Hales CN. Relation of infant feeding to adult serum cholesterol concentration and death from ischaemic heart disease. *BMJ.* 1992;304:801-805.

102. Davis K, Harper JM. Nutritional limitation in early postnatal life and its effect on aging and longevity in rodents. *Exp Gerontol.* 2016:Dec 15;86:84-89.

103. Mueller AJ, Cox WM Jr. The effect of changes in diet on the volume and composition of rat milk. *J Nutr.* 1946;Feb:249-259.

104. Ortiz-Valladares M, Torrero C, Regalado M, Salas M. Late-emerging effects of perinatal undernutrition in neuronal limbic structures underlying the maternal response in the rat. *Brain Res.* 2018:Dec 1; 1700:1731-1740.

105. Grigor MR, Allan JE, Carrington JM, et. al. Effect of dietary protein and food restriction on milk production and composition, maternal tissues and enzymes in lactating rats. *J Nutr.* 1987;Jul.:117(7);1247-1258.

106. Grimble RF, Mansaray YK. Effects in rats of dietary protein inadequacy on lactose production, milk volume and components of the lactose synthetase complex (EC 2.4.1.22). *Ann Nutr Metab.* 1987;31:179-184.

107. Merritt C, Tan SY. Willem Einthoven (1860-1927): father of electrocardiography. -. *Singapore Med J.* 2012:Jan;53(51):17-18.

108. Barold SS. Willem Einthoven and the birth of clinical electrocardiography a hundred years ago. *Card Electrophysiol Rev.* 2003:Jan;7(1):99-104.

109. Schweitzer P, Keller S. Willem Einthoven--inventor of electrocardiography. *Vnitr Lek.* 2002:Dec;48 Suppl 41:20-23.

110. Konopelski P, Ufnal M. Electrocardiography in rats: a comparison to human. *Physiol Res.* 2016:Nov 23;65(25):717-725.

111. Goldbarg AN, Bruell JH, Daroczy AF. Electrocardiogram of the normal mouse, Mus musculus: general considerations and genetic aspects. *Cardiovasc Res.* 1968;2:93-99.

112. Ho D, Gao S, et. al. Heart Rate and Electrocardiography Monitoring in Mice. *Curr Protoc Mouse Biol.* 2011:Mar 1;1:123-139.

113. Berul CI, Aronovitz MJ, Wang PJ, et. al. In vivo cardiac electrophysiology studies in the mouse. *Journal of the American Heart Association.* 1996;Nov 15:2641-2648.

114. Fenske S, Probstle R, Auer F, et. al. Comprehensive multilevel in vivo and in vitro analysis of heart rate fluctuations in mice by ECG telemetry and electrophysiology. *Jan;11.* 2016;11(1):61-86.

115. Kaese S, Frommeyer G, Verheule S, et. al. The ECG in cardiovascular-relevant animal models of electrophysiology. *Herschrittmacherther Elektophsiol*. 2013 Jun;24(2):84-91.

116. Ferguson DP, Dangott LJ, Schmitt EE, Vellers HL, Lightfoot JT. Differential skeletal muscle proteome of high- and low-active mice. *J Appl Physiol (1985).* 2014;116:1057-1067.

117. Ferguson DP, Dangott LJ, Vellers HL, Schmitt EE, Lightfoot JT. Differential protein expression in the nucleus accumbens of high and low active mice. *Behav Brain Res.* 2015;291:283-288.

118. Klose J. Protein mapping by combined isoelectric focusing and electrophoresis of mouse tissues. A novel approach to testing for induced point mutations in mammals. *Humangenetik.* 1975;26:231-243.

119. Meleady P. 2D gel electrophoresis and mass spectrometry identification and analysis of proteins. *Methods Mol Biol.* 2011;784:123-137.

120. Meleady P. Two-Dimensional Gel Electrophoresis and 2D-DIGE. *Methods Mol Biol.* 2018:1664:1663-1614. doi: 1610.1007/1978-1661-4939-7268-1665_1661.

121. Unlü M, Minden JS. Difference gel electrophoresis: a single gel method for detecting changes in protein extracts. *Electrophoresis.* 1997:Oct;18(11):2071-2077.

122. Alban A, Bjorkesten L, et. al. A novel experimental design for comparative two-dimensional gel analysis: two-dimensional difference gel electrophoresis incorporating a pooled internal standard. *Proteomics.* 2003:Jan;3(1):36-44.

123. Arentz G, Weiland, F, Oehler, MK, Hoffmann, P. State of the art of 2D DIGE. *Proteomics Clin Appl.* 2015;9:277-288.

124. Gaspari M, Cuda G. Nano LC-MS/MS: a robust setup for proteomic analysis. *Methods Mol Biol.* 2011;790:115-126.

125. Fabregat A, Jupe S, Matthews L, et al. The Reactome Pathway Knowledgebase. *Nucleic Acids Res.* 2018;46:D649-d655.

126. Croft D, Mundo AF, Haw R, et al. The Reactome pathway knowledgebase. *Nucleic Acids Res.* 2014;42:D472-477.

127. He M, Lin Y, Xu Y. Identification of prognostic biomarkers in colorectal cancer using a long non-coding RNA-mediated competitive endogenous RNA network. *Oncol Lett.* 2019:Mar;17(13):2687-2694.

128. Zhu K, Chen X, Wang H. Bioinformatic Analyses of Renal Ischaemia-Reperfusion Injury Models: Identification of Key Genes Involved in the Development of Kidney Disease. *Kidney Blood Press Res.* 2018:43(46):1898-1907.

129. Ci LY LD, Yang JQ, et. al. Expression of long non-coding RNA and mRNA in the hippocampus of mice with type 2 diabetes. *Mol Med Rep.* 2018:Dec;18(16):4960-4968.

130. Chung NC MB, Choi H, et. al. Unsupervised classification of multi-omics data during cardiac remodeling using deep learning. *Methods.* 2019:Mar 7. pii:S1046-2023(1018)30359-30351.

131. von Mering C, Huynen M, Jaeggi D, et. al. STRING: a database of predicted functional associations between proteins. *Nucleic Acids Res.* 2003;Jan:258-261.

132. Franceschini A, Szklarczyk D, Frankild S, et. al. STRING v9.1: protein-protein interaction networks, with increased coverage and integration. *Nucleic Acids Res.* 2013;Jan:08-15.

133. Szklarczyk D, Franceschini A, Wyder S, et. al. STRING v10: protein-protein interaction networks, integrated over the tree of life. *Nucleic Acids Res.* 2017;Jan:447-452.

134. Szklarczyk D, Franceschini A, Kuhn M, et. al. The STRING database in 2011: functional interaction networks of proteins, globally integrated and scored. Jan;39(Database issue):D561-8. 2011.

135. Tian K, Liu P, Zhang H, Lu X, Xu C. Characteristic bioanalysis of skeletal muscle cells gene markers in septic patients. *Zhonghua Wei Zhong Bing Ji Jiu Yi Xue.* 2019:Mar;31(33):293-297.

136. Khurana R, Rawoof A, et. al. OncomiRdbB: a comprehensive database of microRNAs and their targets in breast cancer. *BMC Bioinformatics.* 2014:Jan 15;15:15.

137. Karbalaei R, Rezaei-Tavirani M, Asadzadeh-Aghdaei H, Ali MR. Protein-protein interaction analysis of Alzheimer`s disease and NAFLD based on systems biology methods unhide common ancestor pathways. *Gastroenterol Hepatol Bed Bench.* 2018:Winter;11(11):27-33.

138. Zhang X, Liu H, et. al. Identification of key genes and crucial modules associated with coronary artery disease by bioinformatics analysis. *Int J Mol Sci.* 2014:Sep;34(33):863-869.

139. Khan R, Wan YJ, et. al. Protein expression profiling of nuclear membrane protein reveals potential biomarker of human hepatocellular carcinoma. *Clin Proteomics.* 2013;Jun 1;doi:10.1186/1559-0275-1110-1186.

140. Szklarczyk D, Morris JH, Cook H, et. al. The STRING database in 2017: quality-controlled protein-protein association networks, made broadly accessible. *Nucleic Acids Res.* 2017;Jan 4:362-368.

141. Wang HL, Liu L, Qin ZM. A novel method to identify differential pathways in uterine leiomyomata based on network strategy. *Oncol Lett.* 2017;Nov;14(5):5765-5772.

142. Nair J, Ghatge M, Kakkar VV, Shanker J. Network analysis of inflammatory genes and their transcriptional regulators in coronary artery disease. *PLoS One.* 2014;Apr 15;9(4):e94328.

143. Li Y, Jiang Q, Ding Z, et. al. Identification of a Common Different Gene Expression Signature in Ischemic Cardiomyopathy. *Genes (Basel).* 2018:Jan 22;29(21). pii: E56.

144. Khan R, Wan YJ, et. al. Protein expression profiling of nuclear membrane protein reveals potential biomarker of human hepatocellular carcinoma. *Clin Proteomics.* 2013:Jun 1;10(11):16.

145. Han LH, Guo H, Wei W, Chen MM, Yan SF. Network strategy to investigate differential pathways in sporadic amyotrophic lateral sclerosis. *J Cancer Res Ther.* 2018:Dec;14(Supplement):S1057-S1062.

146. Gyulai L, Leigh JS Jr, Chance B. Bioenergetic studies of mitochondrial oxidative phosphorylation using 31phosphorus NMR. *J Biol Chem.* 1985;Apr 10;:3947-3954.

147. Sheeran FL, Pepe S. Mitochondrial Bioenergetics and Dysfunction in Failing Heart. *Adv Exp Med Biol.* 2017;982:65-80.

148. Sommakia S, Houlihan PR, Deane S, et. al. Mitochondrial cardiomyopathies feature increased uptake and diminished efflux of mitochondrial calcium. *J Mol Cell Cardiol.* 2017;Dec;22-32.

149. Sun F, Zhai Y, et. al. Crystal structure of mitochondrial respiratory membrane protein complex II. *Cell.* 2005;Jul 1;1043-1057.

150. Vinnakota KC, Bazil JN, Van den Bergh F, Wiseman RW, Beard DA. Feedback Regulation and Time Hierarchy of Oxidative Phosphorylation in Cardiac Mitochondria. *Biophys J.* 2016;Feb 23;100(4):972-980.

151. Wollenman LC, Vander Ploeg MR, Miller ML, Zhang Y, Bazil JN. The effect of respiration buffer composition on mitochondrial metabolism and function. *PLoS One.* 2017;Nov 1;12(11).

152. Akki A, Smith K, Seymour AM. Compensated cardiac hypertrophy is characterised by a decline in palmitate oxidation. *Mol Cell Biochem.* 2008;Apr:215-224.

153. Balaban RS. Domestication of the cardiac mitochondrion for energy conversion. *J Mol Cell Cardiol.* 2009;Jun;46(6):832-841.

154. Balaban RS. The role of Ca(2+) signaling in the coordination of mitochondrial ATP production with cardiac work. *Biochim Biophys Acta.* 2009;Nov;1787(11):1334-1341.

155. Bazil JN, Buzzard GT, Rundell AE. Modeling mitochondrial bioenergetics with integrated volume dynamics. *PLoS Comput Biol.* 2010;Jan;6(1):e1000632.

156. Bazil JN. Analysis of a Functional Dimer Model of Ubiquinol Cytochrome c Oxidoreductase. *Biophys J.* 2017;Oct 3;133(7):1599-1612.

157. Bishop PD, Atkinson DE. Adenine nucleotide control of the rate of oxygen uptake by rat heart mitochondria over a 15- to 20-fold range. *Arch Biochem Biophys.* 1984;Apr;230(1):335-344.

158. Djouadi F BJ, Munnich A, Bastin J. Characterization of fatty acid oxidation in human muscle mitochondria and myoblasts. *Mol Genet Metab.* 2003;Feb;:112-118.

159. Doerrier C, Krumschnabel G, Wohlfarter Y, Meszaros AT, Gnaiger E. High-Resolution FluoRespirometry and OXPHOS Protocols for Human Cells, Permeabilized Fibers from

Small Biopsies of Muscle, and Isolated Mitochondria. *Methods Mol Biol.* 2018;1782:31-70.

160. Marcovina SM, Sirtori C, Peracino A, et al. Translating the basic knowledge of mitochondrial functions to metabolic therapy: role of L-carnitine. *Transl Res.* 2013;161:73-84.

161. Chance B. Respiratory enzymes in oxidative phosphorylation. I. Kinetics of oxygen utilization. *J Biol Chem.* 1955;Nov;383-393.

162. Chance B. Respiratory enzymes in oxidative phosphorylation. VI. The effects of adenosine diphosphate on azide-treated mitochondria. *J Biol Chem.* 1956;221:477-489.

163. Gnaiger E. Bioenergetics at low oxygen: dependence of respiration and phosphorylation on oxygen and adenosine diphosphate supply. *Respir Physiol.* 2001:Nov 15;128(123):277-297.

164. Haller T, Gnaiger E. A respirometer for investigating oxidative cell metabolism: toward optimization of respiratory studies. *Anal Biochem.* 1994:May 1;218(212):338-342.

165. Luptak I, Panagia M, et. al. Decreased ATP production and myocardial contractile reserve in metabolic heart disease. *J Mol Cell Cardiol.* 2018;Mar;:106-114.

166. Jatain S, Kapoor A, Sinha A, et. al. Metabolic manipulation in dilated cardiomyopathy: Assessing the role of trimetazidine. *Indian J Pediatr.* 2016;Nov-Dec;803-808.

167. Mozaffarian D, Benjamin EJ, Go AS, et al. Heart Disease and Stroke Statistics-2016 Update: A Report From the American Heart Association. *Circulation.* 2016;133:e38-360.

168. Feltes BC, de Faria Poloni J, Bonatto D. The developmental aging and origins of health and disease hypotheses explained by different protein networks. *Biogerontology.* 2011;12:293-308.

169. Ritchey MD, Loustalot F, Bowman BA, Hong Y. Trends in mortality rates by subtypes of heart disease in the United States, 2000-2010. *JAMA.* 2014;Nov.19:2037-2039.

170. Taffet GE, Tate CA. CaATPase content is lower in cardiac sarcoplasmic reticulum isolated from old rats. *Am J Physiol.* 1993;264:H1609-1614.

171. Taffet GE, Pham TT, Bick DL, Entman ML, Pownall HJ, Bick RJ. The calcium uptake of the rat heart sarcoplasmic reticulum is altered by dietary lipid. *J Membr Biol.* 1993;131:35-42.

172. Skilton MR, Phang M. From the α to the ω-3: Breaking the link between impaired fetal growth and adult cardiovascular disease. *Nutrition.* 2016;32:725-731.

173. Hannan RD, Jenkins A, Jenkins AK, et. al. Cardiac hypertrophy: a matter of translation. *Clin Exp Pharmacol Physiol.* 2003;Aug;30:517-527.

174. Whitman SC. A practical approach to using mice in atherosclerosis research. *Clin Biochem Rev.* 2004;Feb;25:81-93.

175. Mongue-Din H, Salmon A, Fiszman MY, Fromes Y. Non-invasive restrained ECG recording in conscious small rodents: a new tool for cardiac electrical activity investigation. *Pflugers Arch.* 2007;April:165-171.

176. Drenckhahn JD, Schwarz QP, Gray S, et. al. Compensatory growth of healthy cardiac cells in the presence of diseased cells restores tissue homeostasis during heart development. *Dev Cell.* 2008;Oct; 15:521-533.

177. Boiten HJ, van Domburg RT, Geleijnse ML, Valkema R, Zijlstra F, Schinkel AF. Cardiac stress imaging for the prediction of very long-term outcomes: Dobutamine stress echocardiography or dobutamine (99m)Tc-sestamibi SPECT? *J Nucl Cardiol.* 2016;Jul 21.

178. Cortigiani L, Sorbo S, Miccoli M, et al. Prognostic value of cardiac power output to left ventricular mass in patients with left ventricular dysfunction and dobutamine stress echo negative by wall motion criteria. *Eur Heart J Cardiovasc Imaging.* 2016;Feb:153-158.

179. Henri C, Piérard LA, Lancellotti P, Mongeon FP, Pibarot P, Basmadjian AJ. Exercise testing and stress imaging in valvular heart disease. *Can J Cardiol.* 2014;30:1012-1026.

180. Kim MN, Kim SA, Kim YH, et al. Head to Head Comparison of Stress Echocardiography with Exercise Electrocardiography for the Detection of Coronary Artery Stenosis in Women. *J Cardiovasc Ultrasound.* 2016;24:135-143.

181. Standbridge K, Reyes E. The role of pharmacological stress testing in women. *J Nucl Cardiol.* 2016;Oct:997-1007.

182. Reeves PG, Nielsen FH, Fahey GC. AIN-93 purified diets for laboratory rodents: final report of the American Institute of Nutrition ad hoc writing committee on the reformulation of the AIN-76A rodent diet. *J Nutr.* 1993;Nov:1939-1951.

183. Sampson DA, Hunsaker HA, Jansen GR. Dietary protein quality, protein quantity and food intake: effects on lactation and on protein synthesis and tissue composition in mammary tissue and liver in rats. *J Nutr.* 1986;Mar:365-375.

184. Pine AP, Jessop NS, Oldham JD. Maternal protein reserves and their influence on lactational performance in rats. *J Nutr.* 1994;Jan:13-27.

185. Lim K, Zimanyi MA, Black MJ. Effect of maternal protein restriction in rats on cardiac fibrosis and capillarization in adulthood. *Pediatr Res.* 2006;Jul.:83-87.

186. Álvarez-García J, Vives-Borras M, Gomis P. Electrophysiological Effects of Selective Atrial Coronary Artery Occlusion in Humans. *Circulation.* 2016;Jun 7:2235-2242.

187. Han Y, Jing J, Tu S, et. al. ST elevation acute myocardial infarction accelerates non-culprit coronary lesion atherosclerosis. *Int J Cardiovac Imaging.* 2014;Feb.:253-261.

188. Gouma E, Simos Y, Verginadis I, et. al. A simple procedure for estimation of total body surface area and determination of a new value of Meeh's constant in rats. *Lab Anim.* 2012;Jan.:46(1);40-45.

189. Byers SL, Wiles MV, Dunn SL, Taft RA. Mouse estrous cycle identification tool and images. *PLoS One.* 2012;7(4):e35538.

190. Matthews PA, Samuelsson AM, Seed P, et. al. Fostering in mice induces cardiovascular and metabolic dysfunction in adulthood. *J Physiol.* 2011;Aug 15:3869-3881.

191. Woo M, Isganaitis E, Cerletti M, et. al. Early life nutrition modulates muscle stem cell number: implications for muscle mass and repair. *Stem Cells Dev.* 2011;Oct.:1763-1769.

192. Wang J, Li D, Dangott LJ, Wu G. Proteomics and its role in nutrition research. *J Nutr.* 2006;136:1759-1762.

193. Wei L, Taffet GE, Khoury DS, et. .al. Disruption of Rho signaling results in progressive atrioventricular conduction defects while ventricular function remains preserved. *FASEB.* 2004;May:857-859.

194. Yagi S, Akaike M, Aihara K, et. al. Endothelial nitric oxide synthase-independent protective action of statin against angiotensin II-induced atrial remodeling via reduced oxidant injury. *Hypertension.* 2010;Apr:918-923.

195. Jansen HJ, Moghtadaei M, Mackasey M, et. al. Atrial structure, function and arrhythmogenesis in aged and frail mice. *Sci Rep.* 2017;Mar 14:44336.

196. Allessie MA, Konings K, Kirchof CJ, et. al. Electrophysiologic mechanisms of perpetuation of atrial fibrillation. *Am J Cardiol.* 1996;Jan 25:10A-23A.

197. Devkota A, Bakhit A, Dufresne A, et. al. Arrhythmias and Electrocardiographic Changes in Systolic Heart Failure. 2016 Apr;8(4):171-4. doi: 10.4103/1947-2714.179931.

198. Friedichs GS. Experimental models of atrial fibrillation/flutter. *J Pharmacol Toxicol Methods.* 2000;Mar-Apr:43(12):117-123.

199. Ozcan C, Battaglia E, Young R, Suzuki G. LKB1 Knockout Mouse Develops Spontaneous Atrial Fibrillation and Provides Mechanistic Insights Into Human Disease Process. Vol 4: *J Am Heart Assoc*; 2015. Mar 15;4(3):e001733. doi: 10.1161/JAHA.114.001733.

200. Zhang Q, Timofeyev V, Lu L, et. al. Functional roles of a Ca2+-activated K+ channel in atrioventricular nodes. *Circ Res.* 2008;Feb 29:465-471.

201. van der Hooft CS, Heeringa J, van Herpen G, Kors JA, Kingma JH, Stricker BHC. Drug-induced atrial fibrillation. *Journal of the American College of Cardiology.* 2004;44:2117-2124.

202. Velasco A, Stirrup J, Reyes E, Hage FG. Guidelines in review: Comparison between AHA/ACC and ESC guidelines for the management of patients with ventricular arrhythmias and the prevention of sudden cardiac death. *J Nucl Cardiol.* 2017; Dec;24(6):1893-1901.

203. Iyer V, Roman-Campos D, Sampson KJ, et. al. Purkinje Cells as Sources of Arrhythmias in Long QT Syndrome Type 3. *Sci Rep.* 2017;Aug 20:13287.

204. Hamaguchi S, Kawakami Y, Honda Y, et. al. Developmental changes in excitation-contraction mechanisms of the mouse ventricular myocardium as revealed by functional and confocal imaging analyses. *J Pharmacol Sci.* 2013;123:167-175.

205. He ZX, Wu DQ, Sun ZH, et. al. Protein or energy restriction during late gestation alters fetal growth and visceral organ mass: an evidence of intrauterine programming in goats. *Anim Reprod Sci.* 2013;Mar;177-182.

206. Patel BB, Sebag IA, Chalifour LE. Lifelong exposure to bisphenol a alters cardiac structure/function, protein expression, and DNA methylation in adult mice. *Toxicol Sci.* 2013;May;174-185.

207. Lang DH, Sharkey NA, Lionikas A, et. al. Adjusting data to body size: a comparison of methods as applied to quantitative trait loci analysis of musculoskeletal phenotypes. *J Bone Miner Res.* 2005;May:748-757.

208. Karp NA, Lilley KS. Maximising sensitivity for detecting changes in protein expression: experimental design using minimal CyDyes. *Proteomics.* 2005 Aug;5(12):3105-15.

209. Karp NA, Lilley KS. Design and analysis issues in quantitative proteomics studies. *Protemics*. 2007. Sep;7 Suppl 1:42-50

210. Gorg A, Boguth G, et. al. The current state of two-dimensional electrophoresis with immobilized pH gradients. *Electrophoresis.* 2000;21:1037-1053.

211. Nabity MB, Lees GE, Dangott LJ, et. al. Proteomic analysis of urine from male dogs during early stages of tubulointerstitial injury in a canine model of progressive glomerular disease. *Vet Clin Pathol*. 2011. Jun;40(2):222-36

212. Bradford MM. A rapid and sensitive method for the quantitation of microgram quantities of protein utilizing the principle of protein-dye binding. *Anal Biochem.* 1976;May 7;72:248-254.

213. Laemmli EK. Cleavage of structural proteins during the assembly of the head of bacteriophage T4. *Nature.* 1970;Aug 15;227(5259):680-685.

214. Zhu C, Guo W. Detection and quantification of the giant protein titin by SDS-agarose gel electrophoresis. *MethodsX.* 2017;Oct.10;4:320-327.

215. Shoulders MD, Raines RT. Collagen structure and stability. *Annu Rev Biochem.* 2009:78: 929-958.

216. Vaidyanathan J, Chinnaswamy K, Vaidyanathan TK. Biomimetic recognition and immunochemical assay of ligand binding to collagen. *J Adhes Dent.* 2003;5:7-17.

217. Mocan E, Nacu V. Aspects of Collagen Isolation Procedure. *Clinical Research Studies.* 2011;NR 2:3-5.

218. Huang L, Li R, Xia Y, Bai G, Siddique KHM, Guo P. A Fast Silver Staining Protocol Enabling Simple and Efficient Detection of SSR Markers using a Non-denaturing Polyacrylamide Gel. *J Vis Exp.* 2018;Apr 20;.

219. Benavides-Vallve C, Corbacho D, Iglesias-Garcia O, et al. New strategies for echocardiographic evaluation of left ventricular function in a mouse model of long-term myocardial infarction. *PloS one.* 2012;7:e41691.

220. Knott MH, Strawser PE, et. al. Neonatal Growth Restriction Slows Cardiomyocyte Development and Reduces Adult Heart Size. *Anat Rec.* 2018:Aug;301(308):1398-1404.

221. Dodson RB, Powers K, et. al. Intrauterine growth restriction influences vascular remodeling and stiffening in the weanling rat more than sex or diet. *Am J Physiol Heart Circ Physiol.* 2017:Feb 1;312(312):H250-H264.

222. Evans-Anderson HJ, Alfieri CM, Yutzey KE. Regulation of cardiomyocyte proliferation and myocardial growth during development by FOXO transcription factors. *Circ Res.* 2008;Mar 28:686-694.

223. Bell JM, Slotkin TA. Postnatal nutritional status influences development of cardiac adrenergic receptor binding sites. *Brain research bulletin.* 1988;21:893-896.

224. Taffet GE, Pham TT, Hartley CJ. The age-associated alterations in late diastolic function in mice are improved by caloric restriction. *The journals of gerontology. Series A, Biological sciences and medical sciences.* 1997;52:B285-290.

225. Leszczynski EC, Visker JR, Ferguson DP. The Effect of Growth Restriction on Voluntary Physical Activity Engagement in Mice. *Med Sci Sports Exerc.* 2019:May 16. doi:10.1249/MSS.

226. Nawathe AR, Christian M, Kim SH, et. al. Insulin-like growth factor axis in pregnancies affected by fetal growth disorders. *Clin Epigenetics*. 2016. Jan 27;8:11.

227. Ferrazzi P, Iascone MR, Senni M, Quaini E. The Titan can help titin: from micro to macro myocardial elasticity. *J Cardiovasc Med.* 2006;Mar;7(3):153-158.

228. Radke MH, Peng J, Wu Y, et. al. Targeted deletion of titin N2B region leads to diastolic dysfunction and cardiac atrophy. *Proc Natl Acad Sci USA.* 2007;Feb 27;104(9):3444-3449.

229. Cahill TJ, Watkins H. Genetic cardiomyopathies causing heart failure. *Circ Res.* 2013;Aug 30;:660-675.

230. Chattergoon NN, Giraud GD, Louey S, Stork P, Fowden AL, Thornburg KL. Thyroid hormone drives fetal cardiomyocyte maturation. *FASEB J.* 2012;Jan;26(1):397-408.

231. Hammer D, Leier CV, Baba N, Vasko JS, Wooley CF, Pinnell SR. Altered collagen composition in a prolapsing mitral valve with ruptured chordae tendineae. *Am J Med.* 1979;Nov;67(5):863-866.

232. Cheah KS. Collagen genes and inherited connective tissue disease. *Biochem J.* 1985;Jul 15;229(2):287-303.

233. Collins D, Lindberg K, McLees B, Pinnell S. The collagen of heart valve. *Biochim Biophys Acta.* 1977;Nov 25;495(1):129-139.

234. Wang JH, Su F, Wang S, et. al. CXCR6 deficiency attenuates pressure overload-induced monocytes migration and cardiac fibrosis through downregulating TNF-α-dependent MMP9 pathway. *Int J Clin Exp Pathol.* 2014;Sep 15;7(10):6514-6523.

235. Henney AM, Schwartz RC, Child AH, Devereux RB, Leech GL. Genetic evidence that mutations in the COL1A1, COL1A2, COL3A1, or COL5A2 collagen genes are not responsible for mitral valve prolapse. *Br Heart J.* 1989;Mar;61(3):292-299.

236. Zhao HP, Lu D, Zhang W, et. al. Protective action of tetramethylpyrazine phosphate against dilated cardiomyopathy in cTnT(R141W) transgenic mice. *Acta Pharmacol Sin.* 2010;Mar;31(3):281-288.

237. Bertoli C, Skotheim JM, de Bruin RAM. Control of cell cycle transcription during G1 and S phases. *Nat Rev Mol Cell Biol.* 2013;14:518-528.

238. Haley SA, Zhao T, Zou L, Klysik JE, Padbury JF, Kochilas LK. Forced expression of the cell cycle inhibitor p57Kip2 in cardiomyocytes attenuates ischemia-reperfusion injury in the mouse heart. *BMC Physiol.* 2008;Feb 29;8:4.doi: 10.1186.

239. Zhang P, Liegeois NJ, Wong C, et al. Altered cell differentiation and proliferation in mice lacking p57KIP2 indicates a role in Beckwith-Wiedemann syndrome. *Nature.* 1997;387:151-158.

240. Evans-Anderson HJ, Alfieri CM, Yutzey KE. Regulation of cardiomyocyte proliferation and myocardial growth during development by FOXO transcription factors. *Circ Res.* 2008;Mar 28;102(6):686-694.

241. Kochilas LK, Li J, Jin F, Buck CA, Epstein JA. p57Kip2 expression is enhanced during mid-cardiac murine development and is restricted to trabecular myocardium. *Pediatr Res.* 1999;May;45(5 Pt 1):635-642.

242. Ikenishi A, Okayama H, Iwamoto N, et. al. Cell cycle regulation in mouse heart during embryonic and postnatal stages. *Dev Growth Differ.* 2012;Oct;54(8):731-738.

243. Wang L, Geist J, Grogan A, et. al. Thick Filament Protein Network, Functions, and Disease Association. *Compr Physiol.* 2018;Mar 13;8(2):631-709.

244. Kimura S, Maruyama K, Huang YP. Interactions of muscle beta-connectin with myosin, actin, and actomyosin at low ionic strengths. *J Biochem.* 1984;Aug;96(2):499-506.

245. Kontrogianni-Konstantopoulos A, Ackermann MA, Bowman AL, et. al. Muscle giants: molecular scaffolds in sarcomerogenesis. *Physiol Rev.* 2018;Oct:89(4):1217-1267.

246. Chauveau C, Rowell J, Ferreiro A. A rising titan: TTN review and mutation update. *Hum Mutat.* 2014;Sep;35(9):1046-1059.

247. Heidenreich PA, Trogdon JG, Khavjou OA, et al. Forecasting the future of cardiovascular disease in the United States: a policy statement from the American Heart Association. *Circulation.* 2011;123:933-944.

248. Ovbiagele B, Goldstein LB, Higashida RT, et al. Forecasting the future of stroke in the United States: a policy statement from the American Heart Association and American Stroke Association. *Stroke.* 2013;44:2361-2375.

249. Yang Q, Zhong Y, Ritchey M, et. al. Predicted 10-year risk of developing cardiovascular disease at the state level in the U.S. *Am J Prev Med.* 2015;48(1):58-69.

250. Wollenman LC, Vander Ploeg MR, Miller ML, Zhang Y, Bazil JN. The effect of respiration buffer composition on mitochondrial metabolism and function. *PLoS One.* 2017;Nov 1;12(11):e0187523.

251. Katz LA, Portman MA, Balaban RD. Relation between phosphate metabolites and oxygen consumption of heart in vivo. *Am J Physiol.* 1989;Jan;:H265-274.

252. Wisneski JA, Neese RA, Gruenke LD, Morris DL, Craig JC. Metabolic fate of extracted glucose in normal human myocardium. *J Clin Invest.* 1985;Nov;:1819-1827.

253. Stanley WC, Lopaschuk GD, Hall JL, et. al. Regulation of myocardial carbohydrate metabolism under normal and ischaemic conditions. Potential for pharmacological interventions. *Cardiovasc Res.* 1997;Feb;33(2):243-257.

254. Stanley WC, Recchia FA, Lopaschuk GD. Myocardial substrate metabolism in the normal and failing heart. *Physiol Rev.* 2005;Jul;85(3):1093-1129.

255. Balaban RD. Regulation of oxidative phosphorylation in the mammalian cell. *Am J Physiol.* 1990;Mar;258(3 Pt 1):C377-389.

256. Jeneson JA, Wiseman RW, Westerhoff HV, Kushmerick MJ. The signal transduction function for oxidative phosphorylation is at least second order in ADP. *J Biol Chem.* 1996;Nov 8;271(45):27995-27998.

257. Saddik M, Lopaschuk GD. Myocardial triglyceride turnover and contribution to energy substrate utilization in isolated working rat hearts. *J Biol Chem.* 1991;May 5:266(13);8162-8170.

258. Lopaschuk GD, Spafford MA, Marsh DR. Glycolysis is predominant source of myocardial ATP production immediately after birth. *Am J Physiol.* 1991;Dec:261(6 Pt 2)H1698-16705.

259. Kolwicz SC Jr, Tian R. Metabolic therapy at the crossroad: how to optimize myocardial substrate utilization? *Trends Cardiovasc Med.* 2009;Aug:19(6);201-207.

260. Taegtmeyer H, Wilson CR, Razeghi P, Sharma S. Metabolic energetics and genetics in the heart. *Ann N Y Acad Sci.* 2005;Jun;1047:208-218.

261. Taegtmeyer H. Myocardial energetics: still only the tip of an iceberg. *Heart Lung Circ.* 2003;12(1):3-6.

262. van der Vusse GJ, Glatz JF, Stam HC, Reneman RS. Fatty acid homeostasis in the normoxic and ischemic heart. *Physiol Rev.* 1992;Oct;72(4):881-940.

263. Lopaschuk GD, Wambolt RB, Barr RL. An imbalance between glycolysis and glucose oxidation is a possible explanation for the detrimental effects of high levels of fatty acids during aerobic reperfusion. *J Pharmacol Exp Ther.* 1993;Jan;264(1):135-144.

264. Griffin TM, Humphries KM, Kinter M, Lim HY, Szweda LI. Nutrient sensing and utilization: Getting to the heart of metabolic flexibility. *Biochimie.* 2016;124:74-83.

265. Walker JM. The bicinchoninic acid (BCA) assay for protein quantitation. *Methods Mol Biol.* 1994:32;5-8.

266. Bazil JN, Beard DA, Vinnakota KS. Catalytic Coupling of Oxidative Phosphorylation, ATP Demand, and Reactive Oxygen Species Generation. *Biophys J.* 2016;Feb 23;110(4):962-971.

267. Osmond C, Barker DJ, Winter PD, Fall CH, Simmonds SJ. Early growth and death from cardiovascular disease in women. *BMJ.* 1993 Dec 11;307(6918):1519-1524.

268. Divakaruni AS, Brand MD. The regulation and physiology of mitochondrial proton leak. *Physiology (Bethesda).* 2011;26:192-205.

269. Affourtit C, Quinlan CL, Brand MD. Measurement of proton leak and electron leak in isolated mitochondria. *Methods Mol Biol.* 2012;810:165-182.

270. Quarrie R, Cramer BM, Lee DS, et. al. Ischemic Preconditioning Decreases Mitochondrial Proton Leak and Reactive Oxygen Species Production in the Postischemic Heart. *J Surg Res.* 2011:Jan; 165(161):165-114.

271. Sharov VG, Todor AV, Silverman N, Goldstein S, Sabbah HN. Abnormal mitochondrial respiration in failed human myocardium. *J Mol Cell Cardiol.* 2000:Dec; 32(12):2361-2367.

272. Lemieux H, Semsroth S, Antretter H, Hofer D, Gnaiger E. Mitochondrial respiratory control and early defects of oxidative phosphorylation in the failing human heart. *Int J Biochem Cell Biol.* 2011:Dec;43(12):1729-1738.

273. Cheng J, Nanayakkara G, Shao Y, et al. Mitochondrial Proton Leak Plays a Critical Role in Pathogenesis of Cardiovascular Diseases. *Adv Exp Med Biol.* 2017;982:359-370.

274. Boraso A, Williams AJ. Modification of the gating of the cardiac sarcoplasmic reticulum Ca(2+)-release channel by H2O2 and dithiothreitol. *Am J Physiol.* 1994:Sep;267(263 pt 262):H1010-1016.

275. Okabe E, Hess ML, Oyama M, Ito H. Characterization of free radical-mediated damage of canine cardiac sarcoplasmic reticulum. *Arch Biochem Biophys.* 1983:Aug;225(221):164-177.

276. Holmberg SR, Cumming DV, Kusama Y, et. al. Reactive oxygen species modify the structure and function of the cardiac sarcoplasmic reticulum calcium-release channel. *Cardioscience.* 1991:Mar;2(1):19-25.

277. Cerbai E, Ambrosio G, Porciatti F, Chiariello M, Giotti A, Mugelli A. Cellular electrophysiological basis for oxygen radical-induced arrhythmias. A patch-clamp study in guinea pig ventricular myocytes. *Circulation.* 1991:Oct;84(84):1773-1782.

278. Chouchani ET, Pell VR, Gaude E, et al. Ischaemic accumulation of succinate controls reperfusion injury through mitochondrial ROS. *Nature.* 2014;515:431-435.

279. Rodríguez-Rodríguez P, Ramiro-Cortijo D, Reyes-Hernandez CG, Lopez de Pablo AL, Gonzalez MC, Arribas SM. Implication of Oxidative Stress in Fetal Programming of Cardiovascular Disease. *Front Physiol.* 2018;May 23;9:602.

280. Tain YL, Hsu CN. Interplay between Oxidative Stress and Nutrient Sensing Signaling in the Developmental Origins of Cardiovascular Disease. *Int J Mol Sci.* 2017;Apr 15;18(4):E841.

281. Kang PT, Chen CL, Lin P, et. al. Mitochondrial Complex I in the Post-Ischemic Heart: Reperfusion-Mediated Oxidative Injury and Protein Cysteine Sulfonation. *Journal of molecular and cellular cardiology.* 2018;121:190-204.

282. Karamanlidis G, Lee CF, Garcia-Menendez L, et al. Mitochondrial Complex I Deficiency Increases Protein Acetylation and Accelerates Heart Failure. *Cell metabolism.* 2013;Aug 6;18(2):239-250.